Mechanism of the F_1 ATPase Molecular Motor as Revealed by Single Molecule Studies

by

James Martin

A Dissertation Presented in Partial Fulfillment
of the Requirements for the Degree
Doctor of Philosophy

Approved November 2012 by the
Graduate Supervisory Committee:

Wayne Frasch, Chair
Roberto Gaxiola
Hao Yan
Douglas Chandler

ARIZONA STATE UNIVERSITY

December 2012

ABSTRACT

The F_1F_o ATP synthase is required for energy conversion in almost all living organisms. The F_1 complex is a molecular motor that uses ATP hydrolysis to drive rotation of the γ-subunit. It has not been previously possible to resolve the speed and position of the γ-subunit of the F_1-ATPase as it rotates during a power stroke. The single molecule experiments presented here measured light scattered from 45X91 nm gold nanorods attached to the γ-subunit that provide an unprecedented 5 μs resolution of rotational position as a function of time. The product of velocity and drag, which were both measured directly, resulted in an average torque of 63±8 pN nm for the *Escherichia coli* F_1-ATPase that was determined to be independent of the load. The rotational velocity had an initial (I) acceleration phase 15° from the end of the catalytic dwell, a slow (S) acceleration phase during ATP binding/ADP release (15°-60°), and a fast (F) acceleration phase (60°-90°) containing an interim deceleration (ID) phase (75°-82°). High ADP concentrations decreased the velocity of the S phase proportional to 'ADP-release' dwells, and the F phase proportional to the free energy derived from the [ADP][Pi]/[ATP] chemical equilibrium. The decreased affinity for ITP increased ITP-binding dwells by 10%, but decreased velocity by 40% during the S phase. This is the first direct evidence that nucleotide binding contributes to F_1-ATPase torque. Mutations that affect specific phases of rotation were identified, some in regions of F_1 previously considered not to contribute to rotation.

Mutations βD372V and γK9I increased the F phase velocity, and γK9I increased the depth of the ID phase. The conversion between S and F phases was specifically affected by γQ269L. While γT273D, βD305E, and αR283Q decreased the velocity of all phases, decreases in velocity due to βD302T, γR268L and γT82A were confined to the I and S phases. The correlations between the structural locations of these mutations and the phases of rotation they affect provide new insight into the molecular basis for F_1-ATPase γ-subunit rotation.

DEDICATION

I dedicate this work to my family, and especially my wife, who has been patient and understanding despite times of stress. I am thankful to her for her care of our family when I have been absent, for preparing lunches, and driving long distances to come see me. I finally would like to thank her for sending me uplifting messages throughout each day. Also my kids, who in their youth, do their best to support me and look forward to when I come home every night. In addition, thanks to my parents who have supported me both financially and emotionally. Thanks to all of my other friends and family who have put up with me and helped me despite myself.

ACKNOWLEDGMENTS

Thanks to my committee members for being patient and constructive. I appreciate their wisdom and for their ability to spark creativity. Whether in class or out, I give thanks for supporting me and helping me to think outside the box. Special thanks to my advisor Wayne Frasch for his endless patience, for prodding me when I needed prodding, and for believing in me. Thanks for your many hours in training, teaching, lecturing, and especially in helping to prepare this manuscript.

TABLE OF CONTENTS

LIST OF TABLES

LIST OF FIGURES

Figure Page

Figure Page

Figure Page

Chapter 1

INTRODUCTION

The F_oF_1 ATP Synthase

The F_1F_o ATP synthase can be found in most living things, and utilizes the available energy formed from a proton gradient to combine ADP and Pi to catalyze the formation of ATP. The two complexes of the synthase allow protons to pass through the membrane embedded $ab_2c_{10\text{-}15}$ collection of subunits referred to as F_o, and subsequently causes each of 3 catalytic sites located between each $\alpha\beta$ heterodimer within the F_1 to catalyze the formation of ATP. In photosynthetic organisms, the ATP synthase can be found in the thylakoid membrane oriented with the F_1 portion facing the stroma of the chloroplast. Conversely, in organisms that utilize mitochondria, the ATP synthase resides in the membranes that make up the cristae, with the ATP generating F_1 subunits facing the matrix. Organisms that lack either chloroplast or mitochondria, such as bacteria, locate the F_oF_1 ATP synthase to their inner membrane, with the F_1 turned toward the cytosol.

A high proton gradient potential is maintained either through light driven photosynthetic reactions, or through the breakdown of metabolites, and is harnessed by the F_1F_o ATP synthase to phosphorylate ADP to produce ATP and water, despite high concentrations of ATP present in the cell (Nakamoto, Ketchum et al. 1999; Frasch 2000; Stock, Gibbons et al. 2000; Yoshida, Muneyuki et al. 2001; Fillingame, Angevine et al. 2002;

Senior, Nadanaciva et al. 2002). One reason for the ubiquity of the F_oF_1 ATP synthase in living systems is its central role in providing the chemical energy in the form of ATP that cellular processes utilize in order to function. In specialized circumstances however, the F_1F_o ATP synthase can hydrolyze ATP and reverse the flow of protons across the membrane, thus acting as a proton pump.

The conversion of potential energy to the production of chemical energy is accomplished through the rotation of two separate rotary molecular motors, the F_o and F_1 complexes (**Figure 1**). In order to synthesize ATP, protons pass through the F_o and induce rotation of the c-ring, which in E. coli is composed of 10 c subunits and also interacts tightly with the $\gamma\varepsilon$ subunits of the F_1 rotor. Rotational steps of the F_1 rotor have previously been shown by single molecule FRET measurements to occur in 120° intervals (Borsch, Diez et al. 2002). The rotation of the γ subunit induces conformational changes within the F_1 that alternately change the affinities of each site to induce binding of ADP and Pi, and the release of ATP product. Hydrolysis of ATP in the catalytic sites reverses the process by forcing γ in the opposite direction and thus, causing the rotor of F_o to rotate and pump protons back across the membrane. Although this reverse activity is rare when F_1 is bound to F_o, F_1 can be purified away from F_o in a soluble form, in which the primary catalytic activity is hydrolysis powered rotation of the γ subunit (Noji, Yasuda et al. 1997).

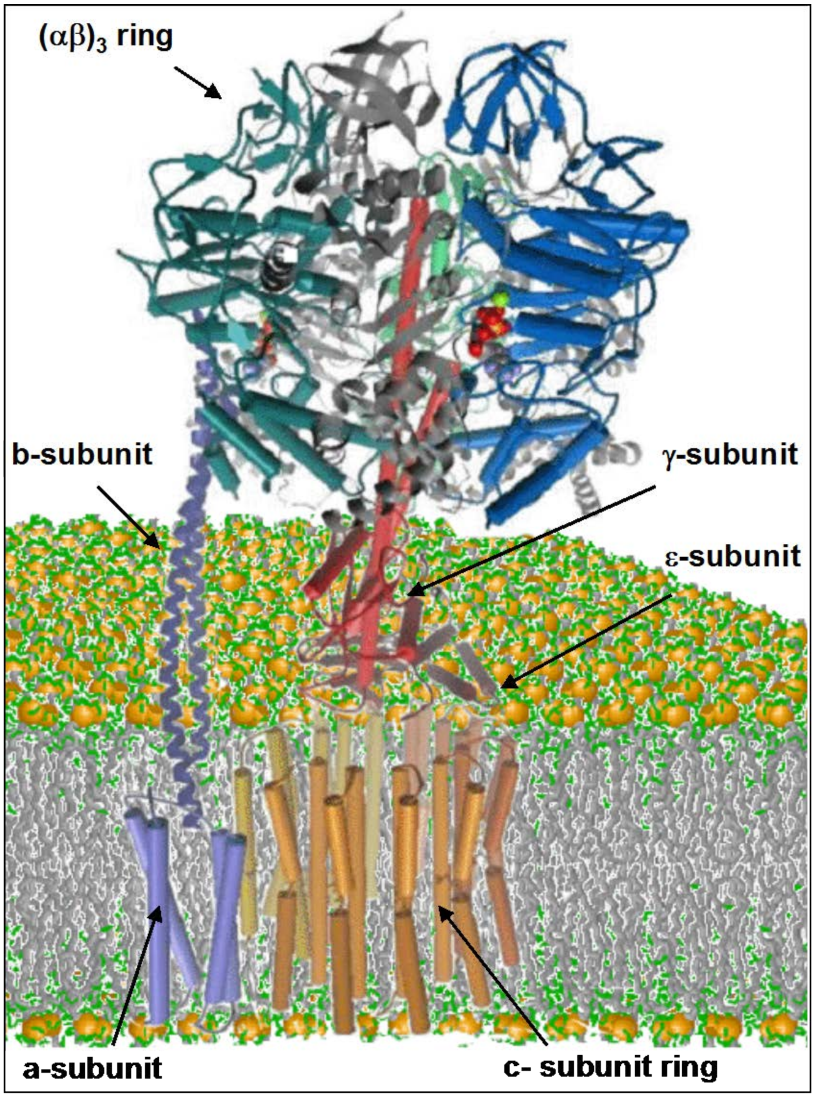

Figure 1. Composite structure of the F_1F_o ATP synthase.

Experiments involving the observation of probes attached to single molecules of F_1 have demonstrated the ability for the γ subunit to rotate (Noji, Yasuda et al. 1997; Cherepanov and Junge 2001; Yasuda, Noji et al. 2001; Spetzler, York et al. 2006). F_1 molecules anchored to a coverslip coated in nickel nitrilotriacetate (Ni-NTA) through histidine tags engineered into the N-terminus of the β subunit were bound so that the long axis of the γ subunit was perpendicular to the surface. In order to examine the rotation of the γ subunit, an actin filament was bound to a biotin-maleimide molecule covalently attached to a cysteine mutation located in the foot of γ. The filament was then observed to rotate counterclockwise in the presence of ATP.

Rotation of the γ subunit occurs in 120° steps when the concentration of ATP has saturated the ability of the F_1 enzyme to catalyze hydrolysis, and results in the consumption of 3 ATP for a full 360° of rotation. Periods of dwelling between rotational events have been observed to last as long as 8 ms for F_1 obtained from *E. coli* (Spetzler, York et al. 2006) and as short as 2 ms in the case of F_1 purified from the thermophile, *PS3* (Yasuda, Noji et al. 2001). At low concentrations of ATP, the 120° power stroke is interrupted by the presence of a pause that is dependent upon the amount of ATP present, indicating that the rotation is halted until nucleotide substrate is bound. Early single molecule experiments determined this dwell to occur about 30° after the catalytic dwell (Yasuda, Noji et al. 2001), but further experiments showed that rotation stopped closer to 40° (Sakaki, Shimo-Kon et al. 2005). In addition, it has been determined that ADP is released from the adjacent catalytic site at the same rotational position that ATP is bound and that high concentrations of Pi lengthened the catalytic dwell, but not the 40 degree dwell under substrate limiting conditions (Adachi, Oiwa et al. 2007). This is consistent with other evidence that suggests product release initiates the final 40º of rotation to complete the catalytic cycle (Sielaff, Rennekamp et al. 2008).

Structure of F_1

The first high resolution structure of F_1 was determined for the enzyme from the bovine mitochondrial. That structure resolved most of the $(\alpha\beta)_3$ ring and part of the γ subunit, but did not include the smaller subunits. The α and β subunits were resolved nearly completely, while subunit γ was resolved only partially (Abrahams, Leslie et al. 1994). Since that time structures of F_1 complexes from several sources have been successfully crystallized under various conditions (Hausrath, Gruber et al. 1999; Gibbons, Montgomery et al. 2000; Menz, Walker et al. 2001; Kabaleeswaran, Puri et al. 2006; Bowler, Montgomery et al. 2007). The most complete F_1 complex structure, including all subunits in the central stalk, was obtained in 2000 (Braig, Menz et al. 2000).

The F_1 ATPase is composed of a hexamer of alternating α and β subunits that surround a coiled-coil structural domain of the γ subunit. Subunit ε acts in conjunction with the γ globular domain that protrudes from the ring formed by the $\alpha_3\beta_3$ subunits to bind F_1 to the F_o complex. The catalytic sites responsible for ATP hydrolysis are located at the interface of each of the 3 αβ heterodimers; with β subunit residues mostly involved in binding and catalysis. Additionally, three more ATP binding sites are located mostly in the α subunits, but remain non-catalytic.

The α and β subunits are very similar in structure and are primarily comprised of three domains. At the end furthest from F_o, a β – barrel provides structural support for the $\alpha_3\beta_3$ ring and provide a solid attachment point for the δ subunit. The central domain is involved in nucleotide binding via the Walker A motif, catalysis, as well as interactions between β and γ. Specifically, the residues referred to as the catch loop form strong electrostatic interactions between the N-terminus of the γ subunit and the β subunit (Greene and Frasch 2003). Residues α287-394 and β274-381 form hydrophobic regions that closely interact with the γ C-terminal hydrophobic end. This structure is called a “sleeve” and appears to ensure friction-free rotation of γ.

The most mobile domain is an α helical bundle domain that contain a group of negatively charged residues referred to as the DELSEED, based on the sequence of amino acids. It has been previously thought that its function is primarily regulatory (Bi, Watts et al. 2008; Volkov, Zaida et al. 2009), but more recently it has been proposed to be responsible for promoting γ subunit rotation (Tanigawara, Tabata et al. 2012; Usukura, Suzuki et al. 2012). Movement of the α helical bundle domain of the β subunit opens and closes access to the catalytic site dependent upon the occupancy of nucleotide in the site. This results in a structural asymmetry that is key to understanding the mechanism for F_1 rotation as domains open and close upon release of product and binding of substrate and as the rotational position of the γ subunit changes in relation to the hexameric ring.

The γ subunit is composed primarily of two domains, a coiled-coil structure formed from α-helixes in the C and N termini, and a globular domain referred to as the foot. The coiled-coil extends up through the aperture of the αβ ring for nearly the entire breadth of the ring, and is composed of anti-parallel α-helixes that are bound together by a band of nonpolar residues (Wilkens 2005). The foot extends toward the membrane from the hexamer, and in conjunction with ε -subunit, docks the F_1 to the F_o c-ring (Pogoryelov, Nikolaev et al. 2008). The γ–subunit functions as the rotor of the molecular motor for the F_1 ATPase and is responsible for transferring rotational torque from F_o during ATP synthesis.

The δ subunit is thought to hold the b subunit stalks from F_o to the α subunits of F_1. The N terminus is composed of six α-helixes that form a helical bundle that previous studies demonstrated interacts with the N-terminal region of subunit α (Greie, Deckers-Hebestreit et al. 2000). In a previous NMR study, the C-terminus was shown to have few structural elements (Dmitriev, Jones et al. 1999), but was shown to associate with the C terminal end of the subunit b dimer (Caviston, Ketchum et al. 1998).

The ε subunit has two domains; a β-barrel domain in the N-terminus, and a C-terminal helix-turn-helix domain. Although ε is involved in the binding of F_1 to F_o through the foot of the γ subunit, it has also been shown to have a regulatory role. Recently, a crystal structure was solved in which the F_1 was inhibited by the helix turn helix (Cingolani and Duncan 2011). The extension of the normally compact helix-turn helix into the cavity of the βα ring disrupted rotation of the γ-subunit, presumably through steric restrictions.

Observation of Single Molecule Rotation

The F_1 ATPase was first shown to rotate in a counterclockwise direction through observations of a fluorescently labeled actin filament bound to the foot of the γ-subunit of single molecules of thermophilic F_1 (TF_1) immobilized onto a glass slide (Noji, Yasuda et al. 1997). Further studies have successfully observed rotation of F_1 derived from *E.coli* and chloroplasts (Hisabori, Kondoh et al. 1999; Noji, Hasler et al. 1999; Omote, Sambonmatsu et al. 1999) using reporter groups other than actin. Some of the probes that have been used include, a single fluorophore (Adachi, Yasuda et al. 2000), spherical bead or bead duplex (Hirono-Hara, Noji et al. 2001; Yasuda, Noji et al. 2001), metal bar (Soong, Bachand et al. 2000), FRET or fluorescence resonance energy transfer (Borsch, Diez et al. 2002) and more recently, gold nanoparticles (Spetzler, York et al. 2006; Spetzler, Ishmukhametov et al. 2009).

Bulk measurements of the *E. coli* F_1 ATPase activity determined that K_m was 10 μM, with a k_{cat} for hydrolysis activity of 120 sec^{-1} (Greene and Frasch 2003). The TF_1 however had a V_{max} of 390 steps s^{-1} and a K_m of 15 μM (Yasuda, Noji et al. 2001). It has been determined that each 120° rotational event is associated with the hydrolysis of a single ATP molecule (Yasuda, Noji et al. 1998; Adachi, Yasuda et al. 2000; Yasuda, Noji et al. 2001). It has been thought previously that the hydrolysis rate for single molecules should be higher than bulk measurements observed in solution due to inhibition by Mg^{2+}-ADP (Jault, Dou et al. 1996; Boyer 1997; Matsui, Muneyuki et al. 1997; Kinosita, Yasuda et al. 2000; Hirono-Hara, Noji et al. 2001). However, when the average catalytic dwell time observed in single molecule experiments was compared to bulk measurements, it was determined that they were comparable (Yasuda, Noji et al. 2001; Spetzler, York et al. 2006).

Rotation of a gold nanosphere attached to the foot of the γ subunit of thermophilic F1 was recorded with a high speed camera capable of collecting data at up to 8000 frames/sec (Yasuda, Noji et al. 2001). The centroid of the nanosphere was tracked and was observed to rotate in 120° steps in ATP saturating conditions, separated by short pauses or dwells. An additional dwell separating the rotation into 40° and 80° sub steps (**Figure 2**) was detected when substrate was limited (20 nM ATP).

The length of the dwell prior to the 80° rotational step was inversely proportional to the concentration of ATP present during the experiment. This dependence provided evidence that ATP binding occurs before the 80° substep, and thus this pause has been labeled the “ATP Binding” dwell.

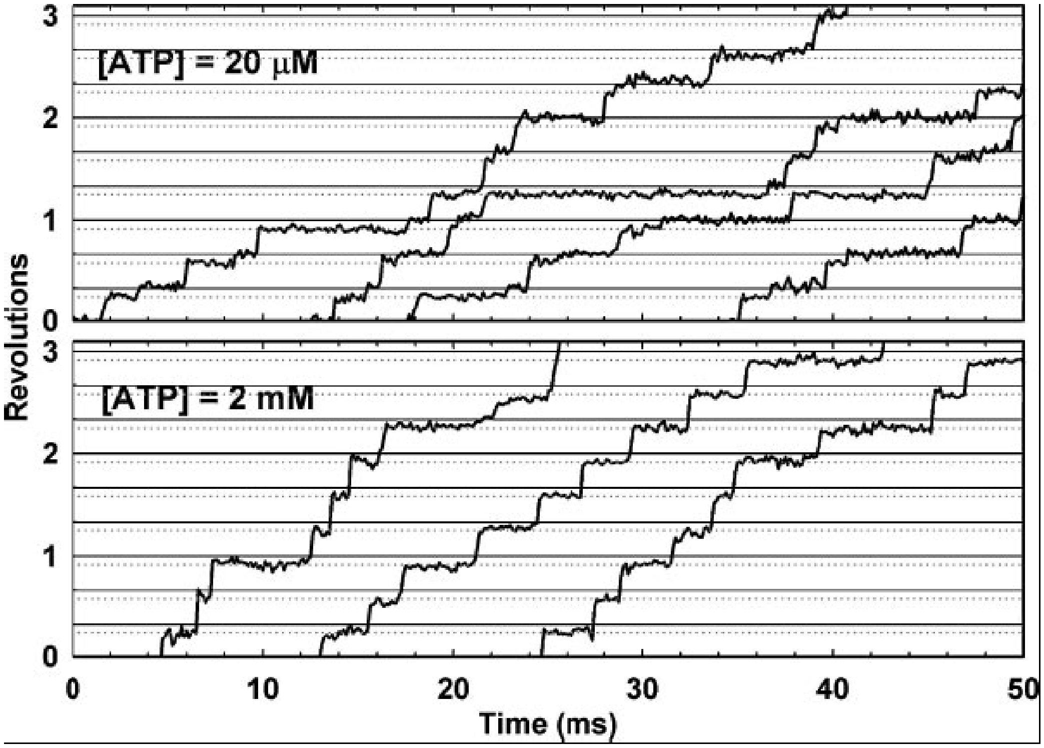

Figure 2. Separation of F_1-ATPase rotation into 40° and 80° sub-steps. Sub-steps in F_1 rotation at 20 mM ATP (upper panel) recorded with a temporal resolution of 0.125 ms (Yasuda, Noji et al. 2001). With this resolution, sub-steps are not discerned at 2 mM ATP (lower panel), implying that the ATP-waiting dwell is <0.125 ms and the next 80° rotation is complete within 0.125 ms of ATP binding; it also implies that F_1 is completely reset and ready to bind a next ATP by the end of a 40° sub-step. Horizontal solid lines are separated by 120°, and dotted lines are drawn 40° below (Taken from (Kinosita, Adachi et al. 2004).

Energy for Rotation

Based on early single molecule experiments (Yasuda, Noji et al. 2001) that showed that each 120° power stroke is split by a pause that occurs 30° after the catalytic dwell, a free energy profile was determined as shown in **Figure 3** (Gao, Yang et al. 2003). The model was constructed under the assumptions that the rotational pause that occurs after 30° is a result of ATP waiting to bind to the empty (E) site, and product release occurs during the catalytic dwell after 90°.

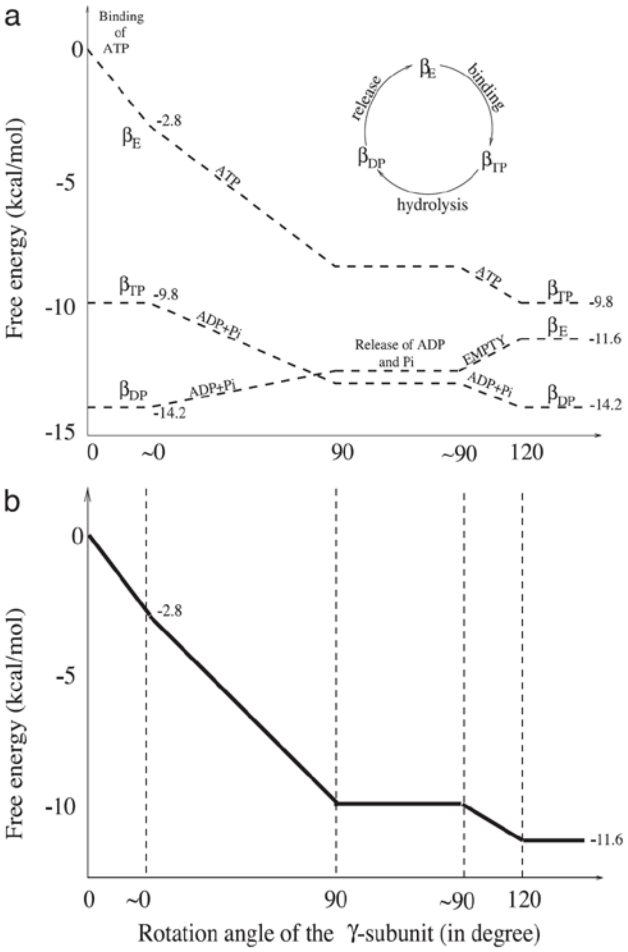

Figure 3. Free energy (kcal/mol) profile for ATP hydrolysis in the tri-site mechanism. (a) The individual free energy changes as a function of the conformational transitions. (b) The change of the total free energy, which is the sum of the free energy changes of the three sites. Taken from (Gao, Yang et al. 2003).

During ATP binding, the E site changes conformation by causing the $\alpha\beta$ subunits to close around the substrate, and becomes the (TP) site observed in crystal structures, which contains a bound ATP. The 19.4 pN nm/molecule of free energy calculated for this change was based on a change in K_D from 25 mM for the E site to 0.3 nM for the TP site and using the cellular level of 3mM ATP (Gao, Yang et al. 2003). It was postulated that the majority of this binding energy is used to drive rotation of the γ-subunit as a result of the conformational changes undergone by the $\alpha\beta$ subunits. Hydrolysis was thought to occur any time after the TP site has formed, due to the equal affinity for both ATP and the products ADP and Pi. The site becomes stabilized however, upon conformational change to the DP site, which has a higher affinity for ADP. The energy derived from binding the ADP to DP site is thought to be a secondary source of energy for γ-subunit rotation.

Due to the cooperative nature of F_1, the changing of E site to the TP site upon ATP binding, causing the former TP site to become the DP site. However, the energy provided by these steps promotes the release of ADP from the DP site resulting in a new E site (Gao, Yang et al. 2003). Through addition of the free energy contributions of each site as they change during 120° of rotation, the net free energy change available for the rotation of the γ-subunit was calculated to be 80.6 pN nm/molecule equivalent to the free energy of hydrolysis.

Torque Determination

Torque is calculated by multiplying the measured velocity, ν, by the frictional drag coefficient, ξ, which represents the drag on the probe as it passes through a liquid medium as shown in Equation 1:

$$T = \xi\nu \qquad (1)$$

One the first measurements of torque were based on the rotational velocity of actin filaments that were attached to the γ-subunit of the F_1 ATPase. Slow rotation of F_1 was the result of viscous drag on the filament, which calculated ξ by Equation 2 (Hunt, Gittes et al. 1994; Adachi, Nishizaka et al. 2003):

$$\xi = \frac{\frac{4\pi}{3}\eta L^3}{\ln(L/r) - 0.447} \qquad (2)$$

for filament of radius r (~5 nm) and length L, and where η is ~10^{-3} nm^{-2} s, the viscosity of the medium at room temperature.

The hydrodynamic drag on a spherical bead with radius *a* attached to F_1 off center with a distance between the center of the bead and axis rotation is x, the frictional drag coefficient, ξ is determined by:

$$\xi = 8\pi\eta a^3 + 6\pi\eta a x^2 \qquad (3)$$

Early single molecule experiments have not been able to measure rotation directly, due to inadequate time resolution during observation of the 120° power stroke. Indirect methods estimated the torque of F_1 as it moves through a viscous medium to range from 44-55 pN nm (Yasuda, Noji et al. 1998; Panke, Cherepanov et al. 2001). The torque was determined to be about 40 pN nm by using an estimated average velocity calculated from a number of full revolutions of an actin filament, during which, stepping was not observed (Yasuda, Noji et al. 1998). However, because this average velocity included periods of dwelling, the torque is an underestimate of that produced only when the γ-subunit is rotating. Using this torque estimate the amount of work performed by the F_1 during 120° of rotation was calculated to be 40–44 pN nm times $(2/3)\pi$ radians, which is, ~20 k_BT or about 80–90 pN nm. Since this is close to the free energy available from hydrolysis, it was concluded that the F_1 is nearly 100% efficient in performing mechanical work using chemical energy.

Further experiments have used alternate methods to determine the torque without using calculations based on drag as determined by Equations 2 and 3 (Hunt, Gittes et al. 1994). Measurements of the drag as determined from the curvature of an actin filament bound to the γ-subunit of F_1, calculated the torque to be 50 ± 6 pN nm (Panke, Cherepanov et al. 2001). Because the bending of the actin filament is a conservative force, this measurement provides a more accurate result than determined previously. However, because the filament was not able to relax during periods when the γ-subunit was not moving during a dwell, this torque estimate is a lower bound for the available torque of the F_1. A 40-nm gold bead (**Figure 4**), shown not to slow the rotation rate, was also used as a probe of rotation (Yasuda, Noji et al. 2001). Despite the use of high speed camera operating at 8000 frames s^{-1} only dwells were recorded, without resolution of the rotational movement between them (**Figure 5**).

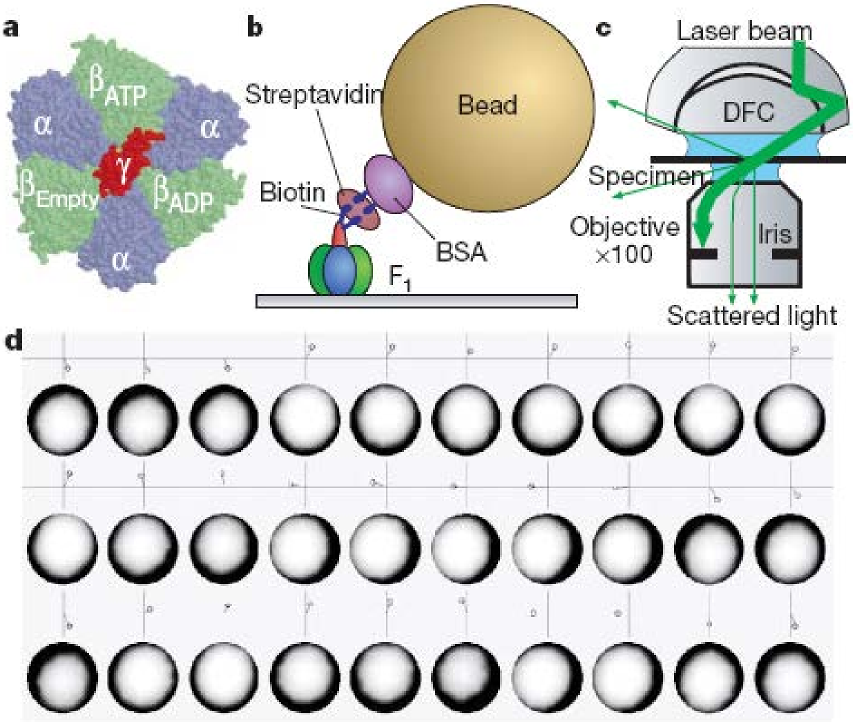

Figure 4. Observation of F_1 rotation via a 40-nm gold bead attached to the γ-subunit (a) Atomic structure of F_1-ATPase viewed from the F_o side (top in b). b, Side view of the observation system. The 40-nm bead gave a large enough optical signal that warranted a sub millisecond resolution; but the bead was small enough not to impede the rotation via viscous drag. c, Laser dark-field microscopy for observation of gold beads. Only light scattered by the beads exited the objective and was detected. DFC, dark-field condenser. d, Sequential images of a rotating bead at 2 mM ATP. Images are trimmed in circles (diameter 370 nm) to aid identification of the bead position; centroid positions are shown above the images at 100X magnification. The interval between images is 0.5 ms. (Taken from (Yasuda, Noji et al. 2001))

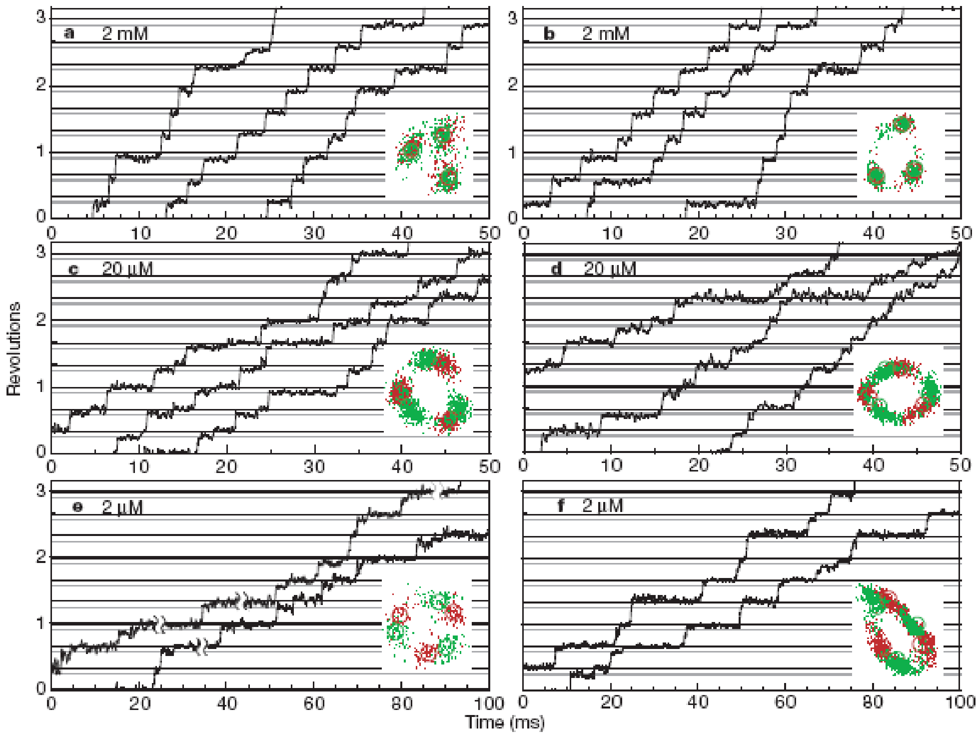

Figure 5. Unfiltered time courses of stepping rotation of 40-nm beads at varying [ATP]. a, b, 2 mM; c, d, 20mM; e, f, 2 mM [ATP]. All curves in a panel are continuous; later curves are shifted, to save space. Grey horizontal lines are placed 30° below black lines. In e, some of the long dwells are cut short. Insets, positions of a bead within 0.25±0.5 ms before (red) and after (green) the main (90° or 120°) steps; runs lasting 0.5 s (2 mM) or 2 s (2mM and 20mM) were analyzed. Circles indicate projection of 0° and 90° dwell points on an obliquely situated circular trajectory that best fit the data. Angles in the time courses are those on the oblique circle. (Taken from (Yasuda, Noji et al. 2001))

Recently, measurements of unprecedented resolution of rotation (Spetzler, York et al. 2006) were observed by recording light scattered from gold nanorods attached to the γ-subunit of the *E. coli* F_1-ATPase (**Figure 6**). Torque was then calculated by measuring the velocity during the power stroke, and through direct measurements of drag, resulted in values as high as 63 ± 8 pN nm (Spetzler, York et al. 2006; Hornung, Ishmukhametov et al. 2008). Less precise experiments estimated torque for F_1 to be 74 ± 20 pN nm using optical clamps (Pilizota, Bilyard et al. 2007), which confirms that the earlier estimated were low.

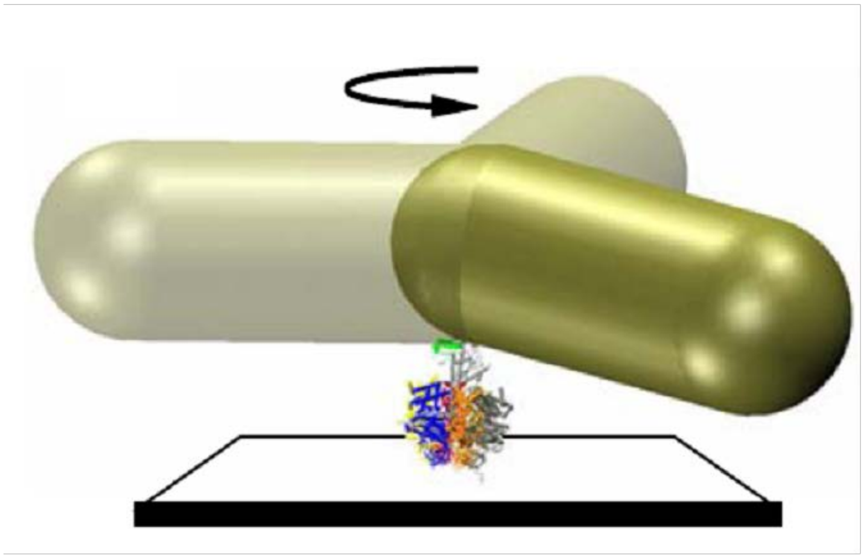

Figure 6. Schematic of F_1-ATPase and a gold nanorod used to determine the torque generated by the enzyme.

Mechanism of the F_1 ATP Synthase

Alternating Site Mechanism of F_1

Each $\alpha\beta$ heterodimer from the hexameric ring of the F_1 ATPase forms a catalytic site that functions cooperatively via an alternating site mechanism in which the binding of ATP to one site prompts release of product in an adjacent site (Boyer 1975). The binding of ATP and release of products depend upon which of three unique binding affinities that each catalytic site adopts; tight, loose, or open. Rotation of the γ subunit occurs when ATP is bound to the open site which then transitions to the loose binding conformation. The loose site then becomes tight, at which point hydrolysis occurs since the tight site has the same affinity for ATP and ADP. Upon binding of ATP to the open site, ADP is released from the tight site. This sequence of substrate binding, hydrolysis, and product release is shown in **Figure 7**.

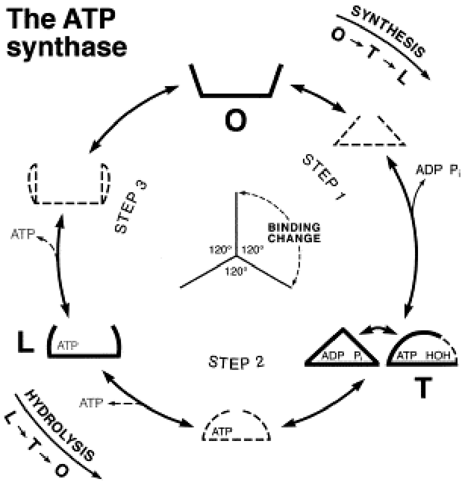

Figure 7: The Binding Change Mechanism. Conformations assumed by one catalytic site of the ATP synthase during synthesis or hydrolysis of ATP during one complete rotation of the γ subunit in 120° steps. The sites are designated as O (open), T (tight) or L (loose), and are related to forms designated as β_E, β_D, or β_T in the Walker structure. Tightness of ATP binding is indicated by the degree of openness of the depicted sites. Intermediate forms during a 120° binding change event are indicated with lighter dashed lines. Forms with some curved lines preferentially bind ATP and those with all straight lines preferentially bind ADP and P_i. The sequence of conformational events during ATP synthesis or hydrolysis occurs is shown. Appropriate arrows indicate reversible substrate binding or release for rapid bisite catalysis. Dashed arrows and dotted ATP indicate that whether ATP is released primarily from the L or the O form during rapid synthesis is not known. A dashed portion of the T site indicates that H_2O formed when ATP is made interchanges readily with the medium water (Boyer 2000).

This mechanism was determined from measurements of the binding affinities of various nucleotides to the three catalytic sites, and from conformational differences in the three catalytic sites as observed in crystal structures. Examination of the three catalytic sites from the first F_1 crystal structure revealed that the nonhydrolyzable ATP analog AMPPNP was bound in what is referred to as the β_{TP} site, ADP in the β_{DP} site, and no nucleotide was bound to the β_E site. The conformations of these sites are all different, with the largest difference seen between the β_E site and the other two. This is due to the β subunit helical domain containing the DELSEED sequence of residues being observed in an open conformation that had a deviation of 30°, versus the closed confirmation seen in the other two sites.

Affinity for nucleotide for the three catalytic sites has been determined to different by several orders of magnitude. Measurements that determined the dissociation constants for each catalytic site were made using the βY331W mutant in *E. coli* F_1 (Weber, Wilke-Mounts et al. 1993). F_1 enzyme that was fully depleted of nucleotides, was monitored for successive quenching of tryptophan fluorescence as each site filled with nucleotide when added in increasing amounts. Quenching was due to masking of fluorescence from π–π bonding of the nucleotide with the tryptophan residue (Shimabukuro, Yasuda et al. 2003).

A modified version of this alternating site mechanism was proposed (**Figure 8**) in which all three sites become occupied once ATP binds

(Weber and Senior 1997). This mechanism labels the three sites according to their nucleotide affinities of high (H), medium, (M) or low (L). The catalytic cycle begins when ATP binds to the low affinity site, which causes the other two sites to alter their binding affinities (M → L, L → H, H → M). Hydrolysis of ATP in the high affinity site produces ADP and Pi as products which are released upon conformational change to the medium binding affinity state. Product release then induces the medium site to become a low affinity site once again, resetting the system.

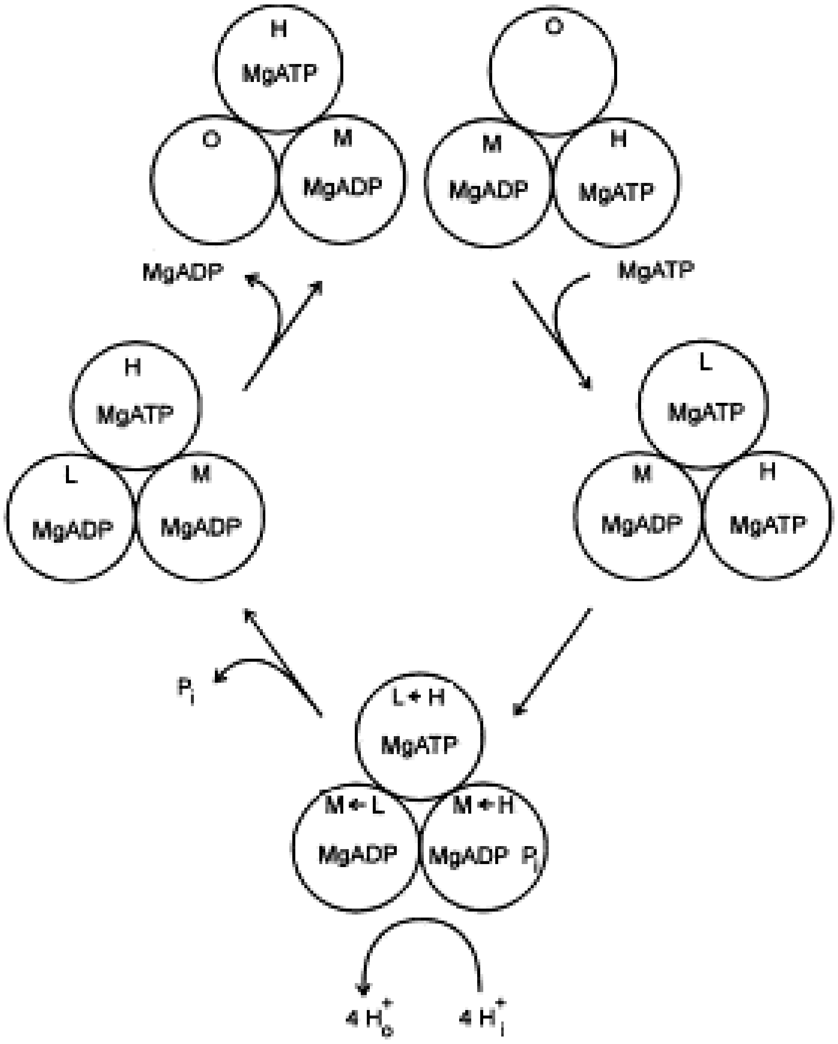

Figure 8 Tri-site Catalysis Model. Conformations of each of the β catalytic subunits that occur during one catalytic cycle of the enzyme with all the catalytic sites in a ‘closed’ conformation with nucleotide bound and where the time that the open conformation exists is negligible. Taken from (Weber and Senior 1997).

The Binding Zipper Model

The Binding Zipper model proposes that ATP-binding-induced rotation of the γ subunit is powered by the gradual closing of the N-terminal helical domain of the β-subunit (**Figure 9**). As this domain draws to closed position, it acts as a lever arm that pushes against the γ-subunit similar to a cam shaft for approximately 90° of rotation that ends upon formation of the catalytic dwell. To explain the energy source for the 30° of rotation subsequent to ATP hydrolysis during the catalytic dwell, elastic energy stored in the closed lever arm conformation of the β–subunit is relaxed upon Pi release. Consequently, 120° of γ-subunit rotation requires the binding of substrate to one site, and elastic recoil in another such that rotation occurs in two separate steps.

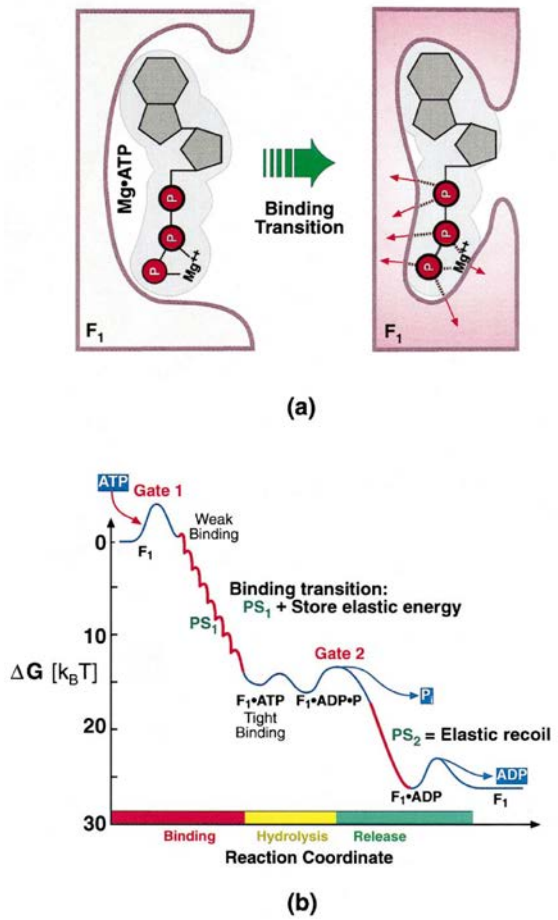

Figure 9. Modeling the power stroke. (a) The Binding Zipper: ATP binds to the catalytic site by a rapid thermal `zippering' of hydrogen bonds. The closing of the site around the nucleotide creates constant torque about the hinge point in β, causing the upper portion of β to rotate with respect to the lower portion. (b) Free energy diagram for the hydrolysis cycle. The second drop reflects release of elastic strain energy stored in β during nucleotide binding. There are two power strokes: the primary power stroke (PS1) is driven by the Binding Zipper, and the secondary powerstroke (PS2) is driven by the elastic recoil of the passive spring. Taken from (Oster and Wang 2000).

The Gamma Dictator Model

The hypothesis that the rotational position of the γ-subunit in relationship to the $(\alpha\beta)_3$ ring dictates the steps of hydrolysis, has been referred to as the Gamma-Dictator model. This was deduced from single molecule experiments where a magnetic particle was attached to the foot of the γ-subunit and the rotational position controlled through the influence of an external magnetic field, so that the position where product is released could be determined (Adachi, Oiwa et al. 2007). It was concluded that upon phosphate release, rotation was initiated and the ADP was released between 30°-40° of rotation afterward.

Application of a magnetic force to drive the rotation of the γ-subunit limits the velocity of the power stroke and therefore encumbers the rotation. Because the force applied was constant, it changed the rate limiting step of the reaction as it was forced to rotate during the catalytic dwell, when rotation is normally dormant. Catalytic site occupancy as measured by tryptophan fluorescence quenching produced results (Nadanaciva, Weber et al. 2000; Weber and Senior 2000; Weber and Senior 2004) contrary to those using a magnetic bead (Adachi, Oiwa et al. 2007), but it was suggested (Senior 2007) that interactions with the γ-subunit are inducing changes that do not normally occur under circumstances in which the rotation is not forced. Single molecule experiments have primarily attached probes for visualizing rotation to the foot domain of the γ-subunit (Sabbert, Engelbrecht et al. 1996; Noji, Yasuda et al. 1997; Omote, Sambonmatsu et al. 1999; Spetzler, York et al. 2006; Spetzler, Ishmukhametov et al. 2009), and therefore measurements reflect the movement of only this domain. Forced restriction in linear motors has been shown to alter the order of substrate binding and the release of products (Spudich 2006), and may also affect F_1 in a similar way.

Dissertation Introduction

The velocity of rotation of the F_1-ATPase was directly observed by microscopy in Chapter 2, after F_1 was mounted on a slide and a visible probe was attached to the γ subunit. Rotation of the γ subunit occurs in discrete 120° steps, each of which is associated with hydrolysis of an ATP molecule (Futai, Omote et al. 1995; Junge, Sabbert et al. 1996; Noji, Yasuda et al. 1997). The torque generated by the molecule is dependent upon the strength of the power stroke associated with each hydrolysis event. The power stroke is dependent upon the velocity of the γ subunit when it rotates. At saturating ATP conditions, the velocity is determined by the transition time; i.e. the time required for γ to move from one dwell location to the next. By measuring the number of rotations per second as a function of the length of an actin filament (200-3000 μm) the first torque calculations of 40 pN nm were obtained by estimating the drag based upon the length of the probe (Noji, Yasuda et al. 1997). A torque value of 50 pN nm was calculated by estimating the drag from the curvature of an actin filament induced by the rotation of the γ-subunit (Panke, Cherepanov et al. 2001). This torque estimate was superior to previous attempts since the torque of F_1 is balanced by the elastic recoil of a bent actin filament which, unlike drag, is a conservative force. Similar values were obtained using video imaging systems to measure the rotation of an F_1-ATPase labeled with a gold nanosphere (Yasuda, Noji et al. 1998).

Limitations of the temporal resolution of these methods resulted in using the number of revolutions per second to approximate rotational velocity (Noji, Yasuda et al. 1997; Yasuda, Noji et al. 1998). This method failed to account for the fact that the motor spends most of the time in a state where γ is not rotating. The number of rotations per second gives an average velocity which is the integral of all the instantaneous velocities that occur during one 360° rotation. When the motor is in a dwell state it has a velocity of zero. Thus, the velocity of the power stroke is faster than the average value resulting in an underestimation of the torque. A related, but less significant, problem occurs with the actin filament curvature approach. Since the filament relaxes during each dwell, the net curvature is less than what would occur if the motor rotated continuously.

Recently, the rotational events of the γ-subunit were measured with a time resolution of 5 μs using gold nanorods as probes such that the speed of rotation could be distinguished from the dwell time (Spetzler, York et al. 2006). Based on these measurements, values of torque as high as 61 pN nm were calculated by estimating the drag (Spetzler, York et al.

2006). However, the accuracy of the torque calculations was limited by the ability to estimate the drag on the gold nanorod. Several different models have been proposed to estimate the drag on the probe based on the size, shape, viscosity, and binding orientation (Noji, Yasuda et al. 1997; Soong, Bachand et al. 2000; Yasuda, Noji et al. 2001; Spetzler, York et al. 2006).

In Chapter 2, the torque generated by the power stroke of F1-ATPase as a function of the load on the enzyme was directly determined. Measurements of the velocity were obtained using a 5 μs time resolution and by directly measuring the drag. This result was compared to values of torque calculated using four different drag models. Rotational assays were performed as described recently (Spetzler, York et al. 2006; York, Spetzler et al. 2007) as a function of polyethylene glycol (PEG-400) which increases the viscosity of the reaction medium. Although the γ-subunit was able to rotate with a 20-fold increase in viscosity, the transition time increased from 0.4 ms to 5.26 ms and the torque remained 63±8 pN nm, independent of the load on the enzyme. However, it is important to note that in the determination of this value for torque, it was assumed that the velocity of the 120° power stroke was constant between catalytic dwells.

Chapter 3 directly examines the rotational velocity as a function of rotational position as the γ-subunit rotates during the power stroke. Previous work has determined the torque using a number of various methods including; the number of revolutions of a gold bead (Yasuda, Noji et al. 2001), or of an actin filament (Noji, Yasuda et al. 1997; Cherepanov and Junge 2001), fluctuation theorem (Watanabe, Hayashi et al. 2011), and the transition time of a gold nanorod (the time it takes for a gold nanorod to rotate 90°) (Spetzler, York et al. 2006; Spetzler, Ishmukhametov et al. 2009). These approaches however, rely on the hypothesis that F_1 rotates at a constant velocity based on single molecule results (Noji, Yasuda et al. 1997) showing that the F_1 is nearly 100% efficient (Oster and Wang 2000).

If the rotational velocity were not constant then the efficiency would necessarily be less than 100%. Based on this premise, it was proposed that ATP-binding-induced rotation of the γ subunit is powered by the gradual closing of the N-terminal helical domain of the β-subunit. As this domain draws to closed position, it acts as a lever arm that pushes against the γ-subunit similar to a cam shaft for approximately 80° of rotation that ends upon formation of the catalytic dwell. To explain the energy source for the 40° of rotation subsequent to ATP hydrolysis during the catalytic dwell, elastic energy stored in the closed lever arm conformation of the β-subunit is relaxed upon Pi release. Consequently, 120° of γ-subunit rotation requires the binding of substrate to one site, and release of elastic energy in another such that rotation occurs in two separate steps.

In Chapter 3, it has been clearly shown, through high fidelity observations of the rotational position of the γ-subunit as it traverses a power stroke, that the rotational velocity is not constant, but has an initial (I) acceleration phase during the first 15° from the end of the catalytic dwell, followed by a slow (S) acceleration phase that occurs during ATP binding and ADP release. At ~60°, the SP transitions to a fast (F) acceleration phase that contains an interim deceleration (ID) phase between 75° - 82°. High ADP concentrations decreased the velocity of the slow phase proportional to the increased presence of ‘ADP-release’ dwells but also decreased the velocity of the fast phase proportional to the change in free energy derived from the change in chemical equilibrium with ATP and Pi. The rotational velocities were compared using purine nucleotides that differed in their binding affinities at the catalytic sites. Although the decreased affinity for ITP caused an expected 10% increase in ITP-binding dwells, the ITP- dependent rotational velocity decreased by 40% during the slow acceleration phase. Since torque is proportional to the velocity times the drag, this is the first direct evidence that nucleotide binding contributes to the generation of torque on the F_1-ATPase molecular motor.

Chapter 4 examines the effects of mutations on the velocity of γ-subunit rotation using the gold nanorod-based single molecule assay that provides detailed resolution of the power strokes. In Chapter 3, single molecule measurements of *E. coli* F_1-ATPase rotation resolved the rotational position and velocity with high precision, and revealed initial (I), slow (S), and fast (F) acceleration phases of rotational velocity where the latter included an interim deceleration (ID) phase. However, except for the nucleotide binding and release steps, the association of these phases with conformational changes of F_1 is currently not understood. Chapter 4 identifies for the first time single-site mutations that can affect the velocity of specific phases of γ-subunit rotation. Some residues, including those in the region of the γ-subunit coiled-coil previously considered not to contribute to rotation, were found to change the velocity by as much as 50% from that in the wild type. Mutations βD372V and γK9I were found to increase the velocity specifically during the F phase, while γK9I also increased the depth of the ID phase. The conversion between S and F phases was specifically affected by γQ269L. While γT273D, βD305E, and αR283Q decreased the velocity of all phases, the decreases in velocity due to βD302T, γR268L and γT82A were confined to the I and S phases. The correlations between the structural locations of these mutations and the phases of rotation they affect provide new insight into the molecular basis for the conformational changes of the protein that contribute to rotation of the γ-subunit.

In all available crystal structures of F_1 ATPase the γ-subunit coiled-coil is attached via electrostatic interactions to residues located on the β-subunit of the empty catalytic site known as “the catch loop”. Mutations to residues on the β and γ-subunits that form this catch have dramatic effects on catalytic function, and have been postulated to be involved in an Escapement Mechanism that permits rotation only upon substrate binding to the empty catalytic site (Greene and Frasch 2003). The electrostatic interactions in the Catch include residues βD305 and βD302 of the empty catalytic site and residues γQ269, γT273, and γR268 on the γ-subunit coiled-coil. In the other two catalytic sites where nucleotide is bound, the catch loop residues form salt bridges with αR283 on the α subunit of the αβ heterodimer that comprise those catalytic sites (Boltz and Frasch 2006). Consequently, sometime after ATP binds to the empty site, the β subunit catch loop residues must switch from the γ-subunit to the α subunit of that catalytic site. Conversely, ADP release at the adjacent catalytic site must dissociate the electrostatic interactions between neighboring α and β so that the γ subunit can bind to the next catch loop at the conclusion of that rotational event.

Recently, it was shown that the binding of ATP to the empty catalytic site provides the energy required for the 120° power stroke of F_1 (Chapter 3). To explain why the low affinity substrate ITP decreased the velocity during the 40° of rotation that follows the catalytic dwell but not the 80° of rotation immediately following substrate binding, it was proposed that the binding energy only needs to exceed a minimal threshold value to initiate rotation prior to the catalytic dwell. The remaining binding energy was thought to be stored as elastic energy during the catalytic dwell that propels the remaining 40° of rotation (Oster and Wang 2000). The binding of ATP is believed to induce the movement of the β-subunit helical domain containing the DELSEED motif to move from an open to a closed position.

This movement of the DELSEED-containing domain is thought to push on the on the γ-subunit as a lever arm on a camshaft to induce rotation. It was shown that when the α-helical arm adjacent to the DELSEED was shortened, torque was reduced significantly, yet torque was not affected by the removing the negative charges in the DELSEED region (Hara, Noji et al. 2000; Usukura, Suzuki et al. 2012). It was concluded that the γ-subunit coiled-coil does not contribute to the generation of torque based on experiments that showed that rotation was still observed after most of the coiled-coil had been deleted (Furuike, Hossain et al. 2008).

Chapter 2

DETERMINATION OF TORQUE GENERATION FROM THE POWER STROKE OF *ESCHERICIA COLI* F_1-ATPASE

Abstract

The torque generated by the power stroke of *Escherichia coli* F_1-ATPase was determined as a function of the load from measurements of the velocity of the γ-subunit obtained using a 5 μs time resolution and direct measurements of the drag from 45 to 91 nm gold nanorods. This result was compared to values of torque calculated using four different drag models. Although the γ-subunit was able to rotate with a 20 fold increase in viscosity, the transition time decreased from 0.4 ms to 5.26 ms. The torque was measured to be 63±8 pN nm, independent of the load on the enzyme.

Introduction

The F_1F_o ATP synthase is required for energy conversion in almost all living organisms. It is composed of two complexes, the F_1-ATPase (*Escherichia coli* subunits α, β, γ, δ and ε) that is peripheral to bioenergetic membranes, and F_o (*E. coli* subunits a, b, and c) that is an integral membrane complex. In F_1, a ring of three αβ subunit heterodimers surrounds the γ subunit coiled-coil domain while the γ subunit 'foot' domain anchors F_1 to the c_{10}-subunit ring of *E. coli* F_o (Abrahams, Leslie et al. 1994; Stock, Leslie et al. 1999). Functionally F_1F_o is a rotary machine, where rotor subunits γ, ε and c rotate relative to the stator composed of subunits a, b, α, β and δ (Noji, Yasuda et al. 1997; Borsch, Turina et al. 1998).

Each $\alpha\beta$ heterodimer contains a site that catalyzes ATP synthesis/hydrolysis. The synthesis of ATP is driven by $\Delta\mu_{H+}$ driven rotation the c-ring of F_o that forces conformational changes in the $(\alpha\beta)_3$ ring (Borsch, Turina et al. 1998). Conversely, ATP hydrolysis can drive γ subunit rotation in the opposite direction (Noji, Yasuda et al. 1997). The three catalytic sites operate in an alternating site mechanism in which binding of ATP to the empty catalytic site induces release of ADP and phosphate from an adjacent site concurrent with rotation (O'Neal and Boyer 1984).

Direct observation of ATPase-driven rotation by microscopy is possible when F_1 is mounted on a slide and a visible probe is attached to the γ subunit. Rotation of the γ subunit occurs in discrete 120° steps, each of which is associated with hydrolysis of an ATP molecule (Futai, Omote et al. 1995; Junge, Sabbert et al. 1996; Noji, Yasuda et al. 1997). The torque generated by the molecule is dependent upon the strength of the power stroke associated with each hydrolysis event. The power stroke is dependent upon the velocity of the γ subunit when it rotates. At saturating ATP conditions, the velocity is determined by the transition time; i.e. the time required for γ to move from one dwell location to the next. By measuring the number of rotations per second as a function of the length of an actin filament (200-3000 μm) the first torque calculations of 40 pN nm were obtained by estimating the drag based upon the length of the probe (Noji, Yasuda et al. 1997). A torque value of 50 pN nm was calculated by estimating the drag from the curvature of an actin filament induced by the rotation of the γ-subunit (Panke, Cherepanov et al. 2001). This torque estimate was superior to previous attempts since the torque of F_1 is balanced by the elastic recoil of a bent actin filament which, unlike drag, is a conservative force. Similar values were obtained using video imaging systems to measure the rotation of an F_1-ATPase labeled with a gold nanosphere (Yasuda, Noji et al. 1998).

Limitations of the temporal resolution of these methods resulted in using the number of revolutions per second to approximate rotational velocity (Noji, Yasuda et al. 1997; Yasuda, Noji et al. 1998). This method failed to account for the fact that the motor spends most of the time in a state where γ is not rotating. The number of rotations per second gives an average velocity which is the integral of all the instantaneous velocities that occur during one 360° rotation. When the motor is in a dwell state it has a velocity of zero. Thus, the velocity of the power stroke is faster than the average value resulting in an underestimation of the torque. A related, but less significant, problem occurs with the actin filament curvature approach. Since the filament relaxes during each dwell, the net curvature is less than what would occur if the motor rotated continuously.

Recently, the rotational events of the γ-subunit were measured with a time resolution of 5 μs using gold nanorods as probes such that the speed of rotation could be distinguished from the dwell time (Spetzler, York et al. 2006). Based on these measurements, values of torque as high as 61 pN nm were calculated by estimating the drag (Spetzler, York et al. 2006). However, the accuracy of the torque calculations was limited by the ability to estimate the drag on the gold nanorod. Several different models have been proposed to estimate the drag on the probe based on the size, shape, viscosity, and binding orientation (Noji, Yasuda et al. 1997; Soong, Bachand et al. 2000; Yasuda, Noji et al. 2001; Spetzler, York et al. 2006).

The torque generated by the power stroke of F1-ATPase as a function of the load on the enzyme has now been determined as presented here. Measurements of the velocity were obtained using a 5 μs time resolution and directly measuring the drag. This result was compared to values of torque calculated using four different drag models. Rotational assays were performed as described recently (Spetzler, York et al. 2006; York, Spetzler et al. 2007) as a function of polyethylene glycol (PEG-400) which increases the viscosity of the reaction medium. Although the γ-subunit was able to rotate with a 20× increase in viscosity, the transition time decreased from 0.4 ms to 5.26 ms and the torque remained 63±8 pN nm, independent of the load on the enzyme.

Results

Figure 10 shows the measured viscosity of the assay buffer as a function of the percentage (vol/vol) of PEG 400. These data were used to calculate the shear stress as a function of the shear rate (**Figure 11**). The linear dependence between these parameters indicates that the assay buffer containing PEG 400 behaves as a Newtonian fluid. Thus, PEG 400 molecules are too small to be pulled along by the rotating nanorod, and do not make secondary nonlinear contributions to the drag.

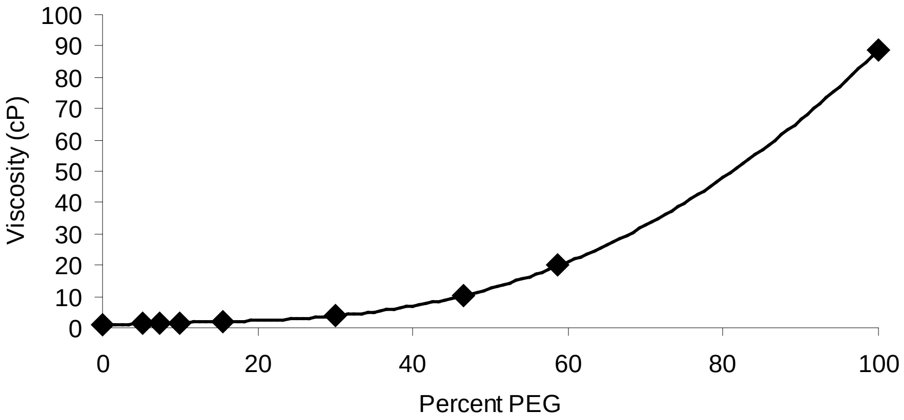

Figure 10. Viscosity of the assay buffer as a function of percent PEG-400 added. The viscosity of the buffer used to make single molecule rotation measurements (Rotation Buffer (50 mM Tris–Cl/pH 8.0, 10 mM KCl)) as a function of its percent composition of PEG 400 (vol/vol). The measurements were made using a Brookfield DVE viscometer with a UL adapter at 28 °C.

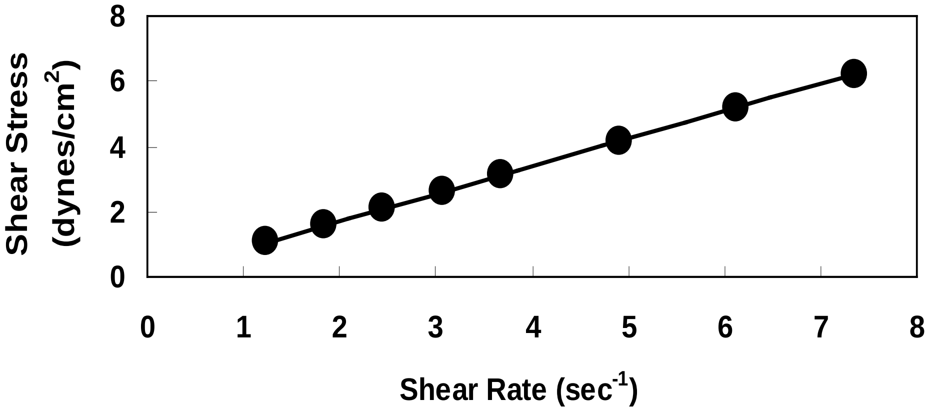

Figure 11. Shear stress as a function of the shear rate. The shear stress as a function of the shear rate of the Rotation Buffer containing PEG 400. This was determined by measuring the effect of increasing the velocity on a rotating probe in the Brookfield DV-E viscometer

The drag coefficient was determined directly as described by Hunt et al. (Hunt, Gittes et al. 1994) by measuring the amount of angular change in individual gold nanorods near the surface in the absence of F_1 (**Figure 12**). Nanorods were selected which displayed a color change indicative of rotational movement, and which did not move significantly in the z direction, i.e. remained in focus. The dynamic range of scattered light intensity from a nanorod was measured by rotating the polarizer 360° in 10° increments. The angular change is related to the intensity by:

$$I = A\sin(\phi) + B, \qquad (1)$$

where ϕ is the difference in angle between the plane of polarization and the gold nanorod, *A* is the dynamic range, and *B* is the sum of the background noise level and half the dynamic range. The angular change was used to determine the diffusion constant by:

$$D = \frac{\Delta\phi^2}{2\Delta t}. \qquad (2)$$

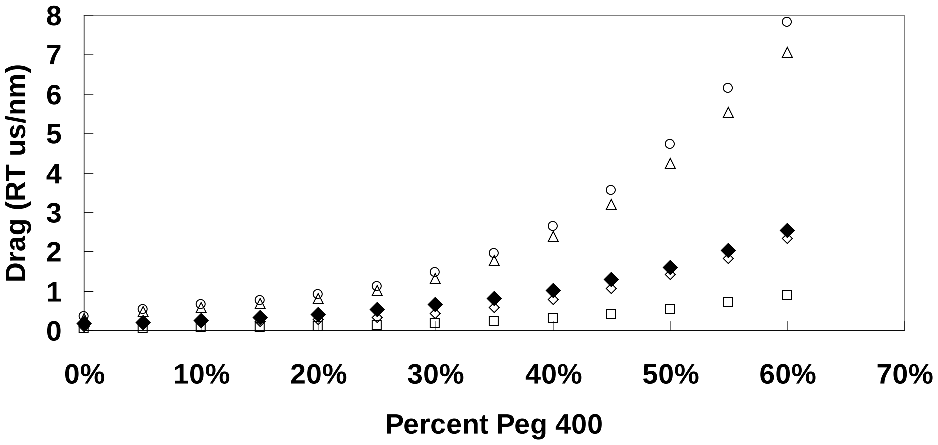

Figure 12. Drag coefficient as a function of viscosity. The solid symbol (♦) is the experimental value, while the open symbols are the theoretical values for a rod (Δ), a sphere (○), a filament (□), and a propeller (◊) calculated from Eqs. (4)–(7).

The change in the angle of gold nanorods near the surface was measured at data acquisition rates from 10 to 200 kHz in 10 kHz increments, which made the determination of the diffusion constant, *D*, independent of time artifacts. Using Einstein's relation (Eq. 3) the drag coefficient, Γ, was determined from the diffusion coefficient,

$$\Gamma = \frac{k_B T}{D} \,. \qquad (3)$$

Figure 12 also shows a comparison of the various drag values calculated from models that assume that the gold nanorod has the properties of a propeller (Soong, Bachand et al. 2000), a nanosphere (Yasuda, Noji et al. 2001), a rod (Spetzler, York et al. 2006), and a long filament (Noji, Yasuda et al. 1997). Based on the model for a propeller, the drag force is approximated by Eq. 4:

$$\Gamma = \frac{4\pi\mu(L_1^3 + L_2^3)}{3\cosh^{-1}(h/r)} \,, \qquad (4)$$

where L_1 and L_2 are the lengths of the propeller extending from the rotational axis, *r* is the radius of the rod, μ is the viscosity of the medium, and *h* is the height of the cylinder axis relative to the surface. The height of the propeller was estimated to be 17 nm based on the dimensions of F_1 and avidin from crystal structures (Al-Shawi, Ketchum et al. 1997; Ketchum, Al-Shawi et al. 1998). When *h* is small, most energy dissipation is believed to occur in the gap between the propeller and the surface (Al-Shawi and Nakamoto 1997).

The models used to estimate the drag force generated by a nanoscale rod, a nanosphere, and a filament are described by Eqs. 5-7, respectively:

$$\Gamma = 8\pi\mu r^3 \tag{5}$$

$$\Gamma = 16\pi\mu r^3 + 12\pi\mu r L_1^2 + 12\pi\mu r L_2^2 \tag{6}$$

$$\Gamma = \frac{4\pi\mu(L_1^3 + L_2^3)}{3\ln(\frac{L}{2r} - 0.447)} \tag{7}$$

The results in Figure 12 show that the propeller model provides the closest approximation to the experimental data. Other models estimated the drag to be as much as 4-fold higher than the measured value at 60% PEG.

To determine the velocity of the power stroke generated during F_1-ATPase-driven rotation, transition times were measured by tracking a 91×45 nm gold nanorod, through 90° of a rotation as described in Spetzler et al. (Spetzler, York et al. 2006), and the velocity plotted as a function of the viscosity (**Figure 13**).

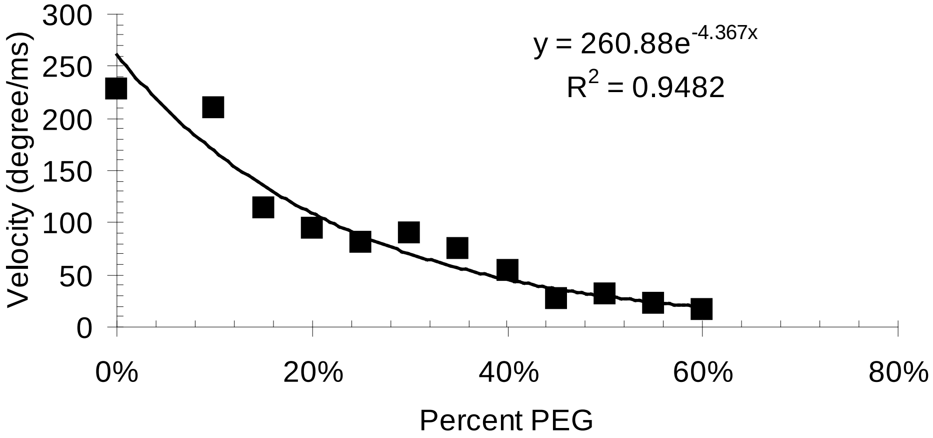

Figure 13. The velocity of the γ-subunit power stroke as a function of viscosity.

The velocity of the transition decreased with increasing viscosity. **Figure 14** shows the torque values calculated from the drag and the velocity by:

$$T = \Gamma w, \tag{8}$$

where w is the angular velocity as a function of viscosity. The value calculated from the direct measurements of the drag was 63 pN-nm ± 8 nm, and was independent of the load applied to the motor. The estimated value for the torque based on the propeller model (~55 pN nm) was similar to the measured result. However, the estimated values based on the sphere, the rod, and filament models were substantially different, indicating that the models provide poor estimates of the drag on the nanorod. For the models of the sphere and rod, the torque values were greater than the maximum amount of energy available to the enzyme in the absence of PEG 400 and increased linearly as a function of the viscosity violating the second law of thermodynamics.

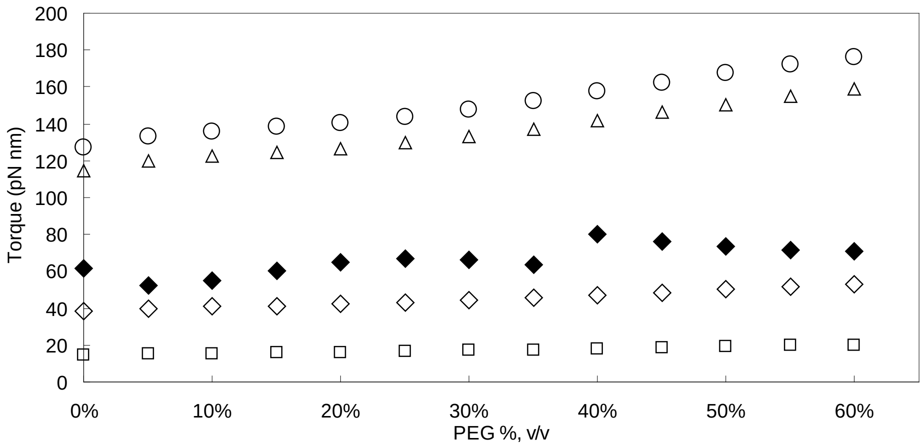

Figure 14. The torque generated by the F1 as a function of the load on the motor. The solid symbol (♦) is the experimental value, while the open symbols are the theoretical values for a rod (Δ), a sphere (○), a filament (□), and a propeller (◊) calculated from Eqs. (4)–(7).

DISCUSSION

The torque value obtained from measured values for both the velocity and the drag reported here was 63 ± 8 pN nm. As the load increased, there was a corresponding decrease in the velocity indicating that the torque was constant over the range of viscous conditions examined. This value is consistent with the highest measured values for the torque generated by the F_1-ATPase (Spetzler, York et al. 2006), but is significantly higher than values obtained elsewhere (Noji, Yasuda et al. 1997; Yasuda, Noji et al. 1998; Panke, Cherepanov et al. 2001). Independent evidence that supports the torque reported here can be derived from measurements of the H+/ATP ratio of proton transport-coupled ATP synthesis and hydrolysis catalyzed by liposomes that contain chloroplast F_oF_1 (Fischer, Graber et al. 2000). In this study, the rates of ATP synthesis and hydrolysis were measured with the luciferin/luciferase assay after an acid-base transition at various [ATP]/([ADP][Pi]) ratios as a function of ΔpH. By determining the point at which the free energy from the [ATP]/([ADP][Pi]) ratio was in equilibrium with the transmembrane electrochemical potential difference such that there was no net synthesis or hydrolysis of ATP, H+/ATP ratios of 3.9–4.0 and standard Gibbs free energies of ATP synthesis of 37±2 kJ/mol and 36±3 kJ/mol at pH 8.45 and 8.05, respectively, were obtained. If the equilibrium point (when there is no net ATP synthesis or hydrolysis) occurs when $\Delta\mu_{H+}$ is equivalent and opposite to the force generated by F1-ATPase hydrolysis, then the Gibbs free energy is equal to the energy used to generate torque. Based on this assumption the chloroplast F1-ATPase generates 61.4±3 pN nm and 59.8±5 pN nm of torque at pH 8.45 and 8.05, respectively. These values are comparable to those reported here for the torque generated by E. coli F1-ATPase.

Previous estimates of the torque F_1 produces against the friction of the viscous medium range from 40 to 50 pN nm (Yasuda, Noji et al. 1998; Panke, Cherepanov et al. 2001). From these estimates, it was calculated that the work F_1 can do in a 120° step is about 80–90 pN nm or ~20 kBT, calculated as 40–44 pN nm times $(2/3)\pi$ radians. This is close to the physiological $|\Delta G|$ for ATP hydrolysis, and was interpreted to mean that the efficiency of the enzyme to convert chemical energy into mechanical energy is nearly 100% under physiological conditions (Kinosita, Yasuda et al. 2000). Since the experiments were not performed under physiological conditions, not all sources of energy were taken into consideration, thus, the efficiency would be lower, consistent with predictions made by Karplus et al. (Karplus, Gao et al. 2005).

The results presented here show that the enzyme is capable of doing more work than would be predicted by the amount of free energy under physiological conditions suggesting that there are additional sources of energy. Gao et al. (2003) and Yang et al. (2003) calculated that the differential in binding constants could yield ~80 PN nm worth of work using cellular concentrations of 3 mM ATP, 0.4 Mm ADP, and 6 mM Pi. In the experiments reported here, there were only trace amounts, < 1%, of ADP and Pi in the 1 mM ATP solution used to induce rotation allowing as much as 60 pN nm of free energy to be generated from the concentration gradient between [ATP]/([ADP][Pi]). Adding the energy from binding to that from the concentration gradient yields a net amount of 140 pN nm of free energy. Based upon the data presented here, the work done by the enzyme is ~130 pN nm. The energy available from substrate binding and subsequent product release, and the concentration gradient yield a net amount of 140 pN nm of free energy, suggesting that the enzyme is at least 90% efficient.

Chapter 3

ANATOMY OF F_1-ATPASE POWERED ROTATION

ABTRACT

Due to poor resolution of single molecule approaches, it has not been possible to resolve the speed and position of the γ-subunit of the F_1-ATPase as it rotates during a power stroke, and thus, was assumed to rotate at a constant velocity. Single molecule experiments are presented here that measure light scattered from gold nanorods attached to the γ-subunit of the motor that provide unprecedented resolution of rotational position as a function of time. Analysis of these results clearly show that the rotational velocity is not constant during a power stroke, but has an initial (I) acceleration phase during the first 15° from the end of the catalytic dwell, followed by a slow (S) acceleration phase that occurs during ATP binding and ADP release. At ~60°, the S transitions to a fast (F) acceleration phase that contains an interim (ID) deceleration phase between 75° - 82°. High ADP concentrations decreased the velocity of the slow phase proportional to the increased presence of 'ADP-release' dwells but also decreased the velocity of the fast phase proportional to the change in free energy derived from the change in chemical equilibrium with ATP and PI. The rotational velocities were compared using purine nucleotides that differed in their binding affinities at the catalytic sites. Although the decreased affinity for ITP caused an expected 10% increase in ITP-binding dwells, the ITP- dependent rotational velocity decreased by

40% during the slow acceleration phase. Since torque is proportional to the velocity times the drag, this is the first direct evidence that nucleotide binding contributes to the generation of torque on the F_1-ATPase molecular motor.

INTRODUCTION

The F_oF_1 ATP synthase is responsible for generating the majority of ATP in nearly all living things. It is composed of two rotary molecular motors, F_o and the F_1 ATPase, that rotate in opposite directions and share a common rotation axle comprised of the $\gamma\varepsilon$ subunits in *Escherichia coli* (Stock, Leslie et al. 1999). The integral membrane F_o motor (Jiang, Hermolin et al. 2001), utilizes the energy available in a transmembrane proton gradient to drive clockwise rotation of $\gamma\varepsilon$. Conformational changes caused by the rotation of the γ subunit within the ring of three αβ-subunit heterodimers that form the stator for F_1, catalyze the synthesis of ATP (Boyer 1997). Each $\alpha\beta$-heterodimer of F_1 forms a catalytic site for ATP synthesis. Conversely, hydrolysis of ATP by the peripheral F_1-ATPase can drive the γ subunit to rotate counterclockwise and cause F_o to pump protons against the proton gradient. The F_1-ATPase can be purified from F_o and the membrane where it can be studied as a soluble protein. In the presence of saturating ATP, the γ subunit of purified *E. coli* F_1-ATPase rotates in 120° power strokes (Sabbert, Engelbrecht et al. 1996; Noji, Hasler et al. 1999; Spetzler, York et al. 2006) separated by 8.3ms catalytic dwells comparable to the turnover time of the rate-limiting step of ATP hydrolysis (Spetzler, York et al. 2006; Hornung, Ishmukhametov et al. 2008).

Each $\alpha\beta$ heterodimer forms a catalytic site that functions cooperatively via an alternating site mechanism in which the binding of ATP to one site prompts release of product in an adjacent site (Boyer 1975). In substrate-limiting conditions, single molecule experiments have observed an additional dwell separating 120° of rotation into a 40° and 80° step (Yasuda, Noji et al. 2001). The duration of the dwell prior to the 80° step was sensitive to the concentration of ATP available and is known as ATP Binding dwell, while the dwell that is insensitive to ATP concentration has been labeled the catalytic dwell, and is believed to include the ATP hydrolysis step. Release of Pi from one catalytic site leaves the site vacant and initiates γ–subunit rotation (Adachi, Oiwa et al. 2007; Watanabe, Iino et al. 2010). If ATP has not bound, or if the ADP generated from the prior hydrolysis has not been released from the adjacent site counterclockwise to that where ATP binds, then the 120° power stroke is interrupted by an ATP Binding dwell ~40° from the catalytic dwell (Watanabe, Okuno et al. 2012).

The binding affinities for nucleotides at the three catalytic sites differ by orders of magnitude, and each changes its affinity sequentially as the result of rotation (Weber and Senior 1997). The F_1-ATPase has been proposed to take advantage of the free energy made available by the change in the affinity for nucleotide at each catalytic site (Gao, Yang et al.

2003). Using cellular concentrations for ATP, ADP, and Pi, and the dissociation constants the free energy for each site was calculated. The overall difference in free energy was then determined for each site after the accompanying change in binding affinities (i.e. low to high, etc.) after 120° of rotation. The net free energy was calculated to be approximately equivalent to the free energy released from hydrolysis of one ATP. Two separate binding steps were proposed to provide the energy needed for the energy consuming step of product release. First, the energy gained in the change from low to high binding affinity once ATP binds, and second, free energy gained when ADP and Pi bind to the medium affinity site.

It was concluded that the rotation must have constant torque (Oster and Wang 2000) based on single molecule measurements that show that the F_1 is nearly 100% efficient (Noji, Yasuda et al. 1997). If the rotational velocity were not constant then the efficiency would necessarily be less than 100%. Based on this premise, it was proposed that ATP-binding-induced rotation of the γ subunit is powered by the gradual closing of the N-terminal helical domain of the β-subunit. As this domain draws to closed position, it acts as a lever arm that pushes against the γ-subunit similar to a cam shaft for approximately 80° of rotation that ends upon formation of the catalytic dwell. To explain the energy source for the 40° of rotation subsequent to ATP hydrolysis during the catalytic dwell, elastic energy stored in the closed lever arm conformation of the β–subunit is relaxed upon Pi release. Consequently, 120° of γ-subunit rotation requires the binding of substrate to one site, and hydrolysis and phosphate release in another such that rotation occurs in two separate steps.

Previous work has determined the torque using a number of various methods including; the number of revolutions of a gold bead (Yasuda, Noji et al. 2001), or of an actin filament (Noji, Yasuda et al. 1997; Cherepanov and Junge 2001), fluctuation theorem (Watanabe, Hayashi et al. 2011), and the transition time of a gold nanorod (the time it takes for a gold nanorod to rotate 90°) (Spetzler, York et al. 2006; Spetzler, Ishmukhametov et al. 2009). These approaches however, rely on the hypothesis that F_1 rotates at a constant velocity based on single molecule results (Noji, Yasuda et al. 1997) showing that the F_1 is nearly 100% efficient (Oster and Wang 2000).

Recently a new method was reported that measured light scattered from gold nanorods attached to the γ-subunit of the *E. coli* F_1-ATPase that provide unprecedented resolution of rotational position as a function of time (Spetzler, York et al. 2006; Spetzler, Ishmukhametov et al. 2009). Rotation was observed as sinusoidal changes in the intensity of red light scattered from the nanorod that correlated to the orientation of the long axis of the nanorod relative to the direction of polarization (**Figure 15**). Upon alignment with the plane of polarized light, the gold nanorods scattered a maximum intensity of red light, and a minimum when aligned perpendicularly (Sonnichsen and Alivisatos 2005). Rotation of the γ-subunit was then determined by observing the intensity of red light scattered from a single nanorod attached to the foot of the γ–subunit. Using this approach, the average rotation was measured to occur in 250 μs, such that the *E. coli* F_1-ATPase generated an average torque of ~61 pN nm.

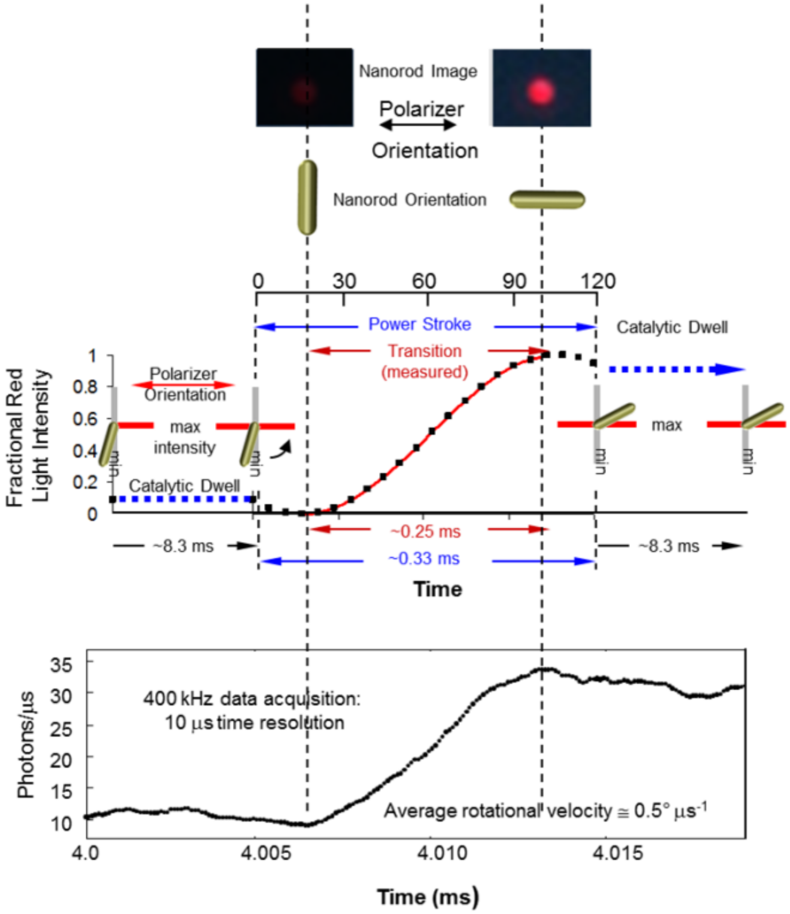

Figure 15. Single molecule measurements of rotation using gold nanorods as a probe. The intensity of the light scattered from the nanorod is proportional to the rotational position of the nanorod in relation to the plane of polarization. A maximum intensity is observed when the nanorod is parallel to the incoming polarized light, and at a minimum when the nanorod is perpendicular. As the foot of the gamma subunit rotates in a counter clockwise direction, the nanorod also rotates, and the intensity of scattered red light increases as the nanorod approaches alignment with the plane of polarized light.

High fidelity observations of the rotational position of the γ-subunit as it traverses a power stroke clearly show that the rotational velocity is not constant, but has an initial (I) acceleration phase during the first 15° from the end of the catalytic dwell, followed by a slow (S) acceleration phase that occurs during ATP binding and ADP release. At ~60°, the SP transitions to a fast (F) acceleration phase that contains an interim deceleration (ID) phase between 75° - 82°. High ADP concentrations decreased the velocity of the slow phase proportional to the increased presence of 'ADP-release' dwells but also decreased the velocity of the fast phase proportional to the change in free energy derived from the change in chemical equilibrium with ATP and PI. The rotational velocities were compared using purine nucleotides that differed in their binding affinities at the catalytic sites. Although the decreased affinity for ITP caused an expected 10% increase in ITP-binding dwells, the ITP-dependent rotational velocity decreased by 40% during the slow acceleration phase. Since torque is proportional to the velocity times the drag, this is the first direct evidence that nucleotide binding contributes to the generation of torque on the F_1-ATPase molecular motor

RESULTS

The most sensitive measure of rotation using gold nanorods occurs during the 90° in which a 120° power stroke passes through a minimum and a maximum of scattered light intensity designated as a transition. **Figure 16A** shows three example transitions collected at 200 KHz after the dynamic range of the intensity of scattered light from the nanorod was maximized. These transitions span a range faster and slower than the average duration of about 0.25 ms for 120° of rotation (Spetzler, York et al. 2006).

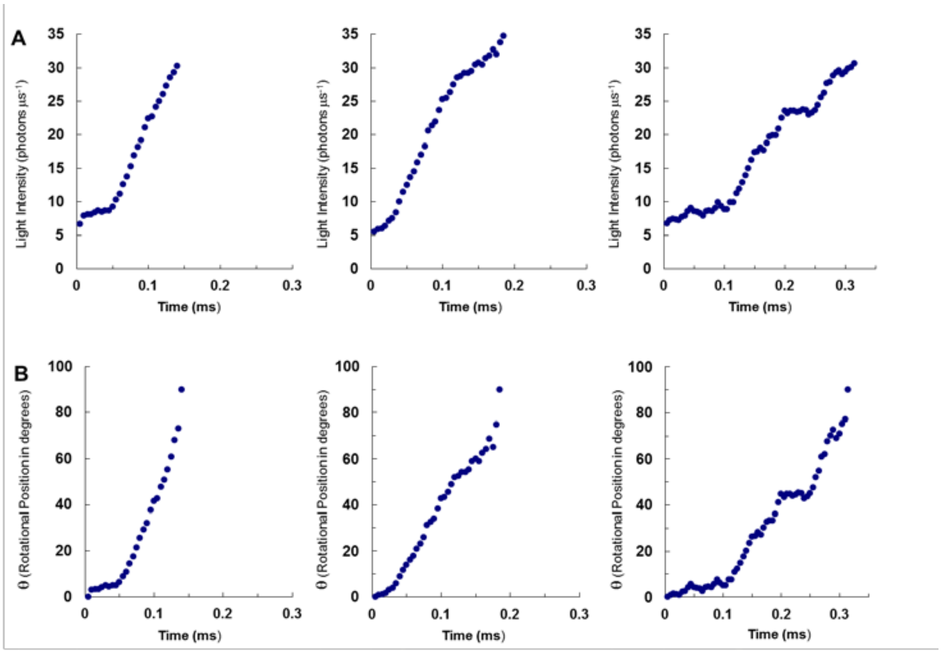

Figure 16. Example Single Transitions of F_1 Power Strokes in the presence of 1 mM Mg^{2+} and 2 mM ATP. (A) Light intensity scattered from a gold nanorod attached to the γ subunit collected at 200kHz as a function of time. The average transition time under these conditions was 0.17 ms. (B) Rotational position of the γ subunit as a function of time calculated from the transitions in (A) using Eq. 1.

In **Figure 16B**, each of the respective transitions was converted to degrees of rotation as a function of time using Eq. 1, where I is the intensity of light scattered from the nanorod.

$$\theta = (\mathrm{asin}\ I)180\pi^{-1} \qquad \text{Eq. 1}$$

It is clear from these example transitions that the rotational velocity is not constant throughout the power stroke. Even though these power strokes occurred at saturating Mg^{2+}-ATP concentrations, occasional short pauses were resolved at this data acquisition speed.

To understand how the velocity of rotation changes as a function of rotational position, the velocity was binned and averaged for every three degrees of rotation. The average velocity of transitions as a function of rotational position from the end of the catalytic dwell is shown in **Figure 17**. Following an Initial (I) Acceleration Phase during the first 10° of rotation, a Slow (S) Acceleration Phase was observed between 10° to 60° of rotation. During the next 30° of rotation a Fast (F) Acceleration Phase occurred that, at its maximum velocity, was about 8 fold of that observed during the slow acceleration phase. Within this fast acceleration phase was a short period of deceleration between 75° and 80° of rotation designated the Interim (ID) Deceleration Phase.

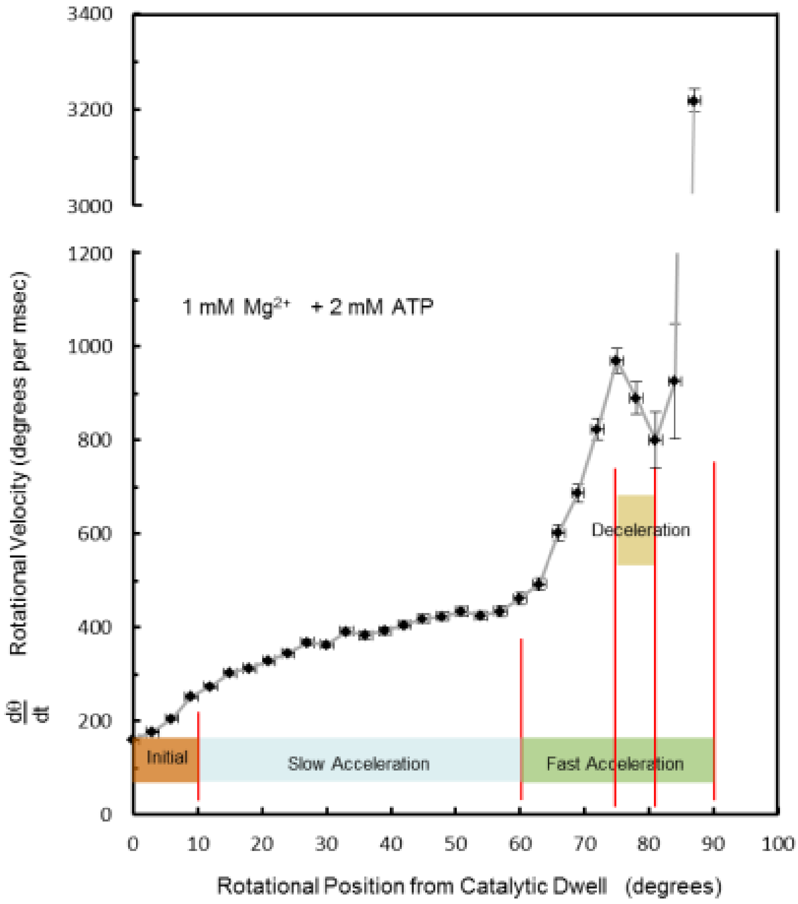

Figure 17. Average velocity of F_1 ATPase-dependent γ subunit rotation as a function of rotational position from the catalytic dwell. The difference in adjacent rotational position data points observed during a transition were used to calculate the rotational velocity of F_1 at each data point. Then, the calculated velocities were binned and averaged for every three degrees of rotation according to the angle in the observable power stroke. The average velocity of transitions was then plotted as a function of rotational position from the end of the catalytic dwell. Four distinct phases are identified in the average velocity profile of F_1 rotation in the presence of 2 mM ATP and 1 mM $MgCl_2$.

It is noteworthy that the average velocity included data when, at given rotational positions, the velocity was zero. The location and duration of pauses were identified by binning the rotational position of each data point within a transition and plotting them as a histogram. A 3D histogram of pause duration and location is shown in **Figure 18A**. The distribution of pauses was fairly constant with small increases in abundance between 15-20° and also between 60-70° of rotation. The duration of the vast majority of these pauses was less than 20 μsec. An ADP-Release dwell is known to occur at about 40° and becomes evident in the presence of elevated concentrations of product (Adachi, Oiwa et al. 2007). **Figure 18B** shows the effect of additional ADP to the 3D dwell profile. The addition of ADP increased the abundance and duration of dwells located around 40° from the catalytic dwell.

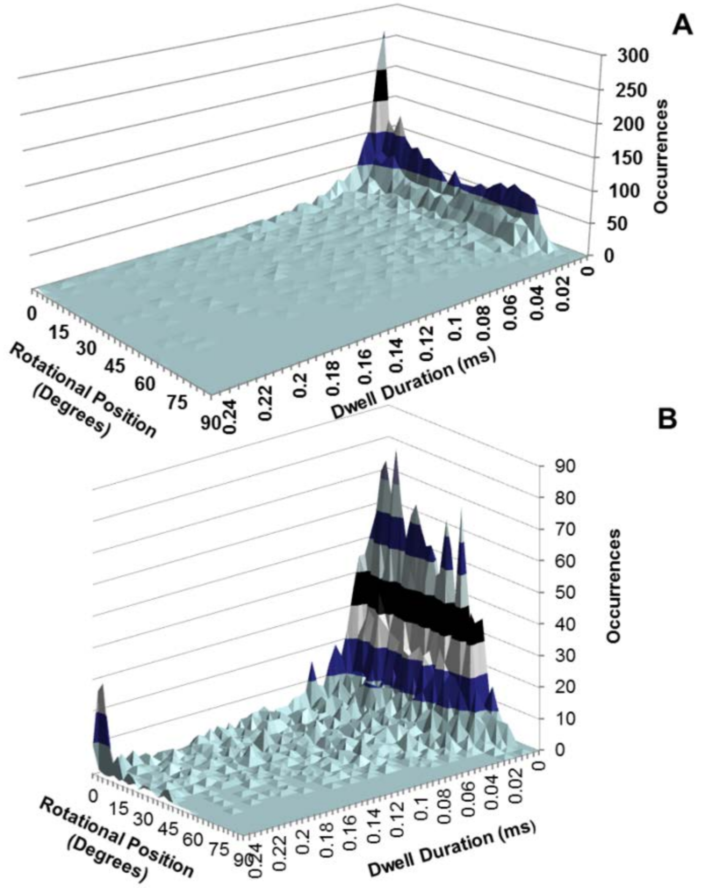

Figure 18. 3D histogram of location and duration of pauses. Distribution of the duration of dwells that occurred during single transitional events as a function of rotational position in the presence of 2mM ATP and 1mM Mg2+ (A) or in the presence of 4 mM ADP, 2mM ATP, and 3 mM Mg2+ (B).

The averaged rotational profile of F_1 in the presence versus the absence of elevated Mg-ADP is shown in **Figure 19A**. The presence of Mg-ADP decreased the initial and slow acceleration phases. As shown in Figure 21B, the fractional differences in rotational velocity due to the addition of Mg-ADP were 40 - 50% during these phases. Although the velocities were about the same at 60° from the catalytic dwell, the rotational position between the slow and rapid acceleration phases, the additional Mg-ADP also decreased the rapid acceleration phase by an average of 22% in a manner that suppressed the magnitude of the deceleration phase.

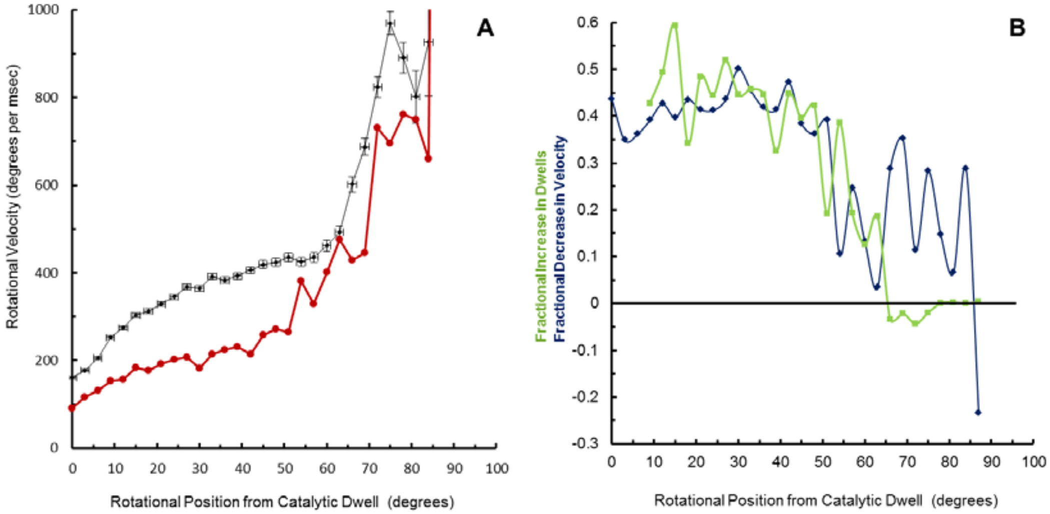

Figure 19. Effect of ADP on Average Rotational Velocity as a Function of Rotational Position. (A) The average rotational velocities of F1 ATPase powered rotation in the presence of 2 mM ATP and Mg2+ (●), versus 4 mM ADP, 2mM ATP and 3 mM Mg2+ (●). (B) The fractional decrease in rotational velocity (●) from (A), and the fractional increase in the occurrence of dwells (●) in the presence versus absence of added ADP as a function of rotational position.

To assess the contribution of the occurrence of Mg-ADP dependent dwells to the decreases in average velocity, the fractional difference in dwell abundance (i.e. the difference in dwell abundance between Figs. 18A and B) as a function of the rotation position is also shown in **Figure 19B**. Comparison of the fractional changes of rotational velocity and Mg-ADP dwell abundance clearly show that the decrease in velocity and increase in dwell abundance during the slow acceleration phase was the same. Thus, the decrease observed during the slow acceleration phase was the result of suppression of Mg-ADP release and not an actual change in rotational velocity.

The contribution of nucleotide binding affinity to the rotational velocity of the γ-subunit was determined by comparing the effects of GTP and ITP to ATP as substrates for hydrolysis. The dissociation constants for GTP, GDP and IDP determined by tryptophan fluorescence quenching are shown in **Table 1** along with a summary of the dissociation constants for ATP, ITP, and ADP as determined by Senior *et al.* (Weber and Senior 2001; Senior, Nadanaciva et al. 2002) using the same method. The binding affinity of GTP and ITP for Catalytic Site 1 was about 300 fold lower than that of ATP. At Catalytic Site 2, the affinities for GTP and ITP were 30 and 40 fold lower than that of ATP. Although Site 3 had similar binding affinities for ATP and GTP, the affinity of ITP was nearly 500 fold lower.

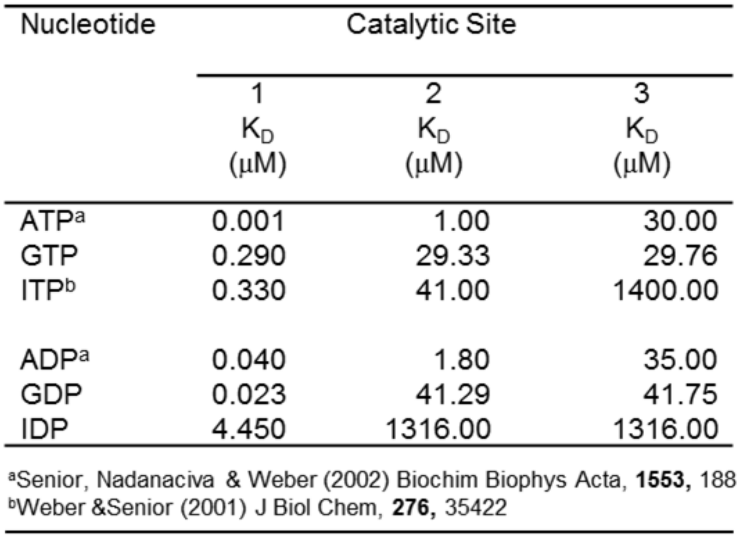

Nucleotide	Catalytic Site		
	1 K_D (μM)	2 K_D (μM)	3 K_D (μM)
ATP[a]	0.001	1.00	30.00
GTP	0.290	29.33	29.76
ITP[b]	0.330	41.00	1400.00
ADP[a]	0.040	1.80	35.00
GDP	0.023	41.29	41.75
IDP	4.450	1316.00	1316.00

[a] Senior, Nadanaciva & Weber (2002) Biochim Biophys Acta, **1553,** 188

[b] Weber &Senior (2001) J Biol Chem, **276,** 35422

Table 1. Binding affinities of purine nucleotides. To the three catalytic site of F_1-ATPase measured by tryptophan fluorescence quenching.

The differences in the affinities of the catalytic sites for ATP, GTP and ITP were reflected in changes in the $k_{cat/}K_M$ of ATP hydrolysis (**Figure 20**), consistent with Michaelis-Menton kinetics. As a consequence, 1 mM Mg-ATP approximated k_{cat} conditions, whereas equivalent concentrations of Mg-GTP and Mg-ITP were rate-limiting. Under substrate-limiting conditions, the rotary mechanism of the F_1-ATPase is known to have an ATP-binding dwell at 40° of rotation from the catalytic dwell (Adachi, Oiwa et al. 2007).

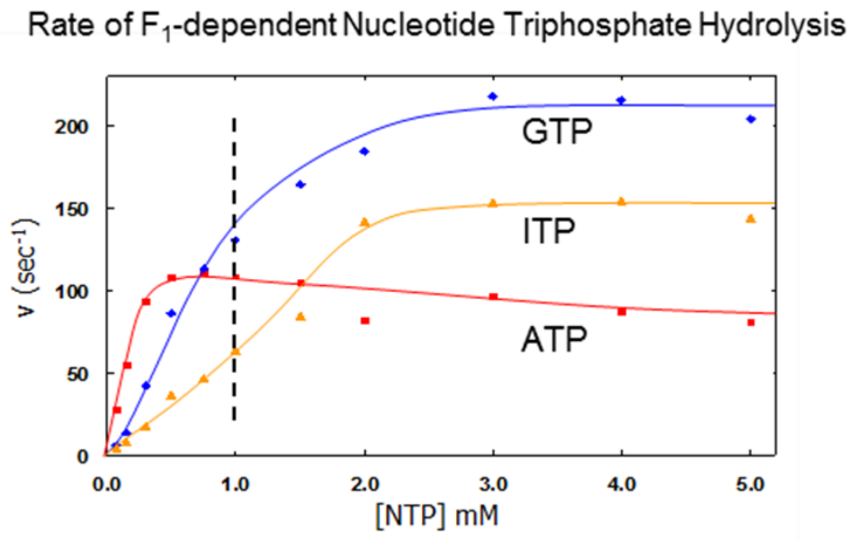

Figure 20. Rate of F_1-dependent hydrolysis as a function of Nucleotide Triphosphate (NTP) concentration. The ATPase activity of F_1 was measured using a coupled assay nucleotide regenerating assay (Greene and Frasch 2003). The k_{cat} of F_1 was calculated and plotted as function of increasing concentrations of the purine nucleotides; ATP, GTP, and ITP. In order reduce possible nucleotide diphosphate inhibition, NTP was added at concentration double that of Mg^{2+}. Thus, the reported concentrations are for Mg^{2+}-NTP, and not for the total nucleotide present in each experiment. Rates were measured and calculated at 0.075, 0.150, 0.300, 0.500, 0.750, 1.00, 1.50, 2.00, 3.00, 4.00, and 5.00 mM Mg^{2+}-NTP.

Figure 21A shows the effects of substrate limiting concentrations of nucleotides on the average rotational velocities of F_1 as a function of rotational position from the catalytic dwell. Although the velocities of both the I and S phases were decreased by 1 mM ITP, only the latter phase was slower in the presence of either 300 μM ATP and 1 mM GTP. In all cases, limiting substrate concentrations resulted in small increases during the fast acceleration phase. The fractional differences in velocity centered on the slow acceleration phase at limiting ATP and GTP were about the same magnitude as the fractional increases in the nucleotide-binding dwells (**Figure 21B and 21C**). The magnitudes of the decreases in dwells during the fast acceleration phase were also about the same as the increases in velocity observed with these nucleotides. These data indicate that the differences in average velocity are the result of dwells, and not from a change in actual rotational velocity.

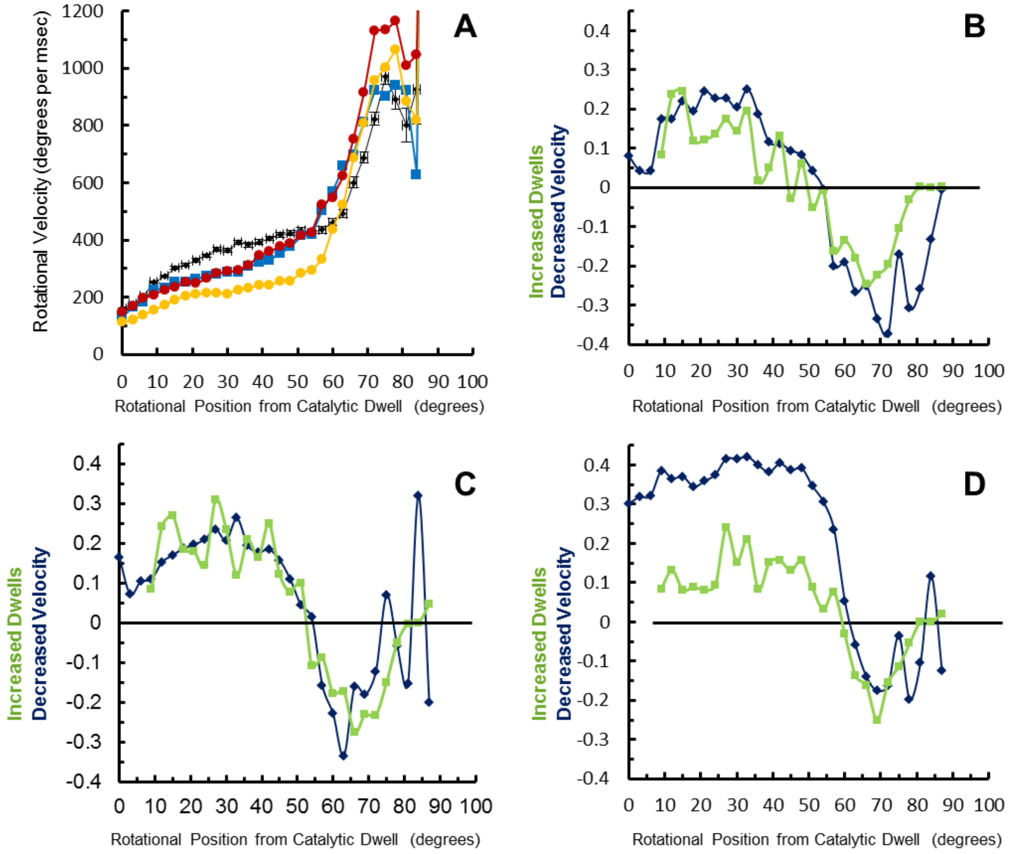

Figure 21. Effects of limiting substrate concentrations for ATP, GTP, and ITP on the nucleotide binding dwells and velocity. (A) Average rotational velocities of F_1 as a function of rotational position from the catalytic dwell for 300μM Mg-ATP (●), 1 mM Mg-GTP (■), and 1mM Mg-ITP (●) compared to 1mM Mg-ATP (♦). The fractional decrease in rotational velocity for (●) from (A), and the fractional increase in the occurrence of dwells (●) for 300 μM ATP (B), 1 mM Mg-GTP (C), and 1mM Mg-ITP (D) versus 1mM Mg-ATP as a function of rotational position.

Limiting ITP also resulted in an increase in the nucleotide-binding dwells during the S phase, and a decrease in dwells during the F phase (**Figure 21D**). The magnitude of the change in velocity during the fast acceleration phase with ITP was comparable to that of the dwells. However, during the slow acceleration phase, the magnitude of the fractional decrease in rotational velocity was 3-fold greater on average than the fractional increase in the nucleotide-binding dwells. Thus, the decrease in velocity during the slow acceleration phase indicates that nucleotide affinity does contribute to the rotational velocity.

Discussion

The use of light scattered from gold nanorods attached to the γ-subunit of the F_1-ATPase presented here provide unprecedented resolution of rotational position as a function of time. These results clearly show that the rotational velocity is not constant during a power stroke, but has an initial (I) acceleration phase during the first 15° from the end of the catalytic dwell, followed by a slow (S) acceleration phase that occurs during ATP binding and ADP release. At ~60°, the S transitions to a fast (F) acceleration phase that contains an interim deceleration (ID) phase between 75° - 82°. The energy conversion efficiency from nucleotide hydrolysis to rotary torque has been estimated to be close to 100% based on early single molecule observations of γ-subunit rotation of F_1 (Noji, Yasuda et al. 1997). Based on this result, the rotary torque generated during rotation was assumed to be nearly constant (Oster and Wang

2000) because the high efficiency implies tight coupling between the mechanics and the chemistry such that entropic losses are small. Since torque is directly proportional to the product of the drag and the velocity, the results presented here clearly show that the torque is not constant, and thus, any conclusions that rely on the assumption of constant torque must be reexamined.

The results presented here that the fractional decrease in ITP-dependent rotational velocity was four-fold larger than the fractional increase in substrate-binding dwells provides the first direct evidence that nucleotide binding contributes to the generation of torque on the F_1-ATPase molecular motor. This is consistent with theoretical studies (Oster and Wang 2000; Gao, Yang et al. 2003). As shown in Figure 23, ATP can bind to *E. coli* F_1 when the γ-subunit has rotated anywhere from 15° – 50° from the catalytic dwell, with the highest binding affinity occurring at ~35°. This is consistent with the probability for ATP binding reported for the thermophilic *PS3* enzyme (Yasuda, Noji et al. 2001).

Following the binding of ATP, the γ-subunit is halted by the catalytic dwell after 80° of rotation. The velocity of F_1 rotation powered by ATP, GTP, or ITP during the fast acceleration phase of this 80° rotation was about the same (Figure 21) even though the affinity for ITP at catalytic site-3 is almost 50-fold lower than ATP and GTP (Table 1). This suggests the binding affinity of all three nucleotides exceed a threshold for the minimum energy required to rotate the γ-subunit during the rapid acceleration phase. To explain how ATP binding energy contributes to torque for the final 40° of the power stroke after the catalytic dwell, Wang and Oster (Oster and Wang 2000) postulated that a portion of the energy from ATP binding is stored during the catalytic dwell as elastic energy in the lever arm of the β subunit. Since a greater fraction of the energy derived from ITP binding would be consumed during the first 80° of rotation, less energy is subsequently available to be stored during the catalytic dwell. This would explain the lower ITP-dependent velocity during the 40° power stroke observed here. More experiments are required to identify how this energy is stored during the catalytic dwell.

In the presence of high ADP concentrations, it was observed that the rotational velocity of the S phase decreased proportional to the increase in 'ADP-release' dwells (Figure 19) similar to that reported for F_1 from the thermophilic bacterium *PS3* (Watanabe, Iino et al. 2008). Furthermore, the addition of ADP to the *E. coli* F_1 also decreased the velocity of the F phase, which was not compensated by a change in the abundance of dwells (Figure 19B). Consequently, the 22% decrease in average rotational rate is solely due to a decrease in velocity. The free energy of the chemical equilibrium of [ADP][Pi]/[ATP] in the presence and absence of the Mg-ADP added here was calculated to be -94.4 pN nm and -116 pN nm, respectively. This 19% difference in free energy approximately corresponded to the fractional decrease in velocity observed during the F phase.

Chapter 4

EFFECT OF CATCH LOOP MUTATIONS ON THE VELOCITY OF F_1 ATPASE ROTATION

ABSTRACT

Recent single molecule measurements of *E. coli* F_1-ATPase rotation that resolve the rotational position and velocity with high precision revealed initial (I), slow (S), and fast (F) acceleration phases to the rotational velocity where the latter included an interim deceleration (ID) phase. Single site mutations that can affect the velocity of specific phases of γ-subunit rotation were observed for the first time, which in some cases, were in regions of F_1 previously considered not to contribute to rotation. Mutations βD372V and γK9I were found to increase the velocity specifically during the F phase, while γK9I also increased the depth of the ID phase. The conversion between S and F phases was specifically affected by γQ269L. While γT273D, βD305E, and αR283Q decreased the velocity of all phases, the decreases in velocity due to βD302T, γR268L and γT82A were confined to the I and S phases. The correlations between the structural locations of these mutations and the phases of rotation they affect provide new insight into the molecular basis for the conformational changes of the protein that contribute to rotation of the γ-subunit.

INTRODUCTION

The F_1-ATPase is a rotary motor composed of the γ subunit that rotates within a hexameric ring of alternating α and β subunits (**Figure 22A**). The three catalytic sites for ATP hydrolysis in the ring, each formed by an αβ subunit heterodimer, function in a sequential manner to promote CCW rotation of the γ-subunit. The γ–subunit is composed of a globular domain known as the foot, and the coiled-coil domain that extends up through the center of the hexameric ring.

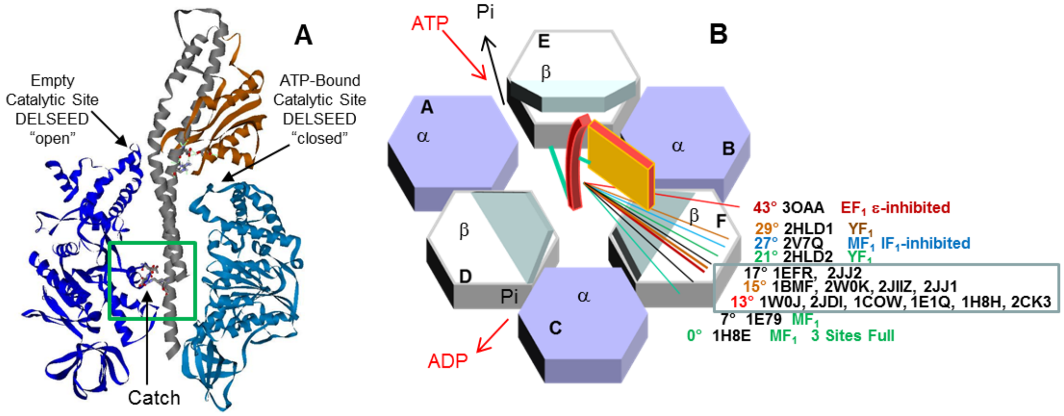

Figure 22. Crystal structures of the F_1 ATPase. (A) Depiction of the F_1 crystal structure (3OAA) from *E.coli* that has been inhibited by ε showing the β subunits designated as E (dark blue) and F (light blue). The γ subunit has two domains, the foot (tan) and the coiled-coil region (grey). This structure also shows that the foot of γ is rotated 43° counterclockwise from that of 1H8E. (B) Model of angular deviations of the foot of the γ subunit in relation to the coiled-coil as determined from available F_1 crystal structures. Hexagonal shapes represent alternating α and β subunits in the F_1 ATPase, and γ is represented by the orange stalk and foot sections, representing the coiled-coil and foot domains of γ, respectively. Crystal structures of various F_1 structures show counterclockwise rotation of the foot while the coiled-coil domain does not move.

Hydrolysis of ATP is believed to occur during Catalytic Dwells that, in the *E. coli* enzyme, last for about 8 ms and are rate-limiting to the overall reaction (Spetzler, York et al. 2006). Release of Pi from one catalytic site ends the catalytic dwell to initiate γ-subunit rotation (Adachi, Oiwa et al. 2007; Watanabe, Iino et al. 2010). At saturating ATP concentrations, rotation occurs in 120° steps separated by catalytic dwells. As rotation proceeds from the end of the catalytic dwell, a second (ATP-Binding) dwell can occur if ATP has not become bound and/or if ADP has not been released (Watanabe, Okuno et al. 2012). Although ATP can bind when the γ-subunit has rotated anywhere from 15° – 50° from the catalytic dwell, it binds with the highest affinity at about 35° - 40° (Chapter 3, (Adachi, Oiwa et al. 2007)). At this point in the rotation, ATP binds to the empty catalytic site vacated by the Pi, while the ADP generated from the prior hydrolysis is released from the adjacent site located on the $\alpha\beta$ ring counterclockwise to the ATP-binding site (Site CD, **Figure 22B).**

It was recently shown that the binding of ATP to the empty catalytic site provides the energy required for the 120° power stroke of F_1 (Chapter 3). To explain why the low affinity substrate ITP decreased the velocity during the 40° of rotation that follows the catalytic dwell but not the 80° of rotation immediately following substrate binding, it was proposed that the binding energy only needs to exceed a minimal threshold value to initiate rotation prior to the catalytic dwell. The remaining binding energy was thought to be stored as elastic energy during the catalytic dwell that propels the remaining 40° of rotation (Oster and Wang 2000). The binding of ATP is believed to induce the movement of the β-subunit helical domain containing the DELSEED motif to move from an open to a closed position (Figure 1A). This movement of the DELSEED-containing domain is thought to push on the on the γ-subunit as a lever arm on a camshaft to induce rotation. It was shown that when the α-helical arm adjacent to the DELSEED was shortened, torque was reduced significantly, yet torque was not affected by the removing the negative charges in the DELSEED region (Hara, Noji et al. 2000; Usukura, Suzuki et al. 2012). It was concluded that the γ-subunit coiled-coil does not contribute to the generation of torque based on experiments that showed that rotation was still observed after most of the coiled-coil had been deleted (Furuike, Hossain et al. 2008).

In the 1H8E crystal structure of bovine F_1 ATPase (Menz, Walker et al. 2001), all catalytic sites contain nucleotide, two of which contain the transition state analog Mg^{2+}-ADP-AlF_n. This suggests that this structure most closely resembles the catalytic dwell, which is consistent with the observation that the γ-subunit foot domain of 1H8E is rotated the furthest clockwise of available F_1 crystal structures (Figure 22B). Two-thirds of available F_1 crystal structures show that the foot of the γ–subunit is rotated 13° - 17° counterclockwise from 1H8E, suggesting that this is the angular position of lowest free energy for the foot domain. At the other extreme, in the *E. coli* F_1 structure (3OAA) , the foot domain is rotated CCW up to 43° relative to the coiled-coil domain as compared to the 1H8E structure.

In all available crystal structures of F_1 ATPase the γ-subunit coiled-coil is attached via electrostatic interactions to residues located on the β-subunit of the empty catalytic site known as “the catch loop”. Mutations to residues on the β and γ-subunits that form this catch have dramatic effects on catalytic function, and have been postulated to be involved in an Escapement Mechanism that permits rotation only upon substrate binding to the empty catalytic site (Greene and Frasch 2003). The electrostatic interactions in the Catch include residues βD305 and βD302 of the empty catalytic site and residues γQ269, γT273, and γR268 on the γ-subunit coiled-coil (**Figure 23A**). In the other two catalytic sites where nucleotide is bound, the catch loop residues form salt bridges with αR283 on the α subunit of the αβ heterodimer that comprise those catalytic sites (Boltz and Frasch 2006) (**Figure 23B**). Consequently, sometime after ATP binds to the empty site, the β subunit catch loop residues must switch from the γ-subunit to the α subunit of that catalytic site. Conversely, ADP release at the adjacent catalytic site must dissociate the electrostatic interactions between neighboring α and β subunits (Catalytic Site CD, Figure 25B) so that the γ subunit can bind to the next catch loop at the conclusion of that rotational event.

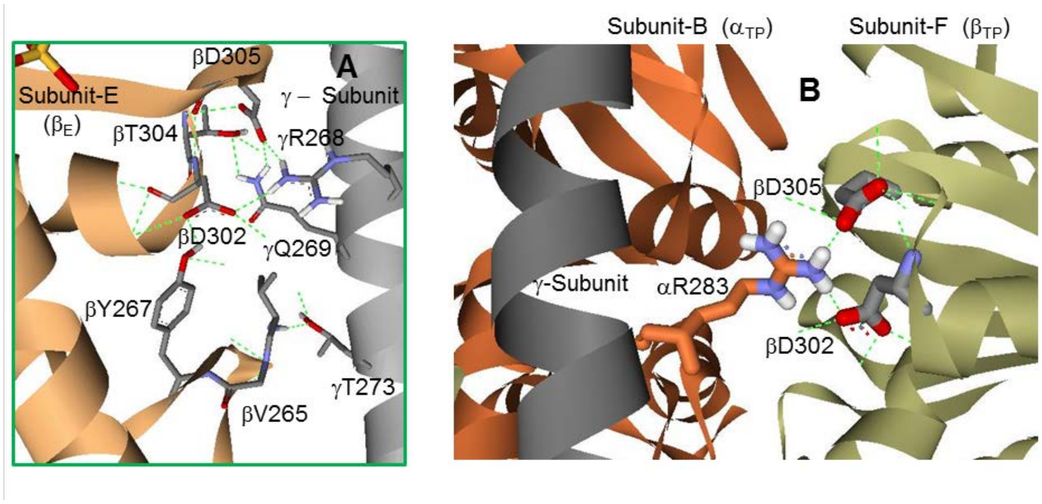

Figure 23. Crystal structures that show interactions of β catch loop residues with the γ-subunit and α-subunits. (A) A close up of the hydrogen bond network formed between the β_E subunit and γ referred to as the catch loop region. This MF_1 structure is from 1E79 as crystallized from bovine. (B) Crystal structure 1H8E of bovine MF_1 showing interactions of βD305 and βD302 with αR283 within the β_{TP} site.

Recently, using the light scattered from gold nanorods as a probe of rotation, the velocity of the γ-subunit as a function of rotational position was observed at much higher resolution than was previously possible (Spetzler, York et al. 2006; Spetzler, Ishmukhametov et al. 2009). This study revealed that the rotational velocity is not constant, but accelerates in four phases. At the end of the catalytic dwell there is an initial acceleration (I) during the first 15° followed by a slow acceleration (S) phase from 15° – 60°. During this latter phase ATP binds and ADP is released with the highest probability occurring from 30° - 40°. From 60° – 90° acceleration is much faster (F), except for a short interim deceleration (ID) that occurs between 75° and 82°. However, except for the nucleotide binding and release steps, the association of these phases with conformational changes of F_1 is currently not understood.

The effects of mutations on the velocity of γ-subunit rotation using the gold nanorod-based single molecule assay have now been examined through detailed resolution of their power strokes. These studies identify for the first time single-site mutations that can affect the velocity of specific phases of γ-subunit rotation. Some residues, including those in the region of the γ-subunit coiled-coil previously considered not to contribute to rotation, were found to change the velocity by as much as 50% from that in the wild type. The correlations between the structural locations of these mutations and the phases of rotation they affect provide new insight into the molecular basis for the conformational changes of the protein that contribute to rotation of the γ-subunit.

RESULTS

The 1H8E crystal structure of bovine F_1 shown in **Figure 24**, depicts a salt bridge linking the *E. coli* equivalent of βD372, which is adjacent to the DELSEED domain, to γK9. The effects of γK9I and βD372V on the average rotational velocities as a function of rotational position are shown in **Figure 25A**. The γ–subunit rotational position of 0° is defined as the end of the catalytic dwell. The average rotational velocities observed with both mutants were the same as that of the wild type during the I and S phases. While the velocity during the F phase was increased by these mutants relative to wild type, the βD372V mutant showed a greater effect during this phase than γK9I. However, γK9I also slowed the rotational velocity by an additional 33% during the ID phase compared to wild type.

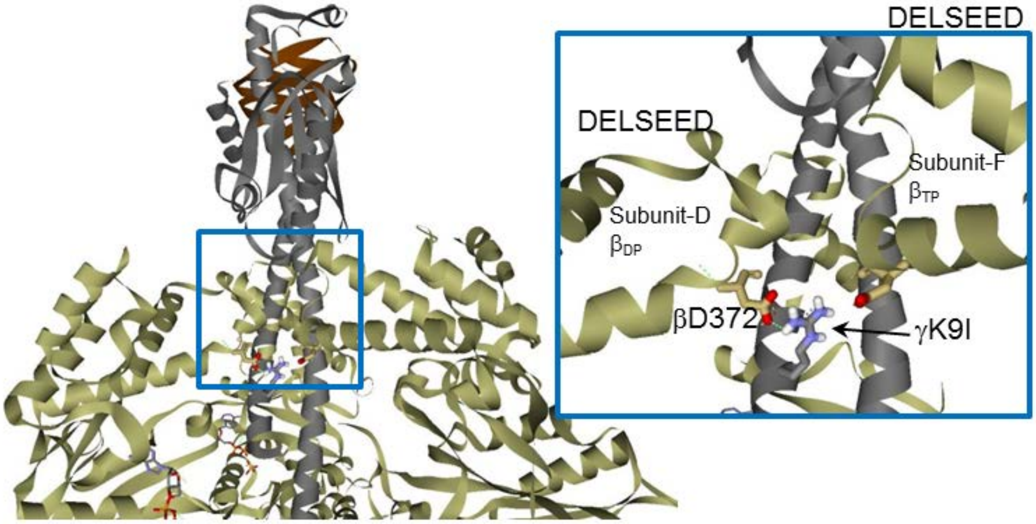

Figure 24. Interaction of the DELSEED lever arm and the γ-subunit coiled-coil. Crystal structure 1H8E of bovine MF_1 that shows the interaction of βD372 adjacent to the DELSEED domain with residue γK9 on the coiled-coil domain of the γ subunit. This interaction does not occur in other F_1 crystal structures for analogous residues.

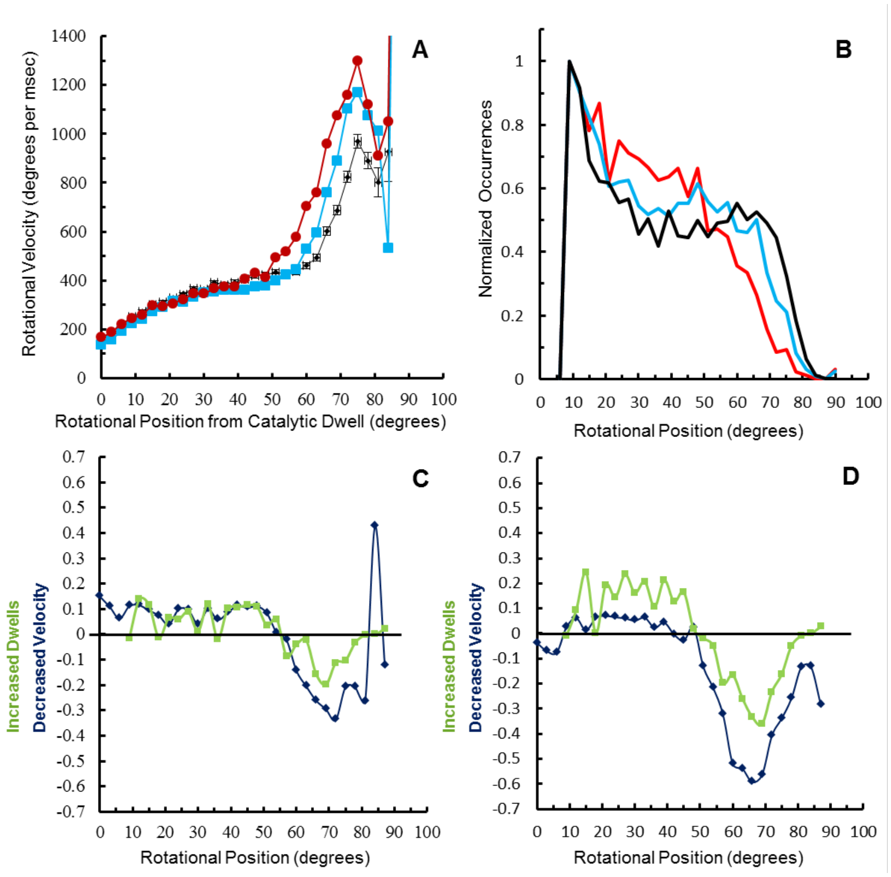

Figure 25. The effects of the βD372V and γK9I mutations on the average velocity of F_1 rotation and dwell abundance as a function of rotational position. (A) The average rotational velocity of F_1 ATPase powered rotation of wild type (♦), versus the βD372V (●), and γK9I (■) mutations. (B) Normalized occurrences of the abundance of dwells for each rotational position for wild type (black), versus the βD372V (red), and the γK9I (blue) mutations. The first nine degrees were excluded from all dwell analysis due to interference from catalytic dwells. The fractional decrease in rotational velocity (●) from (A), and the fractional increase in the occurrence of dwells (●) as calculated from (B) for γK9I in (C), and βD372V in (D) over wild type as a function of rotational position.

The average velocities in Figure 25A include data from contributing individual transitions that have paused at various rotational positions. The distributions of these pauses in the wild type, γK9I, and βD372V mutants were plotted as a function of rotational position (**Figure 25B**). Although, at saturating ATP, pauses in the wild type occur throughout the transition, the abundance is at a local minimum around 40° of rotation where the ATP-binding dwell is observed at limiting substrate concentrations (Chapter 3). When these data were plotted as the fractional differences in dwell abundance between the wild type and the βD372V mutant (**Figure 25C**), the mutant had up to 30% fewer dwells during the F phase, yet there was a corresponding increase of 60% in the velocity of γ subunit rotation. Thus, the βD372V mutant allows the γ-subunit to rotate at higher velocities upon nucleotide binding. The absence of dwells, along with an increase in the rotational velocity suggests that removal of the negative charge of the βD372 residue reduced obstacles that impeded rotation during the F phase.

The fractional differences in dwells observed for γK9I relative to wild type compared to fractional differences in velocity as a function of rotational position is shown in **Figure 25D**. During the F phase, the γK9I mutant had about 20% fewer dwells while at the same time the average rotational velocity increased up to 60%. This increased velocity is likely the result of the elimination of possible electrostatic interactions between γ and the surrounding αβ subunits.

A comparison of the average rotational velocities of the γQ269L and γT273N mutants to wild type as a function of rotational position is shown in **Figure 26A.** Although I and S phases were not affected by the γQ269L mutation, the average rotation rate was 20% slower than wild type from 40° to 60° of rotation (**Figure 26B**), which was predominantly the result of a proportionate increase in dwells.

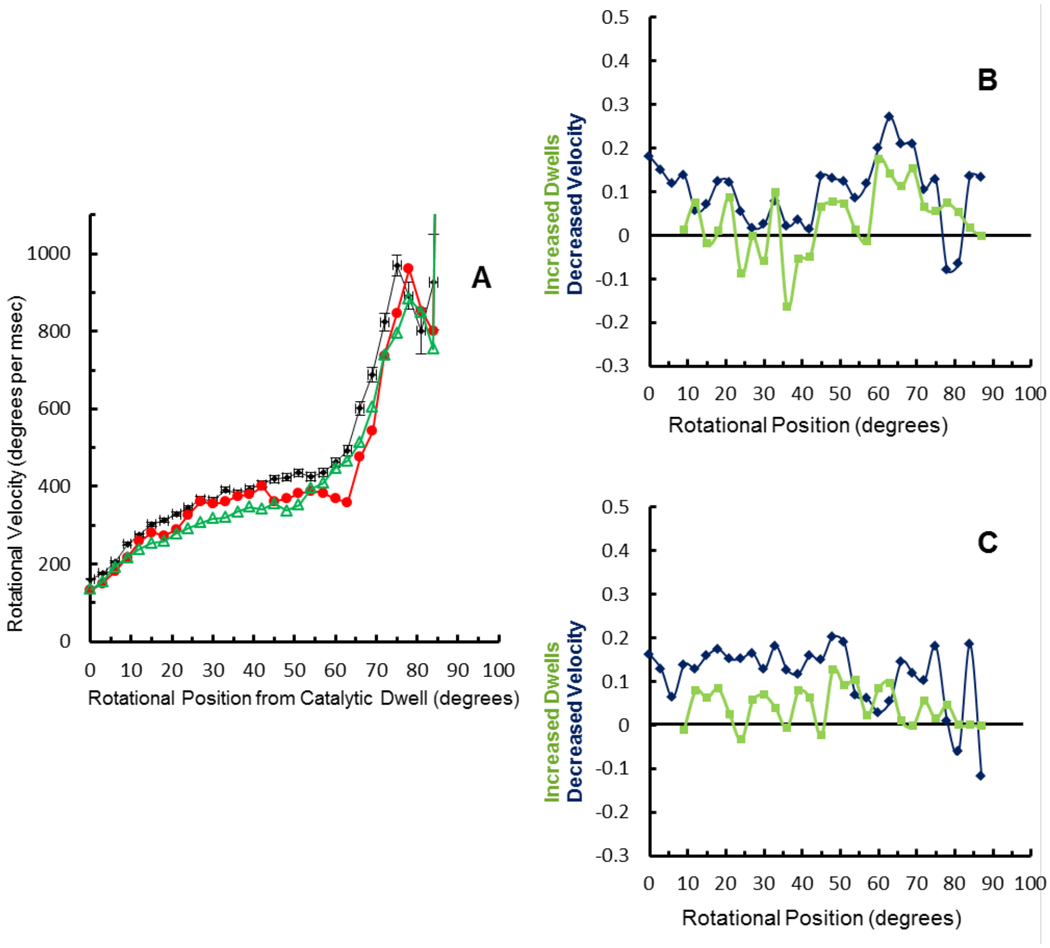

Figure 26. Effects of the γQ269L and γT273N mutations to the average rotational velocity of the γ-subunit and dwell abundance as a function of rotational position. (A) The average rotational velocities of F_1 ATPase powered rotation of wild type (♦), versus the γQ269L (●) and, γT273N (Δ) mutations. (B) The fractional decrease in rotational velocity (●) from (A), and the fractional increase in the occurrence of dwells (●) for the γQ269L mutation as shown in (C), and the γT273N mutation as shown in (D) as compared to wild type and as a function of rotational position.

The γT273 residue is located one helical turn from the γQ269 residue (Figure 23A), where it interacts with the β-subunit through a hydrogen bond to the backbone of βV265. The γT273N mutation, which substituted a group that retained both the size and polarity, slowed γ-subunit rotation by less than 10%. This decrease was primarily the result of an increase in dwells (**Figure 26C**). The γT273D mutant, which converts the polar side chain to a negatively charged group, suppressed the rotational velocity of the γ-subunit during all three phases of rotation (**Figure 27A**), and reduced the magnitude of the ID phase. Although there was a 10% fractional increase in dwells during the S phase (**Figure 27B**), this did not compensate for the 40% decrease in velocity observed during this phase.

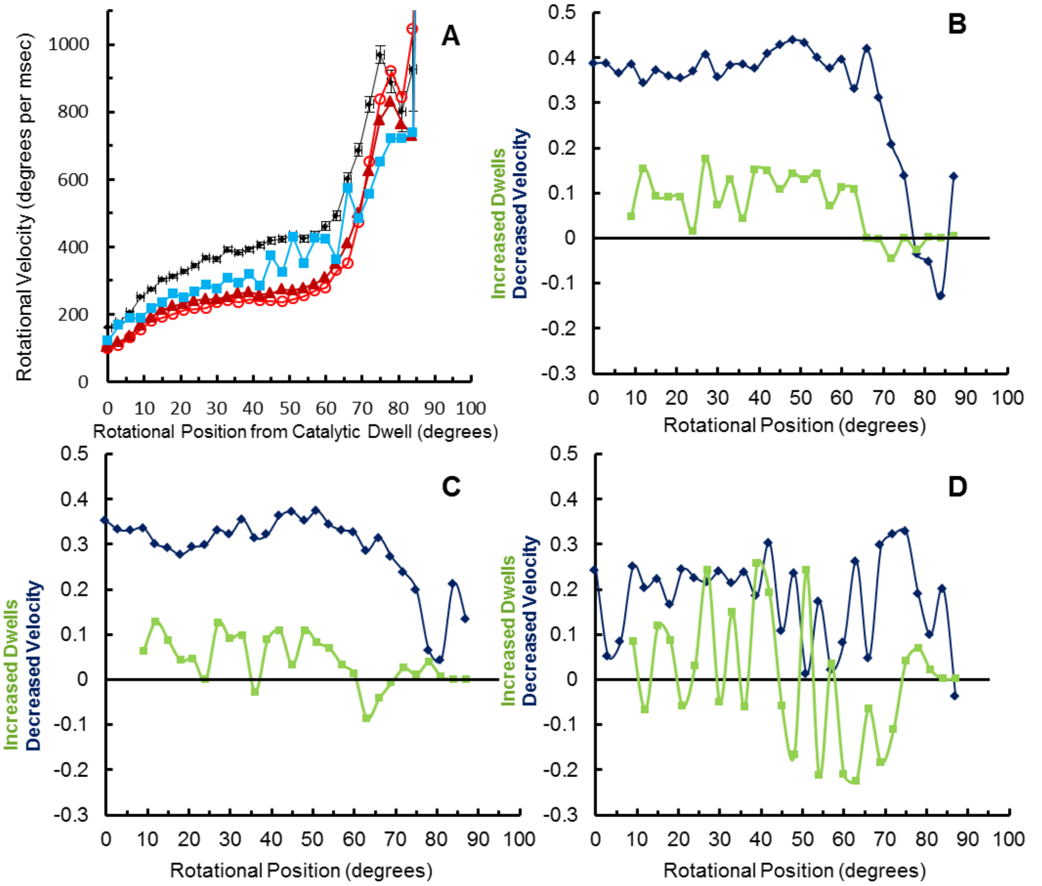

Figure 27. Mutations that affect all three phases of the average rotational velocity of F_1 as a function of rotational (A) The average rotational velocities of F_1 ATPase powered rotation of wild type (♦), versus the γT273D (○), βD305E (▲), and αR283Q (■) mutations. The fractional decrease in rotational velocity (●) from (A), and the fractional increase in the occurrence of dwells (●) for the γT273D mutation as shown in (B), the βD305E mutation as shown in (C), and the αR283Q mutation as shown in (D) compared to wild type and as a function of rotational position.

The βD305E and αR283Q mutants also caused decreases in rotational velocity during all three acceleration phases (Figure 27A). In both cases, the ID phase was suppressed, and was almost eliminated by the αR283Q mutation. The fractional decrease in velocity by about 35% during the I and S phases resulting from the βD305E mutation, was substantially greater than the 10% increase in dwells during these phases (**Figure 27C**). During the F phase, the dwells had little impact on the 20% average decrease in the observed rotational velocity. Although the αR283Q mutation also decreased the I and S phase by 18% (**Figure 27D**), this was largely the result of a very unusual periodic increase in dwells during these phases.

Mutations that decreased the rotational velocity specifically during the I and S phases include γR268L, βD302T and γT82A (**Figure 28A**). The γR268 residue forms a salt bridge to catch loop residue βD302 of the empty catalytic site. Mutations to γR268L and βD302T resulted in a decrease in the rotational velocity of 20%-30% and 40%, respectively (**Figures 28B-C**). The γR268L increased dwells by an average of 5%, while βD302T had 10% fewer dwells such that the actual decrease in rotational approached 50%.

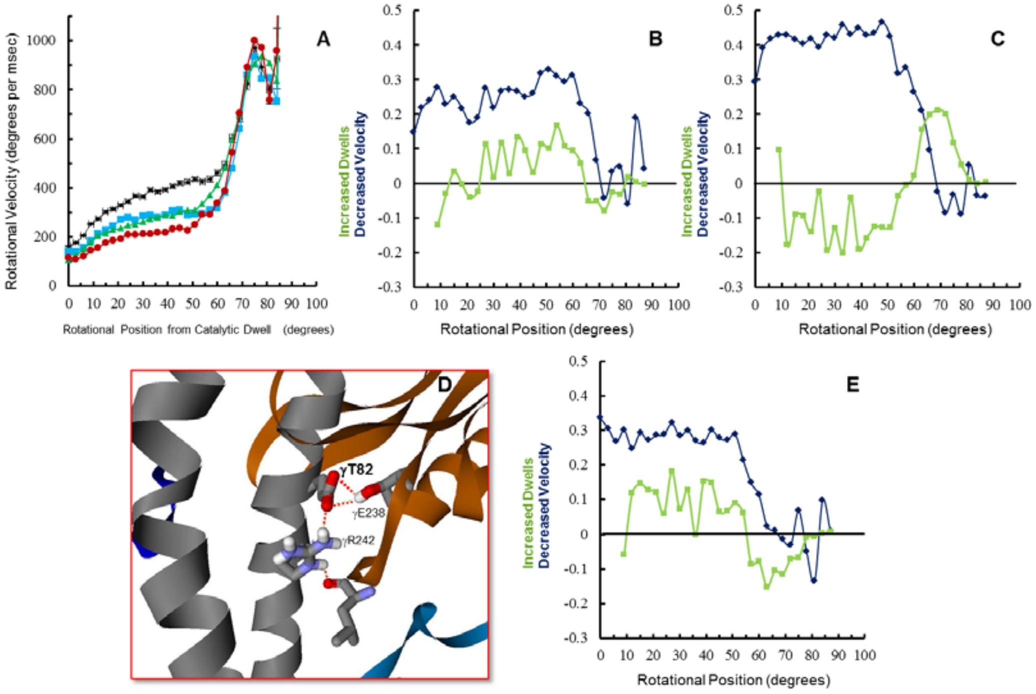

Figure 28. Mutations that affect the average velocity of γ-subunit rotation exclusively during the S phase. (A) The average rotational velocities of F_1 ATPase powered rotation of wild type (♦), versus the γR268L (■), βD302T (●), and γT82A (▲) mutations. (B) The fractional decrease in rotational velocity (●) from (A), and the fractional increase in the occurrence of dwells (●) for the γR268L mutation as shown in (B), and the βD302T mutation as shown in (C). (D) Crystal structure of 1H8E showing electrostatic interactions involving γT82 that connect the foot of the γ subunit to the coiled coil region. (E) The fractional decrease in rotational velocity (●) from (A), and the fractional increase in the occurrence of dwells (●) for the γT82A mutation.

Residue γT82 is part of an electrostatic network that strengthens the linkage between the foot and the coiled-coil domain (**Figure 28D)**. This mutant resulted in a 10% average increase in dwells during the S phase, and a 10% decrease in dwells during the F phase. In contrast, the mutant caused a 30% decrease in rotational velocity during the S phase.

DISCUSSION

Single site mutations have been identified for the first time which affect the velocity of specific phases of γ-subunit rotation, and in some cases, are located in regions of F_1 that were previously considered not to contribute to rotation. The correlations between the structural locations of these mutations and the phases of rotation that they affect provide new insight into the molecular basis for the conformational changes of the protein that contribute to rotation of the γ–subunit. Mutations βD372V and γK9I were found to increase the velocity specifically during the F phase. In the F_1 crystal structure from bovine mitochondria (Menz, Walker et al. 2001) the residue analogous to γK9 is member of a ring of positively charged residues known as the ionic track. Since the negatively charged DELSEED residues at the end of the β–subunit lever arms face the ionic track, electrostatic interactions between DELSEED and the track were initially proposed to propel γ-subunit rotation (Ketchum, Al-Shawi et al. 1998). However, many of the ionic track residues are not conserved, and single molecule experiments of mutants that eliminate the negative charges of the DELSEED residues have been shown to have no effect on torque generation (Hara, Noji et al. 2000). The increase in rotational velocity observed here with the βD372V and γK9I mutations not only confirm that these electrostatic interactions are not contributing to torque, but demonstrate that these interactions slow the average rotational velocity. It is likely that although the two mutations both increase the velocity of the F phase, these effects are not necessarily the result of an interaction of the two residues with each other. This is suggested first by the fact that the bD372V and γK9I mutations accelerate the velocities of the F phase to different extents, and second, by the observation that γK9I uniquely exaggerated the deceleration during the ID phase. This latter effect is possibly explained if electrostatic interactions between γK9 and the negative charges on DELSEED assist in repositioning the β subunit in such a way that reduces the extent of deceleration.

The results presented here show that γT82A was found to decrease the velocity specifically during the S and I phases. The foot and coiled-coil domains are connected by two loops at the end of the coiled-coil. Residue γT82 is part of an electrostatic network between the two domains that minimizes movement of the domains relative to each other. The strength of this electrostatic network is evident by the fact that it remains in place in crystal structures that show up to 43° of rotational movement of the foot domain relative to the coiled-coil (Figure 22B). To explain how ATP binding energy contributes to torque for the 40° power stroke following the catalytic dwell, Wang and Oster (Oster and Wang 2000) postulated that a portion of the energy from ATP binding is stored during the catalytic dwell as elastic energy in the lever arm of the β subunit. The decrease in rotational velocity observed here as the result of γT82A, could occur if the release of stored elastic energy caused the DELSEED lever to push the foot of the γ subunit to rotate counterclockwise. In the absence of the electrostatic network, the mechanical advantage is reduced, resulting in a slower rotation of the foot.

Although the γQ269L mutation had little effect on the rotational velocity during the S and F phases, there was a unique decrease in the velocity during the transition from the S to the F phase. This transition region is likely where the β-subunit catch interactions with the γ–subunit are disrupted and reform with the neighboring α-subunit residue triggered by the binding of ATP. Since the decrease in rotational velocity occurred at this point due to the conversion of a polar to a hydrophobic residue, γQ269 may be important for disengaging the catch from the γ-subunit by forming a hydrogen bond with γR268. This possibility is supported by the relative positions of γQ269, γR268, and β subunit catch loop residues of the empty catalytic site in the *E. coli* F_1 structure where the foot of the γ subunit is rotated 43° relative to the coiled-coil.

The results presented here show that the mutations βD302T and γR268L slowed the velocity only in the I and S phases. Rotation during the

I and S phases has been proposed to result from the release of elastic energy stored during the catalytic dwell that opens the DELSEED lever arm to push against the γ-subunit (Chapter 3). The observation that ITP-driven rotation results in a decrease in velocity specifically during the I and S phases supports the hypothesis that energy from substrate binding has been stored in some conformational state of the protein during the catalytic dwell (Oster and Wang 2000). In order for the DELSEED arm to apply the leverage needed to drive γ-subunit rotation of the foot by 40° following the catalytic dwell, the β subunit needs to be anchored opposite to where the leverage is applied. Since the βD302T and γR268L mutations weaken the catch interaction with the γ-subunit, the decreased velocity observed for these mutations may be the result of decreased leverage as the DELSEED arm pushes against the foot of the γ-subunit. This is supported by the position of the DELSEED arm in the site where ADP is released (Site CD in Figure 2B) relative to the foot of the γ–subunit in the bovine F_1 crystal structure 1H8E (Menz, Walker et al. 2001).

All phases of rotation were observed here to decrease as the result of the γT273D, βD305E, and αR283Q mutations (Figure 6). Since these residues interact with multiple partners at the three catalytic sites in the course of a rotational event, the underlying causes for the observed differences on rotational velocity are complex. The enzyme is extremely sensitive to mutation at position βD305 such that only the most conservative substitution to the longer glutamate that retains the carboxyl group is tolerated (Boltz and Frasch 2006). This increase in the length of the side chain is likely to cause the decreases in velocity by disrupting the electrostatic networks between the γ-subunit and the β-subunit of the empty catalytic site as well as the salt bridges this residue forms with the αR283 at the other two catalytic sites.

Chapter 5

SUMMARY

Single molecule experiments are critical to understanding the mechanism of F_1 rotation. Examination of the details that the effects of treatments and mutations provide on an individual level, provide a different perspective that is important in determining subtleties that can be missed with bulk experiments. The results presented in the preceding three chapters, as well as the appendices provide unique insights into the mechanism of F_1 rotation and can be used to help model this mechanism.

In Appendix A, the abundance of *E. coli* F_1-ATPase molecules observed to rotate using gold nanorods attached to the γ- subunit was quantitated. Individual F_1 molecules were determined to be rotating based upon time dependent fluctuations of red and green light scattered from the nanorods when viewed through a polarizing filter. The average number of F_1 molecules observed to rotate in the presence of GTP, ATP, and without nucleotide was ~50, ~25, and ~4% respectively. In some experiments, the fraction of molecules observed to rotate in the presence of GTP was as high as 65%. These data indicate that rotational measurements made using gold nanorods provide information of the F_1-ATPase mechanism that is representative of the characteristics of the enzyme population as a whole.

In chapter 2, the torque generated by the power stroke of *Escherichia coli* F_1-ATPase was determined as a function of the load from measurements of the velocity of the γ-subunit obtained using a 5 μs time resolution and direct measurements of the drag from 45 to 91 nm gold nanorods. This result was compared to values of torque calculated using four different drag models. Although the γ-subunit was able to rotate with a 20 fold increase in viscosity, the transition time decreased from 0.4 ms to 5.26 ms. The torque was measured to be 63±8 pN nm, independent of the load on the enzyme.

Appendix B measured increases in the power stroke and dwell durations of single molecules of Escherichia coli F_1-ATPase in response to viscous loads applied to the motor and inhibition of ATP hydrolysis. The load was varied using different sizes of gold nanorods attached to the rotating γ subunit and/or by increasing the viscosity of the medium using PEG-400, a noncompetitive inhibitor of ATPase activity. Conditions that increase the duration of the power stroke were found to cause 20-fold increases in the length of the dwell. These results suggest that the order of hydrolysis, product release, and substrate binding may change as the result of external load on the motor or inhibition of hydrolysis.

The use of light scattered from gold nanorods attached to the γ-subunit of the F_1-ATPase presented in chapter 3 provided unprecedented resolution of rotational position as a function of time. These results clearly show that the rotational velocity is not constant during a power stroke, but has an initial (I) acceleration phase during the first 15° from the end of the catalytic dwell, followed by a slow (S) acceleration phase that occurs during ATP binding and ADP release. At ~60°, the S transitions to a fast (F) acceleration phase that contains an interim deceleration (ID) phase between 75° - 82°. The energy conversion efficiency from nucleotide hydrolysis to rotary torque has been estimated to be close to 100% based on early single molecule observations of γ-subunit rotation of F_1 (Noji, Yasuda et al. 1997). Based on this result, the rotary torque generated during rotation was assumed to be nearly constant (Oster and Wang 2000) because the high efficiency implies tight coupling between the mechanics and the chemistry such that entropic losses are small. Since torque is directly proportional to the product of the drag and the velocity, the results presented chapter 3 clearly show that the torque is not constant, and thus, any conclusions that rely on the assumption of constant torque must be reexamined.

The results presented in chapter 3 also show that the fractional decrease in ITP-dependent rotational velocity was four-fold larger than the fractional increase in substrate-binding dwells; thus, providing the first direct evidence that nucleotide binding contributes to the generation of torque on the F_1-ATPase molecular motor. This is consistent with theoretical studies (Oster and Wang 2000; Gao, Yang et al. 2003). As shown in Figure 19, ATP can bind to *E. coli* F_1 when the γ-subunit has rotated anywhere from 15° – 50° from the catalytic dwell, with the highest binding affinity occurring at ~35°. This is consistent with the probability for

ATP binding reported for the thermophilic *PS3* enzyme (Yasuda, Noji et al. 2001).

Following the binding of ATP, the γ-subunit is halted by the catalytic dwell after 80° of rotation. The velocity of F_1 rotation powered by ATP, GTP, or ITP during the fast acceleration phase of this 80° rotation was about the same (Figure 21) even though the affinity for ITP at catalytic site-3 is almost 50-fold lower than ATP and GTP (Table 1). This suggests the binding affinity of all three nucleotides exceed a threshold for the minimum energy required to rotate the γ-subunit during the rapid acceleration phase. To explain how ATP binding energy contributes to torque for the final 40° of the power stroke after the catalytic dwell, Wang and Oster (Oster and Wang 2000) postulated that a portion of the energy from ATP binding is stored during the catalytic dwell as elastic energy in the lever arm of the β subunit. Since a greater fraction of the energy derived from ITP binding would be consumed during the first 80° of rotation, less energy is subsequently available to be stored during the catalytic dwell. This would explain the lower ITP-dependent velocity during the 40° power stroke observed in chapter 3. More experiments are required to identify how this energy is stored during the catalytic dwell, although the results presented in chapter 3 provide some insight into this process.

In the presence of high ADP concentrations, it was observed that the rotational velocity of the S phase decreased proportional to the increase in ‘ADP-release’ dwells (Figure 19) similar to that reported for F_1 from the thermophilic bacterium *PS3* (Watanabe, Iino et al. 2008). Furthermore, the addition of ADP to the *E. coli* F_1 also decreased the velocity of the F phase, which was not compensated by a change in the abundance of dwells (Figure 19B). Consequently, the 22% decrease in average rotational rate is solely due to a decrease in velocity. The free energy of the chemical equilibrium of [ADP][Pi]/[ATP] in the presence and absence of the Mg-ADP added in chapter 3 was calculated to be -94.4 pN nm and -116 pN nm, respectively. This 19% difference in free energy approximately corresponded to the fractional decrease in velocity observed during the F phase.

Chapter 4 shows for the first time, single site mutations that can affect the velocity of specific phases of γ-subunit rotation, which in some cases, were in regions of F_1 that were previously considered not to contribute to rotation. The correlations between the structural locations of these mutations and the phases of rotation that they affect provide new insight into the molecular basis for the conformational changes of the protein that contribute to rotation of the γ-subunit. Mutations βD372V and γK9I were found to increase the velocity specifically during the F phase. In the F_1 crystal structure from bovine mitochondria (Menz, Walker et al. 2001) the residue analogous to γK9 is member of a ring of positively charged residues known as the ionic track. Since the negatively charged DELSEED residues at the end of the β-subunit lever arms face the ionic track, electrostatic interactions between DELSEED and the track were initially proposed to propel γ-subunit rotation (Ketchum, Al-Shawi et al. 1998). However, many of the ionic track residues are not conserved, and single molecule experiments of mutants that eliminate the negative charges of the DELSEED residues have been shown to have no effect on torque generation (Hara, Noji et al. 2000). The increase in rotational velocity observed in chapter 4 with the βD372V and γK9I mutations not only confirm that these electrostatic interactions are not contributing to torque, but demonstrate that these interactions slow the average rotational velocity. It is likely that although the two mutations both increase the velocity of the F phase, these effects are not necessarily the result of an interaction of the two residues with each other. This is suggested first by the fact that the bD372V and γK9I mutations accelerate the velocities of the F phase to different extents, and second, by the observation that γK9I uniquely exaggerated the deceleration during the ID phase. This latter effect is possibly explained if electrostatic interactions between γK9 and the negative charges on DELSEED assist in repositioning the β subunit in such a way that reduces the extent of deceleration.

The results presented in chapter 4 show that γT82A was found to decrease the velocity specifically during the S and I phases. The foot and coiled-coil domains are connected by two loops at the end of the coiled-coil. Residue γT82 is part of an electrostatic network between the two domains that minimizes movement of the domains relative to each other. The strength of this electrostatic network is evident by the fact that it remains in place in crystal structures that show up to 43° of rotational movement of the foot domain relative to the coiled-coil (Figure 22B). To explain how ATP binding energy contributes to torque for the 40° power stroke following the catalytic dwell, Wang and Oster (Oster and Wang 2000) postulated that a portion of the energy from ATP binding is stored during the catalytic dwell as elastic energy in the lever arm of the β subunit. The decrease in rotational velocity observed in chapter 4 as the result of γT82A, could occur if the release of stored elastic energy caused the DELSEED lever to push the foot of the γ subunit to rotate counterclockwise. In the absence of the electrostatic network, the mechanical advantage is reduced, resulting in a slower rotation of the foot.

Although the γQ269L mutation had little effect on the rotational velocity during the S and F phases, there was a unique decrease in the velocity during the transition from the S to the F phase. This transition region is likely where the β-subunit catch interactions with the γ-subunit are disrupted and reform with the neighboring α-subunit residue triggered by the binding of ATP. Since the decrease in rotational velocity occurred at this point due to the conversion of a polar to a hydrophobic residue, γQ269 may be important for disengaging the catch from the γ-subunit by forming a hydrogen bond with γR268. This possibility is supported by the relative positions of γQ269, γR268, and β subunit catch loop residues of the empty catalytic site in the *E. coli* F_1 structure where the foot of the γ subunit is rotated 43° relative to the coiled-coil.

The results presented in chapter 4 show that the mutations βD302T and γR268L slowed the velocity only in the I and S phases. Rotation during the I and S phases has been proposed to result from the release of elastic energy stored during the catalytic dwell that opens the DELSEED lever arm to push against the γ-subunit (Chapter 4). The observation that ITP-driven rotation results in a decrease in velocity specifically during the I and S phases supports the hypothesis that energy from substrate binding has been stored in some conformational state of the protein during the catalytic dwell (Oster and Wang 2000). In order for the DELSEED arm to apply the leverage needed to drive γ-subunit rotation of the foot by 40° following the catalytic dwell, the β subunit needs to be anchored opposite to where the leverage is applied. Since the βD302T and γR268L mutations weaken the catch interaction with the γ-subunit, the decreased velocity observed for these mutations may be the result of decreased leverage as the DELSEED arm pushes against the foot of the γ-subunit. This is supported by the position of the DELSEED arm in the site where ADP is released (Site CD in Figure 22A) relative to the foot of the γ-subunit in the bovine F_1 crystal structure 1H8E (Menz, Walker et al. 2001).

All phases of rotation were observed chapter 4 to decrease as the result of the γT273D, βD305E, and αR283Q mutations (Figure 27). Since these residues interact with multiple partners at the three catalytic sites in the course of a rotational event, the underlying causes for the observed differences on rotational velocity are complex. The enzyme is extremely sensitive to mutation at position βD305 such that only the most conservative substitution to the longer glutamate that retains the carboxyl group is tolerated (Boltz and Frasch 2006). This increase in the length of the side chain is likely to cause the decreases in velocity by disrupting the electrostatic networks between the γ-subunit and the β-subunit of the empty catalytic site as well as the salt bridges this residue forms with the αR283 at the other two catalytic sites.

Figure 29 shows a model of γ-subunit rotation illustrating the proposed timing of events that occur during each 120° of rotation. Subunits A, B, and C represent conformations of the α subunits while D, E, and F are β subunits of a specific conformation. Together the αβ-heterodimers of the three catalytic site conformations are designated AE, BF, and CD. The AE site is the conformation in which the DELSEED arm of the β-subunit is in the open position in the absence of bound nucleotide. The BF site contains ATP bound to the catalytic site, and the β-subunit DELSEED lever is in the closed position. The final site, CD has ADP and Pi bound with the lever arm in the closed position.

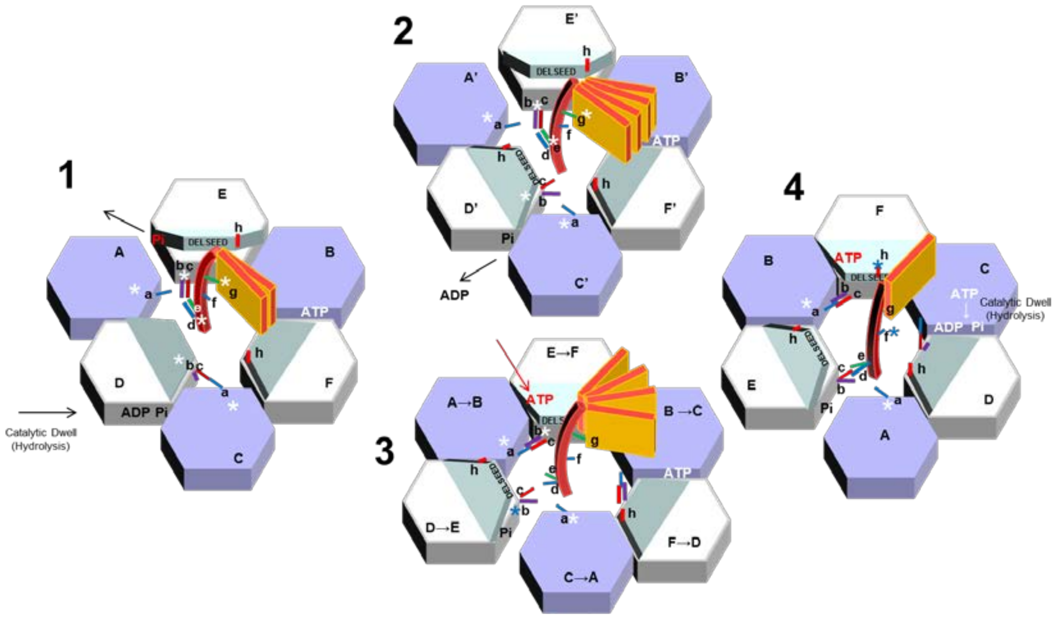

Figure 29. Model of γ-subunit rotation illustrating the proposed timing of events that occur during each 120° rotational event. Conformations of α subunits (A, B, and C) and β subunits (D, E, and F) form catalytic site conformations AE, BF, and CD. Steps 1→2 and 2→3 represent the I (0° - 15°) and S (15 – 60) phases, while Step 3→4 represents the F phase. The asterisks indicate the steps in which changes in velocity were observed as the result of a mutation to residues: a, αR283; b, βD302; c, βD305; d, γR268; e, γQ269; f, γK9; g, γT82; h, βD372.

The model starts at the end of the catalytic dwell during which ATP hydrolysis is believed to occur. Although definitive evidence for Pi release is currently lacking, this product is thought to be released from Site AE during the catalytic dwell, or it defines the end of the catalytic dwell. During Step 1, the elastic energy stored in the DELSEED lever arm located at site CD (the β_{DP} site) is released and drives rotation during the initial 40° (the I and S phases) by pushing on the γ-subunit in a cam shaft manner. At some point during the rotation (Step 2), and likely within the first 40°, Site CD releases ADP but not Pi. However, release of ADP is not necessarily concurrent with the opening of the DELSEED lever arm for Subunit D. The resulting CD conformational change releases the subunit D catch loop residues from interacting with αR283 on C to make them available for binding to the γ-subunit after the final 80° rotational step. In addition the other interactions that hold the D and C subunits together are weakened, and begin to draw apart as the A and E subunits of Site AE draw together during ATP binding.

During Step 3, ATP binds to the AE site and γ-subunit rotation resumes as the DELSEED lever arm of E draws the closed position and pushes on the most eccentric point of the γ-subunit coiled-coil. However, the fast acceleration phase can only be reached after the catch loop residues in the E subunit disengage from the γ-subunit and bind to the adjacent α-subunit A, pulling A and E. During ATP binding, the empty (AE) catalytic site changes its binding affinity and adopts the BF conformation, and in turn the other subunits change from BF→CD, and CD→AE in a cooperative fashion.

Rotation proceeds for 80° (F phase), until the catch loop residues from the newly formed E site stop the rotation and hold the γ-subunit in place (Step 4) to initiate the catalytic dwell and ATP hydrolysis at the end of the rotational event.

Chapter 6

METHODS

Preparation of F_1 Protein

The F_1-ATPase was purified from *E. coli* XL-10 strain. F_1 contains a His_6 tag on the N-terminus of the α-*subunit and γS193C for biotinylation as described previously (Greene and Frasch 2003; York, Spetzler et al. 2007). Membranes were resuspended in Buffer A containing 5.0 mM TES, pH 7, 40 mM ε-amino-caproic acid, 1 mM EDTA, 1 mM DTT, 5.0% (v/v) glycerol, and the mixture was centrifuged at 180,000 × g for 1 hr at 4°C. The supernatant was mixed with Buffer B (0.5 M TRIS/pH 8.0, 1 M KCl, 300 mM imidazole, 50 mM $MgCl_2$) at a 10:1 (v/v) ratio. Glycerol was added to 15% (v/v), and this mixture was loaded on a Ni-NTA column (0.8 cm in diameter, 1.5 cm^3 of resin) washed initially with water and equilibrated with Buffer C (50 mM TRIS/pH 8.0, 100 mM KCl, 30 mM imidazole, 5 mM $MgCl_2$, 15 % glycerol) to bind the F_1-ATPase to the column, and the column was washed with 20 ml of Buffer C. To biotinylate the enzyme, an excess of biotin maleimide (Pierce) was dissolved in 3 ml of Buffer C, which was used to wash the Ni-NTA column containing bound F_1-ATPase. After a wash with 10ml of Buffer C, the column was then flushed with 3 ml of Buffer C containing 180 mM imidazole instead of 30 mM to elute the F_1-ATPase. The F1-ATPase containing solution was then passed through a desalting column (Pierce) equilibrated with Buffer C in order to remove excess imidazole. Biotinylated F_1 was stored at 0.1 mg/ml at -80°C prior to use. The protein prep demonstrated high rotational activity for half a year.

Gold Nanorod Preparation.

Protocols available to make gold nanorods have primarily optimized factors that give rise to a high yield of nanorods with a narrow distribution of size and aspect ratio. However, optimization of the dynamic range of polarized light scattering has not been a priority. Although adding small amounts of Ag during the synthesis of the gold nanorods has improved the yield and uniformity of the nanorods, the presence of Ag decreased the dynamic range significantly.

Nanorods used in the single molecule experiments presented in this work came from both synthesized and commercial sources, or commercial nanorods that were modified. Synthesis of gold nanorods was accomplished through the reduction of $HAuCl_4$ to form 4-nm seeds (Jana, Gearheart et al. 2001). Commercial nanorods were obtained from Nanopartz, Inc., and were also used as a scaffold for growing larger nanorods. In order to maximize their light scattering properties gold nanorods were required to have an aspect ratio of around 1.7 to 1.9 (Huang, Neretina et al. 2009). In addition, the more gold material present in the rod, the more efficient their light scattering properties. Thus, the ideal rod was large, and yet did not exceed the ideal aspect ratio.

Long and narrow gold nanorods fom Nanopartz, Inc. were used as a substrate in order to increase their girth until they reached the optimum aspect ratio of about 1.8. The gold nanorods were added in 1:4 ratio to Solution A (100 mM CTAB, 67 μM $HAuCl_4$, 69 μM Ascorbic Acid, 67 μM Dehydroascorbic acid). Then the gold nanorod solution was placed in 70° C water bath for 30 mins, and then the nanorods were spun down at 5,200 x g for 10 minutes. The aqueous solution was removed from the nanorod pellet, and the pellet was resuspended in distilled deionized water. The sample was spun again at 5,200 x g for 10 minutes, and the solution was carefully decanted, leaving the nanorod pellet intact. Finally, the gold nanorod pellet was resuspended in 1 mM CTAB and was stored at room temperature for up to six months.

Because the synthesis of nanorods is not precise, each nanorod preparation that was either synthesized or obtained commercially was examined by electron microscopy to confirm the distribution of sizes and shapes before use in single molecule experiments. It has been determined that the drag on the motors can be determined precisely based on their dimensions, with the one minor caveat that the drag may be sensitive to the extent of curvature at the ends of the rods (Spetzler, Ishmukhametov et al. 2009).

The prepared rods were functionalized with Neutravidin in order to facilitate binding to biotinylated F_1-ATPase molecules for single molecule rotation experiments. Neutravidin was added directly to the nanorod/CTAB solution to a final concentration of 40 μg/ml. The solution was then shaken at room temperature for 1 hour, and was diluted with

Buffer D (50 mM Tris-Cl/pH 8.0, 10 mM KCl) containing BSA-c. The coating of the nanorods with avidin was verified by confirming a 4-10 nm red shift in the spectrum obtained from a Cary 100 spectrophotometer, and it was determined that the coating lasted about a day.

PEG-400 Utilization

Where PEG-400 was present, the desired volume of PEG-400 was mixed with Buffer D, 60 μM phenol red pH indicator, and the desired amount of $MgCl_2$ and ATP. A 1:2 mole ratio of Mg^{2+}-ATP ratio was maintained to minimize the presence of free Mg^{2+}. Since high concentrations of PEG-400 interfere with the accuracy of measurements by a pH meter, the pH was adjusted by comparing absorbance of the phenol red at 557 nm in the presence and absence of PEG-400.

The viscosity of the solutions was measured with a Brookfield LVDV viscometer with UL adaptor at 28°C, and varied between 1-20 cP (Hornung, Ishmukhametov et al. 2008). **Figure 30** shows the measured viscosity of the assay buffer as a function of the percentage (vol/vol) of PEG 400. These data were used to calculate the shear stress as a function of the shear rate (**Figure 31**).

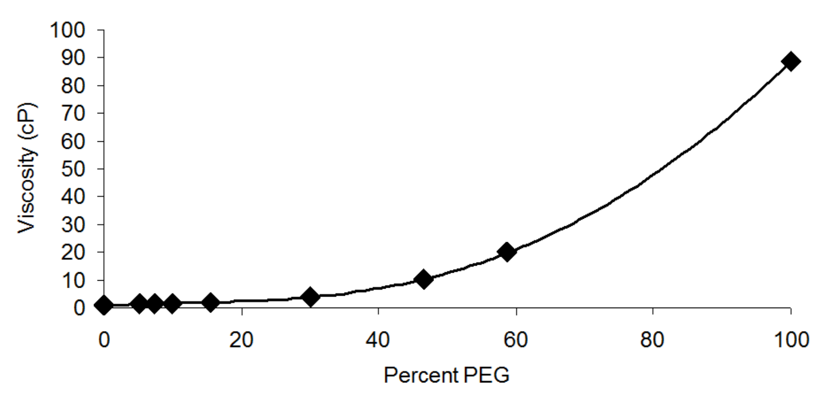

Figure 30. Viscosity of the assay buffer as a function of percent PEG-400 added. The viscosity of the buffer used to make single molecule rotation measurements (Rotation Buffer (50 mM Tris–Cl/pH 8.0, 10 mM KCl)) as a function of its percent composition of PEG 400 (vol/vol). The measurements were made using a Brookfield DVE viscometer with a UL adapter at 28 °C.

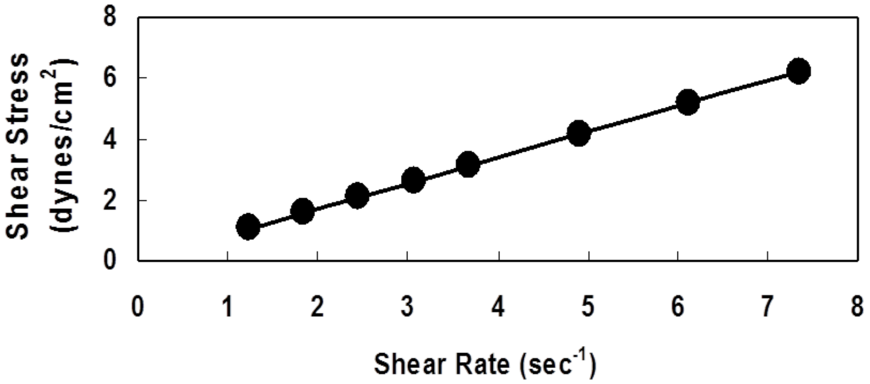

Figure 31. The shear stress as a function of the shear rate of Buffer D containing PEG 400. This was determined by measuring the effect of increasing the velocity on a rotating probe in the Brookfield DV-E viscometer.

The linear dependence between these parameters indicates that the assay buffer containing PEG 400 behaves as a Newtonian fluid. Thus, PEG 400 molecules are too small to be pulled along by the rotating nanorod, and do not make secondary nonlinear contributions to the drag.

ATPase Assay

The bulk activity of F_1 was measured in a buffer containing 55 mM KCl, 5 mM TRIS, pH 8.0, and the indicated amount of ATP in a Cary 100 spectrophotometer at 28°C. Activity was monitored with the ATP regenerating system as described by Greene et al. (Greene and Frasch 2003) and with the phenol red assay as done previously by Ishmukhametov et al. (Ishmukhametov, Galkin et al. 2005). The ATP regenerating system media contained 0.4 mM NADH, 30 mM PEP, 7 units of pyruvate kinase and 7 units of lactate dehydrogenase, except in the case of alternate nucleotides for which the amount of pyruvate kinase added was quadrupled.

Single Molecule Rotation Assay

Single molecule rotation assays were performed as described by Spetzler et al. (Spetzler, York et al. 2006) with the following modifications. A 5 μl droplet of biotinylated F_1-ATPase was bound to the surface of non-functionalized glass slide for 5 minutes instead of Ni-NTA coated cover slips, since there was no measurable difference in dwell or transitions times between the substrates. The slide was then washed thoroughly with Buffer D. Nanodevice assembly (**Figure 32**) was completed by addition of saturating amounts of avidin-coated nanorods and incubated for 5 min at room temperature. This allowed the avidin-coated gold nanorods to be captured by the biotinylated γ-subunit. The slide was washed thoroughly in Buffer D to remove excess nanorods and minimize nonspecific binding. Samples that were examined for rotation included a Buffer D containing Mg2+-NTP at a concentration that maximized F_1-ATPase activity. On average 25% of nanorods were observed to rotate (York, Spetzler et al. 2007).

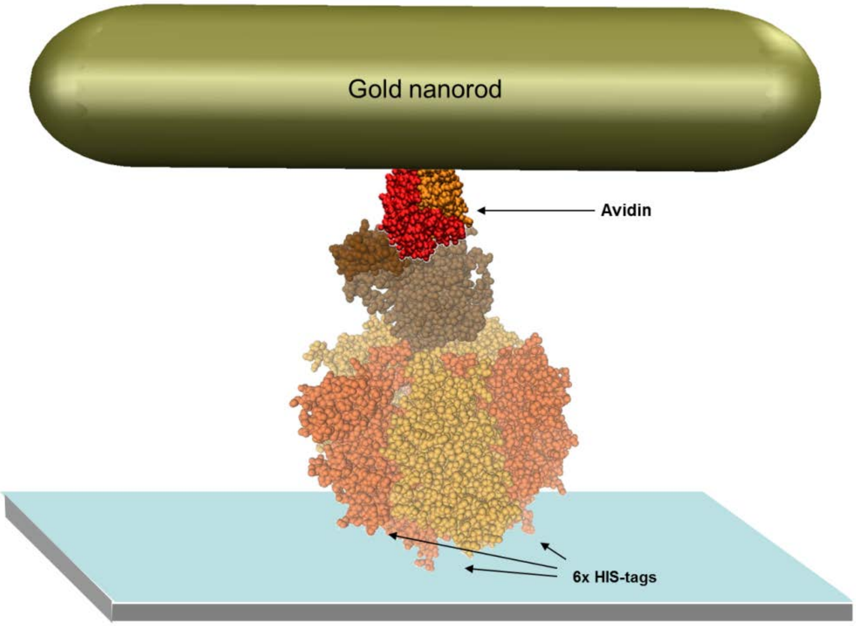

Figure 32. Assembly of gold nanorod probe and the F_1-ATPase on a glass slide. The F_1 is bound to the slide via three 6x His tags engineered onto the N terminus of the α subunit. During purification the F1 is functionalized with biotin through a cysteine residue located on the foot of the γ-subunit. Gold nanorods coated in nuetravidin are then captured by the biotinlylated F_1-ATPase, completing the assembly.

The slide was then observed via dark field microscopy (**Figure 33**), where incident light illuminated the sample at an oblique angle so that only light scattered from the nanorods entered the objective. When scattered light from a nanorod was viewed through a polarizing filter, its intensity changed as a function of the relative angle between its longitudinal and translational axes and the polarizing filter (**Figure 34**).

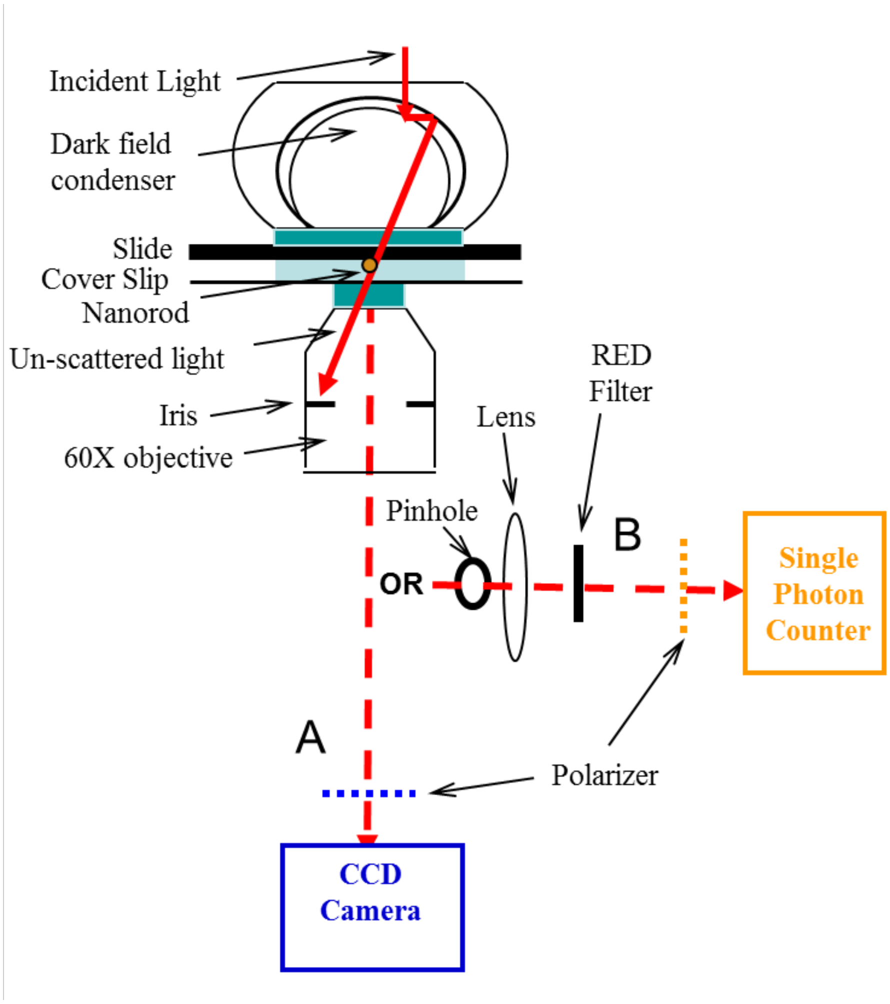

Figure 33. Schematic of the instrument used to make single molecule measurements.

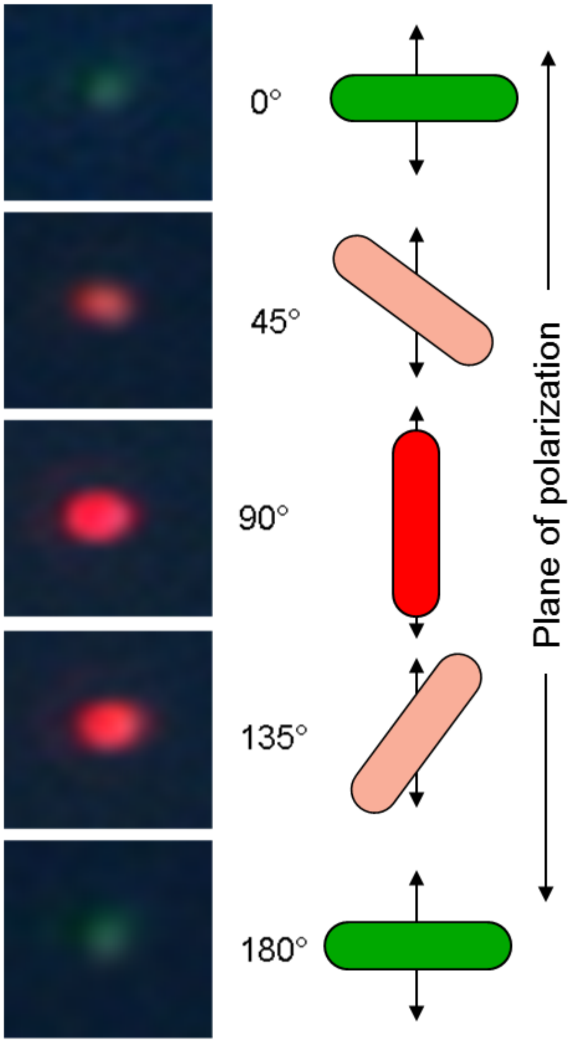

Figure 34. Light-Scattering Properties of Gold Nanorods Viewed Through A Polarizing Filter. (A) Consecutive dark-field micrographs of a stationary rod observed under different positions of the polarized lens. (B) Schematic of a gold nanorod that illustrates the change in red light intensity as the rod is rotated relative to the plane of polarized light.

Light is scattered most efficiently along the rod axes such that the intensity of scattered red light is maximal and minimal when the long and short axes of the rod are parallel and orthogonal to the plane of polarization, respectively. The converse is true for the intensity of scattered green light. Therefore, the intensities of light scattered from a gold nanorod immobilized to a single F_1 γ-subunit change as a function of the polarization angle. The resulting intensity profiles of red and green light follow out-of-phase sine curves.

Single gold nanorods were initially identified to undergo F_1-ATPase-dependent rotation by observing oscillations in light intensity through a polarizing filter via a Zeiss HSC color CCD camera at 55 fps. Each molecule was aligned confocal to a Perkin-Elmer SPCM-AQR-15 single photon detector to quantitate changes in scattered light intensity from the nanorods as a function of time. A total of 100 sec of data was collected in successive 5 sec data sets at each acquisition speed from 10- 200 kHz in 10 kHz increments for each molecule. Temperatures of the slide on the microscope while making the measurements were observed to vary between 27-29° C. The viscosity of the buffer used in these single molecule measurements was varied by increasing the concentration of polyethylene glycol 400 (PEG 400) in the rotation assay buffer (Hornung, Ishmukhametov et al. 2008).

Analysis of Transitions

Since minimum and maximum intensity values of red light scattered from the nanorod occur when the rod is perpendicular and parallel to the plane of polarization, respectively, these minimum and maximum intensity values provide the most sensitive measure of the rotation rate. Thus, the most sensitive measure of a 120° rotational power stroke driven by ATP hydrolysis at saturating Mg^{2+}-ATP will occur in the subset of data that includes the 90° of rotation between these maximum and minimum values. These 90° rotational events in the data set are referred to here as transitions.

The single molecule rotation data is analyzed to identify and measure transitions using custom software written in Mat Lab 6.5 (Spetzler, York et al. 2006). The program first establishes the minimum and maximum intensity values for each data set. Rotational events are then identified as a consecutive group of a minimum of three data points in which the intensity changes from within 5% of the minimum intensity of scattered light to >95% of the maximum or vice versa that also have a linear regression R^2 value of 0.95 or greater. Each group of data points in a transition are stored for use in determining the rotational velocity of each, and collated in a spread sheet. They can be accessed and plotted individually or as a group. The software allows the min/max intensity percentage cut-offs and R^2 values to be varied to examine the variation in the calculation of the rotational velocity. Information concerning the total number of rotational events, average velocity and distribution of events in a given data acquisition is also tabulated.

A schematic of scattered light intensity during three consecutive power strokes (one complete revolution) is shown in **Figure 35** when the nanorod was initially aligned nearly, but not exactly, perpendicular to the polarizer. Since the stochastic nature of the enzyme results in a variation in the rotational position of each catalytic dwell (Yasuda, Noji et al. 2001), the alignment of the nanorod with the polarizer will show small variations during the data collection period. If the nanorod is initially aligned perpendicular to the polarizer and the 3 consecutive power strokes are exactly 120° during a single revolution such that the nanorod is also perpendicular during catalytic dwell 3, the algorithm will analyze transitions from power strokes one and three. In practice, the number of consecutive power strokes analyzed is randomized by the stochastic nature of the molecular motor. Due to the randomization, there is an equal probability that the 90° increments of rotation measured as transitions represents the beginning, the middle, and the end of each 120° power stroke such that the entire power stroke is sampled in the course of the ~3520 power stroke events monitored on average for each molecule during the 50s of data acquisition at 100KHz.

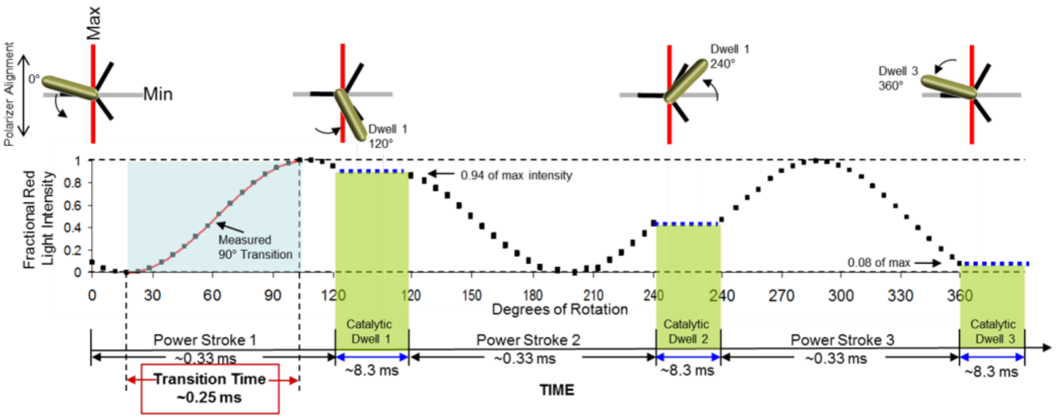

Figure 35. Relationship between a 120° power stroke and a 90° measured rotational transition. Theoretical plot of the intensity of scattered red light from a nanorod during one complete revolution that involves three consecutive power strokes and three consecutive catalytic dwells separated by exactly 120°. The nanorod is initially positioned almost, but not exactly perpendicular to the orientation of the polarizer such that the scattered light intensity goes through a minimum then a maximum prior to catalytic dwell 1. A transition includes the data between the minimum and maximum intensities representing 90° of the 120° of rotation for analysis. When initial alignment of the nanorod is exactly at the minimum and each of the successive power strokes is exactly 120°, the algorithm selects transitions for power strokes 1 (min to max) and 3 (max to min).

Since the intensity of scattered light changes as a sinusoidal function of the rotational position of the nanorod, the degrees of rotation during a transition were derived from the arcsine of the fractional intensity of light scattered from the nanorod by Eq. 1:

$$\theta = (\mathrm{asin}\ I)180\pi^{-1} \qquad (1)$$

where θ is degrees of rotation, and I is the fractional intensity of scattered light. **Figure 36** shows example transitions that have been converted from light intensity to rotational position.

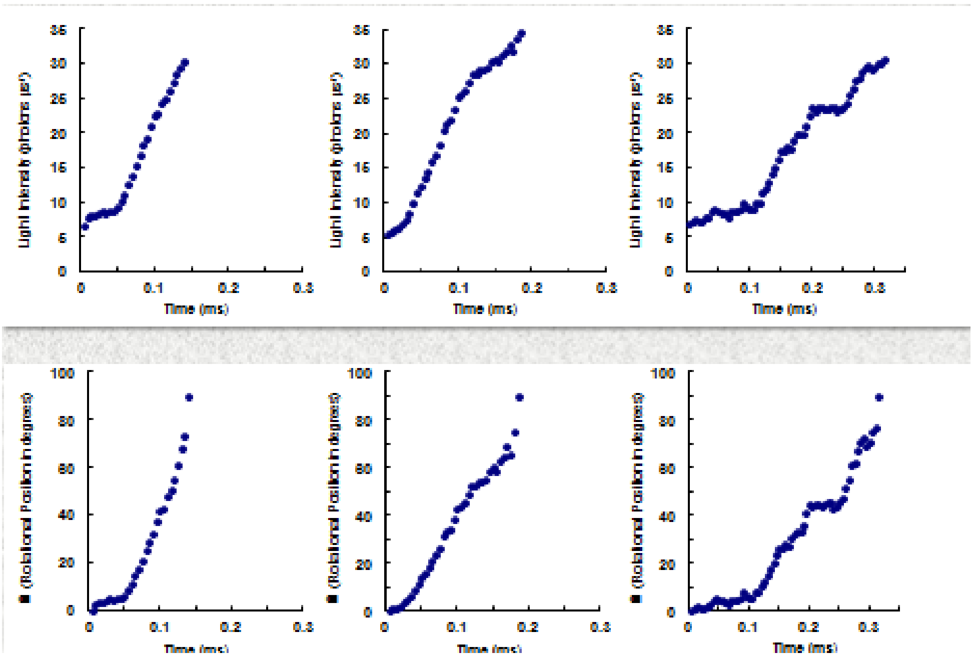

Figure 36. Example Single Transitions of F_1 Power Strokes in the presence of 1 mM Mg^{2+} and 2 mM ATP. (A) Light intensity scattered from a gold nanorod attached to the γ subunit collected at 200kHz as a function of time. The average transition time under these conditions was ~17 ms. (B) Rotational position of the γ subunit as a function of time calculated from the transitions in (A) using Eq. 1.

Analysis of Catalytic Dwells

The average dwell time was calculated by determining the number of hydrolysis events that occurred in a given time frame. This was measured by counting the number of times that the scattered light intensity spanned the 5th and 95th percentile of the dynamic range of the intensity of that data set. The average dwell time was calculated by dividing the total time by the number of 5th-95th percentile events.

Analysis of Rotational Direction

The optional use of two photon counters to acquire rotation data (**Figure 37**) provides the ability to determine the direction of rotation. The exact number of degrees of offset between the two polarizers is not important, but it must be sufficient to distinguish the time that a power stroke is detected by the two single photon counters (**Figure 38A**). Simply, CCW rotation is indicated when photon counter 1 detects a power stroke before photon counter 2 and vice versa for CW rotation. By tracking the changes in intensity with a known polarization phase shift between the detectors, an algorithm can calculate the exact angular position of the Nanorod and the direction of rotation throughout during the entire data set. An example is shown in **Figure 38B and 38C**.

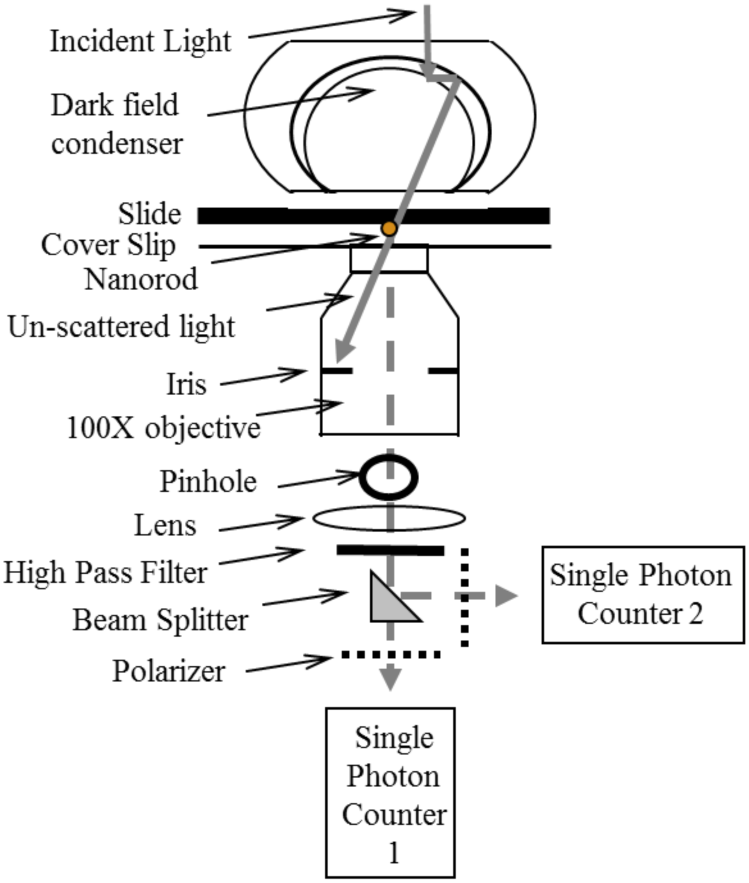

Figure 37. Schematic of the dark-field microscope used to make measurements to determine rotational direction. In this configuration, the scattered light from a single rotating gold nanorod (dashed line) passes through a beam splitter for measurement by two single photon counting avalanche photodiode detectors when the orientation of the polarizer for detector 1 is offset from that of detector 2.

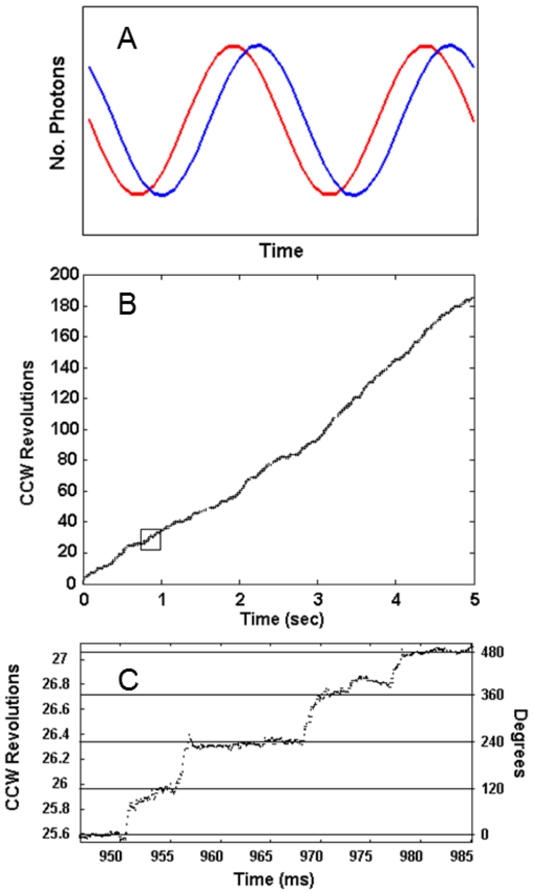

Figure 38. Detection of rotation direction using 2 offset polarizers. (A) Theoretical plot of changes in intensity of red scattered light observed from two single rotating nanorod by two photon counters when the orientation of the polarizer for detector 1 is offset from that of detector 2. (B) Experimental time course of rotational position of the g subunit in a single F1 molecule determined from data acquired at 10 kHz with two photon counters in which the orientation of the polarizer for detector 1 was offset from that of detector 2. The substrate concentration was 1 mM MgCl2 and 2 mM ATP. (C) Detail of the rotational stepping of the boxed region of (b). Horizontal lines indicate the 120° catalytic dwell positions.

Determination of Pauses during Rotation

Determination of the possible impact that dwells have on rotation was accomplished by using an algorithm that determines when rotation has paused. The algorithm examined individual transitions, and using Equation 1, converted the intensity scattered from the nanorod during a transition to degrees of rotation. Then, the data was binned according to the rotational position, and during a pause in rotation, counts would accrue in the bin at which rotation had stopped (**Figure 39**). A threshold value was then calculated by rounding up the average of all the bins between 10° and 90° that were greater than the positive minimum of all the bins. All contiguous bins greater than the threshold, were considered to be a pause, and the duration and location of all pauses in each transition were compiled for further analysis.

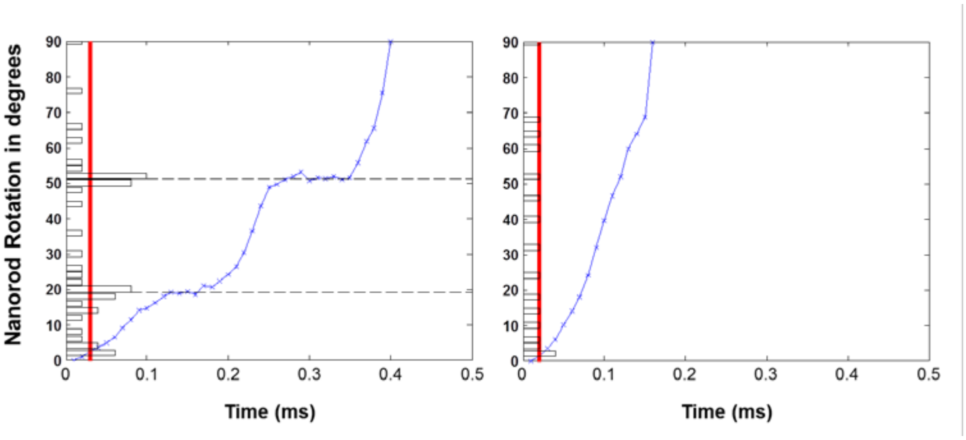

Figure 39. Analysis of transitions using an algorithm to identify pauses. Both panels depict a transition as it rotates 90° after the catalytic dwell. A histogram of rotational position is plotted on the y axis, and as a transition pauses, data points accumulate dependent upon the duration of the pause. Pausing (dotted horizontal line) is identified by bins that are greater than a threshold (red line).

Determination of Average Rotational Velocity

Rotational velocities were calculated using a Matlab algorithm that converted the intensity of scattered light to degrees of rotation for each transition. Then the velocity was calculated between neighboring data points by determining their slope as shown in **Figure 40**. The average velocities were then calculated for every 3 degrees of rotation by collating all the calculated velocities that had an initial starting position within that bin and finding their average.

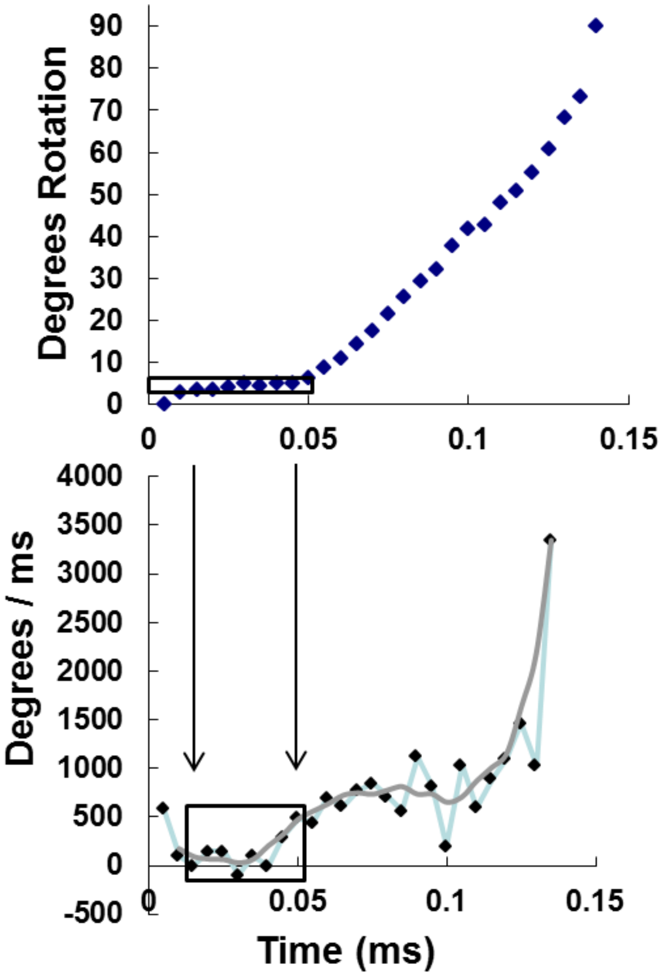

Figure 40. Determination of average rotational velocity of individual transitions for the F_1 ATPase. Velocity was determined at each rotational position by calculating the slope for neighboring data points and plotting it as a function of time. The average rotational velocities for three degrees of rotation was determined by averaging all the calculated velocities (black box, bottom) for data points that originated within a three degree rotational window (black box, top).

Load on F_1 and Torque Calculations

The load imposed on the motor can be varied by changing the size of the nanorod and/or by increasing the viscosity of the medium (REF). The viscosity was varied by the inclusion of PEG400 in the solution because it was determined that PEG400 molecules behave as a Newtonian fluid (Hornung, Ishmukhametov et al. 2008). As such, they are too small to be pulled along by the rotating nanorod, and thus do not make secondary nonlinear contributions to the drag. The increased drag on the gold nanorod due to the viscosity of the PEG400 solution exerts a load on the motor that slows the power stroke velocity, which can be used to determine the torque (Hornung, Ishmukhametov et al. 2008). For a given size of nanorod, the angular velocity is determined by the rotational distance (arc distance) divided by time. In the absence of the transient dwell, the average angular velocity is calculated using the arc distance of the rod moving 90° divided by the transition time. In the presence of the transient dwell, the average angular velocity is the arc distance of the rod moving 36° divided by the average time between transient dwells.

Torque is calculated from the drag and the velocity by Eq. 2:

$$T = \Gamma w, \qquad (2)$$

where Γ is the drag force, and w is the angular velocity of the power stroke.

Comparison of direct measurements of the drag on the nanorod (Hornung, Ishmukhametov et al. 2008) showed that the propeller model provided a close approximation of the drag force as a function of PEG400 concentration. Based on this model, the drag force is approximated by Eq. (3),

$$\Gamma = \frac{4\pi\mu(L_1^3 + L_2^3)}{3\cosh^{-1}(h/r)}, \qquad (3)$$

where L_1 and L_2 are the length of the propeller extending from the rotational axis, *r* is the radius of the rod, μ is the viscosity of the medium, and *h* is the height of the cylinder axis relative to the surface. Values for the viscosity of a solution of PEG400 in the buffer used for these rotation measurements is provided in (Hornung, Ishmukhametov et al. 2008). The drag generated by a 77x39 nm gold nanorod will vary depending on whether the axis of rotation is at the end or in the middle of the nanorod.

Error in scattered light intensities

The error in the determination of rotational position primarily results from variations in the intensity of scattered photons from the nanorod. The distribution of light intensity scattered from the nanorod was narrower at polarizer angles in which the intensity was at a minimum than that observed at the maximum. Based on the data of **Figure 41**, the standard error in the measurement varied between about 0.02° and 0.12° as the scattered light intensity varied between minimum and maximum values (Ishmukhametov 2010).

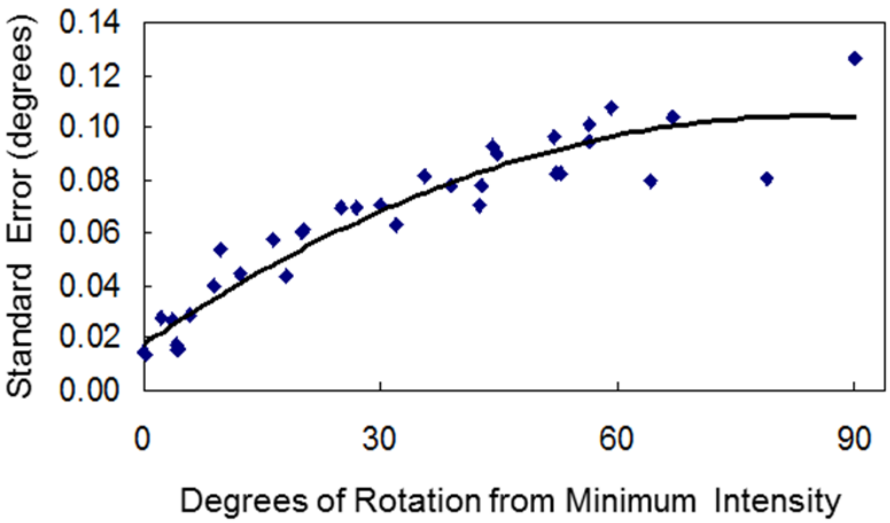

Figure 41. Standard error as determined from scattered light intensities. Standard error of nanorod rotational position versus degrees of rotation of the polarizer from the minimum intensity of light scattered from the nanorod as determined by Equation (1).

REFERENCES

Abrahams, J. P., A. G. Leslie, et al. (1994). "Structure at 2.8 A resolution of F1-ATPase from bovine heart mitochondria." Nature **370**(6491): 621-628.

Abrahams, J. P., A. G. W. Leslie, et al. (1994). "Structure at 2.8-Angstrom Resolution of F1-Atpase from Bovine Heart-Mitochondria." Nature **370**(6491): 621-628.

Adachi, K., T. Nishizaka, et al. (2003). "Imaging of multisite catalysis in F1-ATPase." Biophysical Journal **84**(2): 121a-121a.

Adachi, K., K. Oiwa, et al. (2007). "Coupling of rotation and catalysis in F(1)-ATPase revealed by single-molecule imaging and manipulation." Cell **130**(2): 309-321.

Adachi, K., R. Yasuda, et al. (2000). "Stepping rotation of F1-ATPase visualized through angle-resolved single-fluorophore imaging." Proc Natl Acad Sci U S A **97**(13): 7243-7247.

Al-Shawi, M. K., C. J. Ketchum, et al. (1997). "Energy coupling, turnover, and stability of the F0F1 ATP synthase are dependent on the energy of interaction between gamma and beta subunits." J Biol Chem **272**(4): 2300-2306.

Al-Shawi, M. K. and R. K. Nakamoto (1997). "Mechanism of energy coupling in the FOF1-ATP synthase: the uncoupling mutation, gammaM23K, disrupts the use of binding energy to drive catalysis." Biochemistry **36**(42): 12954-12960.

Bi, Y., J. C. Watts, et al. (2008). "Probing the functional tolerance of the b subunit of Escherichia coli ATP synthase for sequence manipulation through a chimera approach." Biochim Biophys Acta **1777**(7-8): 583-591.

Boltz, K. W. and W. D. Frasch (2006). "Hydrogen bonds between the alpha and beta subunits of the F1-ATPase allow communication between the catalytic site and the interface of the beta catch loop and the gamma subunit." Biochemistry **45**(37): 11190-11199.

Borsch, M., M. Diez, et al. (2002). "Stepwise rotation of the gamma-subunit of EF(0)F(1)-ATP synthase observed by intramolecular single-molecule fluorescence resonance energy transfer." FEBS Lett **527**(1-3): 147-152.

Borsch, M., P. Turina, et al. (1998). "Conformational changes of the H+-ATPase from Escherichia coli upon nucleotide binding detected by single molecule fluorescence." FEBS Lett **437**(3): 251-254.

Bowler, M. W., M. G. Montgomery, et al. (2007). "Ground state structure of F1-ATPase from bovine heart mitochondria at 1.9 A resolution." J Biol Chem **282**(19): 14238-14242.

Boyer, P. D. (1975). "A model for conformational coupling of membrane potential and proton translocation to ATP synthesis and to active transport." FEBS Lett **58**(1): 1-6.

Boyer, P. D. (1997). "The ATP synthase--a splendid molecular machine." Annu Rev Biochem **66**: 717-749.

Boyer, P. D. (2000). "Catalytic site forms and controls in ATP synthase catalysis." Biochimica Et Biophysica Acta-Bioenergetics **1458**(2-3): 252-262.

Braig, K., R. I. Menz, et al. (2000). "Structure of bovine mitochondrial F(1)-ATPase inhibited by Mg(2+) ADP and aluminium fluoride." Structure Fold Des **8**(6): 567-573.

Caviston, T. L., C. J. Ketchum, et al. (1998). "Identification of an uncoupling mutation affecting the b subunit of F1F0 ATP synthase in Escherichia coli." FEBS Lett **429**(2): 201-206.

Cherepanov, D. A. and W. Junge (2001). "Viscoelastic dynamics of actin filaments coupled to rotary F-ATPase: Curvature as an indicator of the torque." Biophysical Journal **81**(3): 1234-1244.

Cingolani, G. and T. M. Duncan (2011). "Structure of the ATP synthase catalytic complex (F-1) from Escherichia coli in an autoinhibited conformation." Nature Structural & Molecular Biology **18**(6): 701-U100.

Dmitriev, O., P. C. Jones, et al. (1999). "Structure of the membrane domain of subunit b of the Escherichia coli F0F1 ATP synthase." J Biol Chem **274**(22): 15598-15604.

Fillingame, R. H., C. M. Angevine, et al. (2002). "Coupling proton movements to c-ring rotation in F(1)F(o) ATP synthase: aqueous access channels and helix rotations at the a-c interface." Biochim Biophys Acta **1555**(1-3): 29-36.

Fischer, S., P. Graber, et al. (2000). "The activity of the ATP synthase from Escherichia coli is regulated by the transmembrane proton motive force." Journal of Biological Chemistry **275**(39): 30157-30162.

Frasch, W. D. (2000). "The participation of metals in the mechanism of the F(1)-ATPase." Biochim Biophys Acta **1458**(2-3): 310-325.

Furuike, S., M. D. Hossain, et al. (2008). "Axle-less F-1-ATPase rotates in the correct direction." Science **319**(5865): 955-958.

Futai, M., H. Omote, et al. (1995). "Escherichia coli H(+)-ATPase (ATP synthase): catalytic site and roles of subunit interactions in energy coupling." Biochem Soc Trans **23**(4): 785-789.

Gao, Y. Q., W. Yang, et al. (2003). "A model for the cooperative free energy transduction and kinetics of ATP hydrolysis by F1-ATPase." Proc Natl Acad Sci U S A **100**(20): 11339-11344.

Gibbons, C., M. G. Montgomery, et al. (2000). "The structure of the central stalk in bovine F(1)-ATPase at 2.4 A resolution." Nat Struct Biol **7**(11): 1055-1061.

Greene, M. D. and W. D. Frasch (2003). "Interactions among gamma R268, gamma Q269, and the beta subunit catch loop of Escherichia coli F1-ATPase are important for catalytic activity." J Biol Chem **278**(51): 51594-51598.

Greie, J. C., G. Deckers-Hebestreit, et al. (2000). "Secondary structure composition of reconstituted subunit b of the Escherichia coli ATP synthase." Eur J Biochem **267**(10): 3040-3048.

Hara, K. Y., H. Noji, et al. (2000). "The role of the DELSEED motif of the beta subunit in rotation of F1-ATPase." J Biol Chem **275**(19): 14260-14263.

Hara, K. Y., H. Noji, et al. (2000). "The role of the DELSEED motif of the beta subunit in rotation of F-1-ATPase." Journal of Biological Chemistry **275**(19): 14260-14263.

Hausrath, A. C., G. Gruber, et al. (1999). "Structural features of the gamma subunit of the Escherichia coli F(1) ATPase revealed by a 4.4-A resolution map obtained by x-ray crystallography." Proc Natl Acad Sci U S A **96**(24): 13697-13702.

Hirono-Hara, Y., H. Noji, et al. (2001). "Pause and rotation of F(1)-ATPase during catalysis." Proc Natl Acad Sci U S A **98**(24): 13649-13654.

Hisabori, T., A. Kondoh, et al. (1999). "The gamma subunit in chloroplast F(1)-ATPase can rotate in a unidirectional and counter-clockwise manner." FEBS Lett **463**(1-2): 35-38.

Hornung, T., R. Ishmukhametov, et al. (2008). "Determination of torque generation from the power stroke of Escherichia coli F1-ATPase." Biochim Biophys Acta **1777**(7-8): 579-582.

Huang, X. H., S. Neretina, et al. (2009). "Gold Nanorods: From Synthesis and Properties to Biological and Biomedical Applications." Advanced Materials **21**(48): 4880-4910.

Hunt, A. J., F. Gittes, et al. (1994). "The force exerted by a single kinesin molecule against a viscous load." Biophys J **67**(2): 766-781.

Ishmukhametov, R., Hornung, T., Spetzler, D. and Frasch, W. D. (2010). "Direct Observation of Stepped proteolipid ring rotation in *E. coli* F_oF_1 ATP Synthase." EMBO J **29**: in press.

Ishmukhametov, R. R., M. A. Galkin, et al. (2005). "Ultrafast purification and reconstitution of His-tagged cysteine-less Escherichia coli F1Fo ATP synthase." Biochim Biophys Acta **1706**(1-2): 110-116.

Jana, N. R., L. Gearheart, et al. (2001). "Wet Chemical Synthesis of high aspect ratio cylindrical gold nanorods." Phys.Chem **105**: 4065-4067.

Jault, J. M., C. Dou, et al. (1996). "The alpha3beta3gamma subcomplex of the F1-ATPase from the thermophilic bacillus PS3 with the betaT165S substitution does not entrap inhibitory MgADP in a catalytic site during turnover." J Biol Chem **271**(46): 28818-28824.

Jiang, W. P., J. Hermolin, et al. (2001). "The preferred stoichiometry of c subunits in the rotary motor sector of Escherichia coli ATP synthase is 10." Proceedings of the National Academy of Sciences of the United States of America **98**(9): 4966-4971.

Junge, W., D. Sabbert, et al. (1996). "Rotatory catalysis by F-ATPase: Real-time recording of intersubunit rotation." Berichte Der Bunsen-Gesellschaft-Physical Chemistry Chemical Physics **100**(12): 2014-2019.

Kabaleeswaran, V., N. Puri, et al. (2006). "Novel features of the rotary catalytic mechanism revealed in the structure of yeast F1 ATPase." EMBO J **25**(22): 5433-5442.

Karplus, M., Y. Q. Gao, et al. (2005). "Protein structural transitions and their functional role." Philosophical Transactions of the Royal Society of London Series a-Mathematical Physical and Engineering Sciences **363**(1827): 331-355.

Ketchum, C. J., M. K. Al-Shawi, et al. (1998). "Intergenic suppression of the gammaM23K uncoupling mutation in F0F1 ATP synthase by betaGlu-381 substitutions: the role of the beta380DELSEED386 segment in energy coupling." Biochem J **330 (Pt 2)**: 707-712.

Kinosita, K., Jr., K. Adachi, et al. (2004). "Rotation of F1-ATPase: How an ATP-driven molecular machine may work." Annu Rev Biophys Biomol Struct **33**: 245-268.

Kinosita, K., Jr., R. Yasuda, et al. (2000). "A rotary molecular motor that can work at near 100% efficiency." Philos Trans R Soc Lond B Biol Sci **355**(1396): 473-489.

Matsui, T., E. Muneyuki, et al. (1997). "Catalytic activity of the alpha3beta3gamma complex of F1-ATPase without noncatalytic nucleotide binding site." J Biol Chem **272**(13): 8215-8221.

Menz, R. I., J. E. Walker, et al. (2001). "Structure of bovine mitochondrial F(1)-ATPase with nucleotide bound to all three catalytic sites: implications for the mechanism of rotary catalysis." Cell **106**(3): 331-341.

Nadanaciva, S., J. Weber, et al. (2000). "New probes of the F1-ATPase catalytic transition state reveal that two of the three catalytic sites can assume a transition state conformation simultaneously." Biochemistry **39**(31): 9583-9590.

Nakamoto, R. K., C. J. Ketchum, et al. (1999). "Rotational coupling in the F0F1 ATP synthase." Annu Rev Biophys Biomol Struct **28**: 205-234.

Noji, H., K. Hasler, et al. (1999). "Rotation of Escherichia coli F(1)-ATPase." Biochem Biophys Res Commun **260**(3): 597-599.

Noji, H., K. Hasler, et al. (1999). "Rotation of Escherichia coli F-1-ATPase." Biochemical and Biophysical Research Communications **260**(3): 597-599.

Noji, H., R. Yasuda, et al. (1997). "Direct observation of the rotation of F1-ATPase." Nature **386**(6622): 299-302.

O'Neal, C. C. and P. D. Boyer (1984). "Assessment of the rate of bound substrate interconversion and of ATP acceleration of product release during catalysis by mitochondrial adenosine triphosphatase." J Biol Chem **259**(9): 5761-5767.

Omote, H., N. Sambonmatsu, et al. (1999). "The gamma-subunit rotation and torque generation in F1-ATPase from wild-type or uncoupled mutant Escherichia coli." Proc Natl Acad Sci U S A **96**(14): 7780-7784.

Oster, G. and H. Wang (2000). "Reverse engineering a protein: the mechanochemistry of ATP synthase." Biochim Biophys Acta **1458**(2-3): 482-510.

Panke, O., D. A. Cherepanov, et al. (2001). "Viscoelastic dynamics of actin filaments coupled to rotary F-ATPase: Angular torque profile of the enzyme." Biophysical Journal **81**(3): 1220-1233.

Pilizota, T., T. Bilyard, et al. (2007). "A programmable optical angle clamp for rotary molecular motors." Biophysical Journal **93**(1): 264-275.

Pogoryelov, D., Y. Nikolaev, et al. (2008). "Probing the rotor subunit interface of the ATP synthase from Ilyobacter tartaricus." Febs Journal **275**(19): 4850-4862.

Sabbert, D., S. Engelbrecht, et al. (1996). "Intersubunit rotation in active F-ATPase." Nature **381**(6583): 623-625.

Sakaki, N., R. Shimo-Kon, et al. (2005). "One rotary mechanism for F1-ATPase over ATP concentrations from millimolar down to nanomolar." Biophysical Journal **88**(3): 2047-2056.

Senior, A. E. (2007). "ATP synthase: motoring to the finish line." Cell **130**(2): 220-221.

Senior, A. E., S. Nadanaciva, et al. (2002). "The molecular mechanism of ATP synthesis by F1F0-ATP synthase." Biochim Biophys Acta **1553**(3): 188-211.

Shimabukuro, K., R. Yasuda, et al. (2003). "Catalysis and rotation of F1 motor: cleavage of ATP at the catalytic site occurs in 1 ms before 40 degree substep rotation." Proc Natl Acad Sci U S A **100**(25): 14731-14736.

Sielaff, H., H. Rennekamp, et al. (2008). "Functional halt positions of rotary FOF1-ATPase correlated with crystal structures." Biophys J **95**(10): 4979-4987.

Sonnichsen, C. and A. P. Alivisatos (2005). "Gold nanorods as novel nonbleaching plasmon-based orientation sensors for polarized single-particle microscopy." Nano Lett **5**(2): 301-304.

Soong, R. K., G. D. Bachand, et al. (2000). "Powering an inorganic nanodevice with a biomolecular motor." Science **290**(5496): 1555-1558.

Spetzler, D., R. Ishmukhametov, et al. (2009). "Single molecule measurements of F1-ATPase reveal an interdependence between the power stroke and the dwell duration." Biochemistry **48**(33): 7979-7985.

Spetzler, D., J. York, et al. (2006). "Microsecond Time Scale Rotation Measurements of Single F(1)-ATPase Molecules." Biochemistry **45**(10): 3117-3124.

Spudich, J. A. (2006). "Molecular motors take tension in stride." Cell **126**(2): 242-244.

Stock, D., C. Gibbons, et al. (2000). "The rotary mechanism of ATP synthase." Curr Opin Struct Biol **10**(6): 672-679.

Stock, D., A. G. Leslie, et al. (1999). "Molecular architecture of the rotary motor in ATP synthase." Science **286**(5445): 1700-1705.

Tanigawara, M., K. V. Tabata, et al. (2012). "Role of the DELSEED Loop in Torque Transmission of F-1-ATPase." Biophysical Journal **103**(5): 970-978.

Usukura, E., T. Suzuki, et al. (2012). "Torque Generation and Utilization in Motor Enzyme F0F1-ATP Synthase HALF-TORQUE F-1 WITH SHORT-SIZED PUSHROD HELIX AND REDUCED ATP SYNTHESIS BY HALF-TORQUE F0F1." Journal of Biological Chemistry **287**(3): 1884-1891.

Volkov, O. A., T. M. Zaida, et al. (2009). "De-novo modeling and ESR validation of a cyanobacterial F(o)F(1)-ATP synthase subunit bb' left-handed coiled coil." Biochim Biophys Acta **1787**(3): 183-190.

Watanabe, R., K. Hayashi, et al. (2011). "Structural Fluctuation and Catalytic Function of F-1-ATPase." Biophysical Journal **100**(3): 226-226.

Watanabe, R., R. Iino, et al. (2010). "Phosphate release in F-1-ATPase catalytic cycle follows ADP release." Nat Chem Biol **6**(11): 814-820.

Watanabe, R., R. Iino, et al. (2008). "Temperature-sensitive reaction intermediate of F1-ATPase." EMBO Rep **9**(1): 84-90.

Watanabe, R., D. Okuno, et al. (2012). "Mechanical modulation of catalytic power on F1-ATPase." Nat Chem Biol **8**(1): 86-92.

Watanabe, R., D. Okuno, et al. (2012). "Mechanical modulation of catalytic power on F-1-ATPase." Nat Chem Biol **8**(1): 86-92.

Weber, J. and A. E. Senior (1997). "Catalytic mechanism of F1-ATPase." Biochim Biophys Acta **1319**(1): 19-58.

Weber, J. and A. E. Senior (2000). "Features of F(1)-ATPase catalytic and noncatalytic sites revealed by fluorescence lifetimes and acrylamide quenching of specifically inserted tryptophan residues." Biochemistry **39**(18): 5287-5294.

Weber, J. and A. E. Senior (2001). "Bi-site catalysis in F1-ATPase: does it exist?" J Biol Chem **276**(38): 35422-35428.

Weber, J. and A. E. Senior (2004). "Fluorescent probes applied to catalytic cooperativity in ATP synthase." Methods Enzymol **380**: 132-152.

Weber, J., S. Wilke-Mounts, et al. (1993). "Specific placement of tryptophan in the catalytic sites of Escherichia coli F1-ATPase provides a direct probe of nucleotide binding: maximal ATP hydrolysis occurs with three sites occupied." J Biol Chem **268**(27): 20126-20133.

Wilkens, S. (2005). "Rotary molecular motors." Adv Protein Chem **71**: 345-382.

Yang, W., Y. Q. Gao, et al. (2003). "The missing link between thermodynamics and structure in F1-ATPase." Proc Natl Acad Sci U S A **100**(3): 874-879.

Yasuda, R., H. Noji, et al. (1998). "F1-ATPase is a highly efficient molecular motor that rotates with discrete 120 degree steps." Cell **93**(7): 1117-1124.

Yasuda, R., H. Noji, et al. (2001). "Resolution of distinct rotational substeps by submillisecond kinetic analysis of F-1-ATPase." Nature **410**(6831): 898-904.

York, J., D. Spetzler, et al. (2007). "Abundance of Escherichia coli F1-ATPase molecules observed to rotate via single-molecule microscopy with gold nanorod probes." J Bioenerg Biomembr **39**(5-6): 435-439.

Yoshida, M., E. Muneyuki, et al. (2001). "ATP synthase--a marvellous rotary engine of the cell." Nat Rev Mol Cell Biol **2**(9): 669-677.

APPENDIX A

ABUNDANCE OF ESCHERICHIA COLI F_1-ATPASE MOLECULES OBSERVED TO ROTATE VIA SINGLE-MOLECULE MICROSCOPY WITH GOLD NANOROD PROBES

J Bioenerg Biomembr (2007) 39:435–439
DOI 10.1007/s10863-007-9114-x

TRANSPORT ATPASES: STRUCTURE, MECHANISM AND RELEVANCE TO MULTIPLE DISEASES

Abundance of *Escherichia coli* F_1-ATPase molecules observed to rotate via single-molecule microscopy with gold nanorod probes

Justin York · David Spetzler · Tassilo Hornung · Robert Ishmukhametov · James Martin · Wayne D. Frasch

Abstract The abundance of *E. coli* F_1-ATPase molecules observed to rotate using gold nanorods attached to the γ-subunit was quantitated. Individual F_1 molecules were determined to be rotating based upon time dependent fluctuations of red and green light scattered from the nanorods when viewed through a polarizing filter. The average number of F_1 molecules observed to rotate in the presence of GTP, ATP, and without nucleotide was ~50, ~25, and ~4% respectively. In some experiments, the fraction of molecules observed to rotate in the presence of GTP was as high as 65%. These data indicate that rotational measurements made using gold nanorods provide information of the F_1-ATPase mechanism that is representative of the characteristics of the enzyme population as a whole.

Keywords F_1-ATPase · Gold nanorods · Plasmon resonance · Molecular motors · Single molecule microscopy

Introduction

The F_1F_o ATP synthase is composed of a transmembrane F_o complex and extrinsic membrane F_1 complex that work together to couple the energy from a nonequilibrium transmembrane proton gradient into the synthesis of ATP from ADP and phosphate. Both complexes are rotary molecular motors that use a common drive shaft composed of the γ and ε subunits. The F_1-ATPase driven rotation and F_o-proton gradient driven rotation of the ε and γ subunits occur in opposite directions (Noji et al. 1997; Borsch et al. 2002).

The F_1-ATPase can be purified from F_o and the membrane, and studied as a soluble protein. Hydrolysis of ATP occurs at the interface of each of the three $\alpha\beta$ subunit heterodimers that form a ring around the coiled-coil domain of the γ subunit (Abrahams et al. 1994). When F_1 is attached to a Ni-NTA coated microscope slide via histidine tags on α or β subunits, and a visible probe is attached to the γ-subunit, single molecules of the γ-subunit can be observed to rotate via microscopy (Noji et al. 1997). In the presence of saturating amounts of substrate, the F_1 γ-subunit rotates in 120° step increments that correspond to the hydrolysis of one ATP per event (Yasuda et al. 1998).

When fluorescent actin filaments were used as a reporter group to visualize rotation, Noji et al. (1997) observed less than 2% of F_1 from the thermophilic bacterium *PS3* to rotate, whereas Adachi et al. (2000) observed 10%. About 5% of *E. coli* F_1-ATPase molecules examined using actin filaments were observed to rotate (Panke et al. 2000). Actin filaments are very large with respect to $F_{1,}$ which increases the potential for these probes to interfere significantly with the ability of the motors to drive rotation. Rotation has also been detected using nanospheres that varied from 40 nm to 1 μm in diameter as probes. These measurements rely on the ability to detect the eccentricity of γ subunit rotation through calculation of the centriod movement of a diffraction-limited 250 nm diameter spot of green light scattered from the nanosphere, and measured with a video

Electronic supplementary material The online version of this article (doi: 10.1007/s10863-007-9114-x) contains supplementary material, which is available to authorized users.

This work was supported by National Institutes of Health grant GM50202 to W.D.F.

J. York · D. Spetzler · T. Hornung · R. Ishmukhametov · J. Martin · W. D. Frasch (✉)
School of Life Sciences, Arizona State University,
P.O. Box 874501, Tempe, AZ 85287-4501, USA
e-mail: Frasch@asu.edu

or digital camera (Yasuda et al. 2001). The fraction of molecules observed to rotate increased to about 10% for *E. coli* F_1 through the use of nanospheres as rotation probes (Nakanishi-Matsui et al. 2006). Although the causes of such a low yield of rotating molecules remain unclear, this observation has been explained by postulating that only 10% of the molecules in an F_1 preparation are active, and that the active motors hydrolyze ATP at a rate 10-fold higher than would be expected from bulk measurements (Nakanishi-Matsui et al. 2006). However, because such a small percentage of the population of molecules has been observed to rotate, it has been difficult to conclude that the measurements made that characterize rotation are representative of the enzyme population as a whole.

Spetzler et al. (2006) recently reported a new method to detect F_1-ATPase rotation using 35×75 nm gold nanorod probes viewed through a polarizing filter. The nanorods scatter green and red light intensely when the long axis is perpendicular and parallel to the plane of a polarizing filter, respectively (Raschke et al. 2003; Sonnichsen and Alivisatos 2005), such that F_1-ATPase-driven rotation of these probes results in a predictable color change. The large dynamic range of intensity fluctuations of the red and green light as a function of the angular position between the nanorod and the polarizing filter provides a much more sensitive means to identify rotation compared to previous methods. Using a single photon counter, variations in intensity of the scattered red light from one F_1-bound nanorod allowed precise measurement of changes in angular position of the rod below the diffraction limit of light, and also provided the ability to resolve the power stroke of the motor with a time resolution of 2.5 μs.

In the work reported here, the gold nanorod assay with a polarizing filter was used to assess the fraction of *E. coli* F_1-ATPase molecules observed to rotate. A digital color camera with a refresh rate of 50 fps was used to record fields of view of F_1-dependent rotation of nanorods that were determined to be rotating based on their ability to blink red and green. The fraction of rotating molecules observed under these conditions was found to be 5 to 30-fold higher than reported previously with other methods, such that the majority of molecules can be observed to rotate. These data indicate that rotational measurements made using gold nanorods provide information of the F_1-ATPase mechanism that is representative of the characteristics of the enzyme population as a whole.

Materials and methods

E. coli XL-10 strain (Greene and Frasch 2003), containing a His6 tag on the N-terminus of the α-subunit, and a gS193C mutation to provide a biotinylation site, was used to isolate F_1. Cells were grown as explained previously (Lowry and Frasch 2005). Membranes were obtained as in (Ishmukhametov et al. 2005), and were resuspended in Release buffer containing 5.0 mM TES, pH 7, 40 mM ε-amino-caproic acid, 1 mM EDTA, 1 mM DTT, 5.0% (v/v) glycerol. The mixture was centrifuged at 180,000×g for 1 h at 4 °C. The supernatant was mixed with 10-× Binding buffer (0.5M TRIS/pH 8.0, 1M KCl, 300 mM imidazole, 50 mM $MgCl_2$) at a ratio of 10:1 (v/v). Glycerol was then added to 15% (v/v). This mixture was then loaded onto a Ni-NTA column (0.8 cm in diameter, 1.5 cm^3 of resin), which was prepared by first washing with water, and then equilibrating the column with Wash buffer (50 mM TRIS/pH 8.0, 100 mM KCl, 30 mM imidazole, 5 mM $MgCl_2$, 15% glycerol). After binding the protein to the column, it was washed with 4 column volumes of Wash buffer. To elute F_1, 3 ml of Wash buffer, supplemented with 150 mM imidazole, was passed through the column.

In the process of biotinylating the purified F_1 enzyme, 200 μl of F_1 solution was mixed with equimolar amount of biotin-maleimide, and passed through a desalting column equilibrated with Wash buffer. Biotinylated F_1 was stored at 0.1 mg/ml at −80 °C until use. The protein preparation demonstrated high rotational activity for half a year.

Gold nanorods for rotational microscope assay were prepared as in Spetzler et al. (2006). It was found that F_1 binds to the surface of regular glass as sufficiently as it does to a Ni-NTA covered glass surface. A 5 μl droplet of biotinylated F_1 was incubated on the slide for 5 min then washed with F_1 buffer (50 mM Tris-Cl, pH 8.0, and 10 mM KCl). Nanodevice assembly was completed by addition of saturating amounts of avidin-coated nanorods and incubated for 5 min at room temperature. This allowed the avidin-coated gold nanorods to be captured by the biotinylated γ-subunit. The slide was washed thoroughly in F_1 buffer to remove excess nanorods and minimize nonspecific binding. Samples that were examined for rotation included a final buffer containing Mg^{2+}-NTP at a concentration that maximized F_1-ATPase activity.

The bulk activity of F_1 was measured in a buffer containing 20 mM KCl, 100 mM TRIS, pH 8.0, 1 mM $MgCl_2$, and 2 mM ATP or GTP at 25 °C. Activity was monitored with the coupled assay as described by Greene and Frasch (2003). The turnover for ATP and GTP hydrolysis was 108 and 130 s^{-1}, respectively.

Results

Figure 1 shows the amount of gold particles bound to the surface in a typical field of view under the microscope in the absence and presence of immobilized F_1. The F_1-ATPase was immobilized on the slide by incubating for

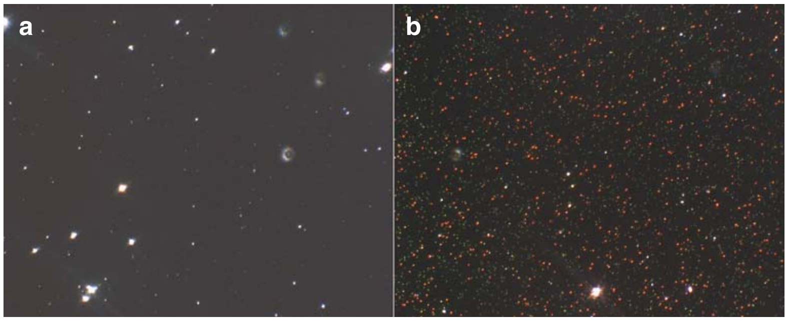

Fig. 1 A field of view under the microscope of gold particles bound to the slide in the absence (**a**) and presence (**b**) of 100 μg/ml F_1 immobilized to the surface. F_1 was immobilized to the surface prior to the addition of the gold nanoparticles. *White spots* are aberrations in the glass

5 min with 100 μg/ml of protein. Under these conditions, the average distance between immobilized F_1 molecules was 1±0.5 μm as measured by atomic force microscopy (Fig. 2), which is large enough to ensure that the gold rods are rarely bound to multiple F_1 molecules. The percent of nonspecifically bound nanorods is <0.1% of that bound when F_1 is present.

The method to prepare the gold nanorods used here is a two-step process that involves the initial formation of gold nanospheres that are subsequently elongated to nanorods with a yield of about 30% (Spetzler et al. 2006). Nanorods prepared in this manner provide a more sensitive measure of rotation compared to preparations that yield nearly 100% nanorods (Jana et al. 2001) due to the larger dynamic range of scattered light as a function of angular position to the polarizer. Consequently, the red spots in Fig. 1b are necessarily the result of light scattered from the long axis of bound nanorods, while the green spots are primarily the result of nanospheres that will not exhibit a rotational-dependent color change when viewed through a polarizer. Thus, for this study, green spots were not counted and not included in the calculation of the fraction of F_1 molecules observed to rotate.

Figure 3 shows a field of view under the microscope which is the first frame of a 500 frame movie of GTP-dependent rotation, where each frame had an exposure time of 20 ms. Determination that a nanorod was rotating was based on the fluctuation in the color between red and green during the course of each movie. Example movies are available as supplemental data. Yellow and red X’s denote rods observed to rotate and not rotate, respectively. Figure 4 shows the first frame of a similar movie in the absence of nucleotide. Without substrate, a small percentage of the nanorods show some color fluctuation due to Brownian motion. While nucleotide-driven rotation can last for hours at a time, Brownian fluctuations are typically sporadic and do not show consistent rotation. The number of nanorods observed to rotate in the presence of ATP was also measured.

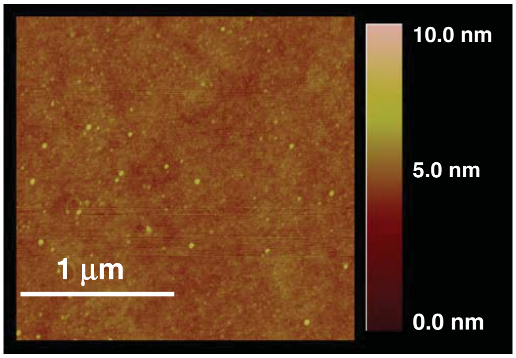

Fig. 2 Atomic force microscopy surface scan of F_1 bound to the surface of the slide after incubation of 100 μg/ml F1 followed by a wash

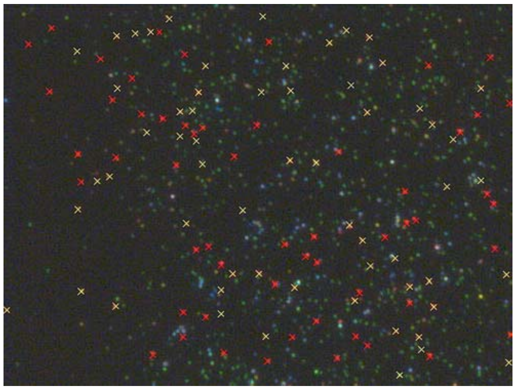

Fig. 3 The first frame from a movie depicting a microscope field of view of GTP-driven F_1 rotation. *Yellow* and *red Xs* denote rotating and non-rotating molecules, respectively. The GTPase activity of F_1 as measured with a coupled assay in the presence of 1 mM Mg^{2+}GTP was 130 s^{-1}. The movie can be viewed online in the supplemental information

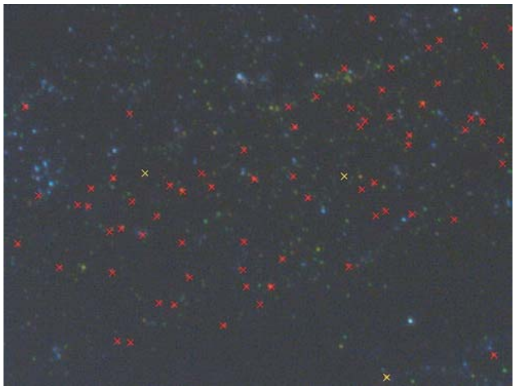

Fig. 4 The first frame from a movie depicting a microscope field of view of F_1 bound nanorods in the absence of nucleotides. *Yellow* and *red Xs* denote fluctuating and non-motile nanorods, respectively. The movie can be viewed online in the supplemental information

The fraction of nanorods observed to rotate was calculated by quantitating the number of rotating rods in each of several movies under the same conditions, then dividing by the total number of nanorods in those movies. As summarized in Fig. 5, the average number of F_1 molecules observed to rotate in the presence of GTP, ATP, and without nucleotide was ~50, ~25, and ~4% respectively. In some experiments, the fraction of molecules observed to rotate in the presence of GTP was as high as 65%.

Discussion

The results here clearly show that a majority of F_1 molecules can be observed to rotate with GTP. These data indicate that rotational measurements made using gold nanorods provide information about the F_1-ATPase mechanism that is representative of the characteristics of the enzyme population as a whole. It has been shown that *E. coli* F_1-ATPase is highly susceptible to inhibition that results from the entrapment of Mg^{2+}-ADP at a catalytic site (Hyndman et al. 1994; Bowler et al. 2006; Galkin et al. 2006). However, Mg^{2+}-GDP has been shown not to cause such an inhibition (Vasilyeva et al. 1980). This is the likely cause of the two-fold difference reported here in the abundance of rotating molecules powered by ATP and GTP, respectively.

The small fraction of molecules observed to rotate as measured by other approaches may be due to inherent limitations of those methods. When 40 nm gold nanospheres are used as the reporter group for rotation, they appear as light diffraction-limited spots ~250 nm in diameter. The eccentricity of the γ-subunit allows for about 5 nm of displacement during rotation (Oster et al. 2000; Sun et al. 2004). Thus, any bead that is attached near the center of the axis of rotation will show little variation in the location of the centroid of the spot when it rotates. Also, due to the substantial amount of surface variation on standard slides, it is possible for F_1 to become immobilized to the surface at an angle to the observation plane that virtually eliminates any variation in the location of the centroid.

The fraction of F_1 observed to rotate in single molecule measurements are likely an underestimate of the total number of those rotating on the slide due to several factors. First, it is possible that surface interactions prohibit rotation. The surface of the slide is not flat relative to the size of the F_1-ATPase and the detection probes. Consequently, it is likely that a fraction of the F_1 molecules bind to the surface at an angle that causes the probe to come in contact with the surface at some point in its trajectory in a manner that interferes with rotation.

Second, Spetzler et al. (2006) have shown that data acquisition rates of at least 50 kHz are required to resolve the 120° rotational steps (0.24 ms duration) of the *E. coli* F_1 γ-subunit that occur between the relatively long 8 ms pauses in rotation. Consequently, in the work presented here, rotation is evident in the movies acquired with a 50 fps color camera due to a strobe effect between rotation rate and the refresh rate of the camera. The strobe effect may not be apparent if the dwell positions for a given functioning F_1 motor are oriented in the field of view relative to the plane of polarization in such a way that there is very little dynamic range in the light intensity scattered by the nanorod. When this occurs, the apparent color of the nanorod will not fluctuate between red and green as a function of time.

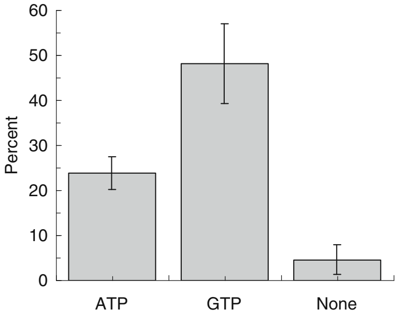

Fig. 5 Percent of nanorods directly observed to fluctuate between *red* and *green* in the presence of ATP, GTP, or in the absence of a nucleotide. Data were compiled from 11, 6, and 9 movies for GTP, ATP, and without nucleotide, respectively. Example movies of each condition can be viewed online in the supplemental information

References

Abrahams JP, Leslie AG, Lutter R, Walker JE (1994) Nature 370 (6491):621–628

Adachi K, Yasuda R, Noji H, Itoh H, Harada Y, Yoshida M, Kinosita K (2000) Proc Natl Acad Sci U S A 97(13):7243–7247

Borsch M, Diez M, Zimmermann B, Reuter R, Graber P (2002) FEBS Lett 527(1–3):147–152

Bowler MW, Montgomery MG, Leslie AG, Walker JE (2006) Proc Natl Acad Sci U S A 103(23):8646–8649

Galkin MA, Ishmukhametov RR, Vik SB (2006) Biochim Biophys Acta 1757(3):206–214

Greene MD, Frasch WD (2003) J Biol Chem 278(51):51594–51598

Hyndman DJ, Milgrom YM, Bramhall EA, Cross RL (1994) J Biol Chem 269(46):28871–28877

Ishmukhametov RR, Galkin MA, Vik SB (2005) Biochimica Et Biophysica Acta-Bioenergetics 1706(1–2):110–116

Jana NR, Gearheart L, Murphy CJ (2001) Phys Chem 105:4065–4067

Lowry DS, Frasch WD (2005) Biochemistry 44(19):7275–7281

Nakanishi-Matsui M, Kashiwagi S, Hosokawa H, Cipriano DJ, Dunn SD, Wada Y, Futai M (2006) J Biol Chem 281(7): 4126–4131

Noji H, Yasuda R, Yoshida M, Kinosita K (1997) Nature 386 (6622):299–302

Oster G, Wang H, Grabe M (2000) Philos Trans R Soc Lond B Biol Sci 355(1396):523–528

Panke O, Gumbiowski K, Junge W, Engelbrecht S (2000) Febs Letters 472(1):34–38

Raschke G, Kowarik S, Franzl T, Sonnichsen C, Klar TA, Feldmann J, Nichtl A, Kurzinger K (2003) Nano Letters 3(7):935–938

Sonnichsen C, Alivisatos AP (2005) Nano Letters 5(2):301–304

Spetzler D, York J, Daniel D, Fromme R, Lowry D, Frasch W (2006) Biochemistry 45(10):3117–3124

Sun SX, Wang H, Oster G (2004) Biophys J 86(3):1373–1384

Vasilyeva EA, Fitin AF, Minkov IB, Vinogradov AD (1980) Biochem J 188(3):807–815

Yasuda R, Noji H, Kinosita K, Yoshida M (1998) Cell 93(7):1117–1124

Yasuda R, Noji H, Yoshida M, Kinosita K, Itoh H (2001) Nature 410 (6831):898–904

APPENDIX B

SINGLE MOLECULE MEASUREMENTS OF F1-ATPASE REVEAL AN INTERDEPENDENCE BETWEEN THE POWER STROKE AND THE DWELL DURATION

BIOCHEMISTRY
including biophysical chemistry & molecular biology
Article

Biochemistry **2009,** *48,* 7979–7985 7979
DOI: 10.1021/bi9008215

Single Molecule Measurements of F_1-ATPase Reveal an Interdependence between the Power Stroke and the Dwell Duration[†]

David Spetzler,[‡] Robert Ishmukhametov,[‡] Tassilo Hornung,[‡] Lixia Jin Day, James Martin, and Wayne D. Frasch*

School of Life Sciences, Arizona State University, P.O. Box 874501, Tempe, Arizona 85287-4501 [‡]*Authors contributed equally*

Received May 12, 2009; Revised Manuscript Received July 15, 2009

ABSTRACT: Increases in the power stroke and dwell durations of single molecules of *Escherichia coli* F_1-ATPase were measured in response to viscous loads applied to the motor and inhibition of ATP hydrolysis. The load was varied using different sizes of gold nanorods attached to the rotating γ subunit and/or by increasing the viscosity of the medium using PEG-400, a noncompetitive inhibitor of ATPase activity. Conditions that increase the duration of the power stroke were found to cause 20-fold increases in the length of the dwell. These results suggest that the order of hydrolysis, product release, and substrate binding may change as the result of external load on the motor or inhibition of hydrolysis.

Mechanical work at the subcellular level is performed by enzymes called molecular motors that convert chemical energy in the form of either ATP or a transmembrane electrochemical gradient into mechanical energy by initiating conformational changes capable of performing work. Molecular motors are classified as either linear or rotary, depending upon the type of work they perform. The effect of external load on some linear molecular motors has been found to alter the relationship between the mechanical output and the kinetics of nucleotide binding, hydrolysis, and product release (*1*−*8*).

Application of a load to several motors perturbs the mechanical transitions in the catalytic cycle, causing a force-dependent shift in both the dwell time distribution and mechanical transitions (*1*). Several groups have observed changes in these distributions resulting from intramolecular strain due to an applied external load that altered the conformations of the active site and affected nucleotide binding, ATP hydrolysis, and product release (*2*, *5*, *8*−*10*). Single molecule studies using a laser trap revealed a 100-fold increase in the rate of ADP binding when 2 pN of load was applied to the linear molecular motor myosin VI (*7*). A biochemical mechanism was derived from this application of an external force that caused this motor to stop its transport function and become a structural linker. Spudich (*1*) has suggested that the use of mechanical strain to alter protein function may serve as a widespread means of enzyme activity regulation.

The F_1F_o ATP synthase is composed of the transmembrane F_o complex and extrinsic membrane F_1 complex that couples the energy from a transmembrane proton gradient to synthesize ATP from ADP and phosphate. Both complexes are rotary molecular motors that use a common drive shaft composed of the γ and ε subunits. Crystal structures show that the F_1 γ subunit is composed of two domains, a coiled-coil domain that protrudes through the center cavity of the $(\alpha\beta)_3$ ring and an open α-helix/β-sheet domain known as the foot that binds to the ε subunit and the c-subunit ring of F_o (*11*). The F_1-ATPase-driven and F_o-proton gradient-driven rotation of the $\gamma\varepsilon$ subunits occur in opposite directions (*12*, *13*).

The rotary cycle of the F_1-ATPase molecular motor at saturating ATP concentrations involves three 120° power strokes each separated by a catalytic dwell (*13*). Catalytic dwell durations of 8 and 2 ms measured in F_1 from *Escherichia coli* and the thermophilic bacterium *PS3*, respectively, are consistent with the turnover time of ATP hydrolysis (*14*, *15*). Early measurements with low temporal resolution were unable to resolve the velocity of the power stroke but estimated torque to be about 40 pN nm (*14*). However, more recent measurements using acquisition rates of 100 kHz have shown that the velocity of the power stroke is 0.45 deg μs^{-1}, which results in a torque of 63 pN nm (*15*, *16*). Torque values of 56−74 pN nm have also been estimated using other methods that do not rely on resolving the power stroke directly (*17*−*20*).

Rotation occurs in discrete 120° steps between the catalytic dwells under saturating ATP concentrations (*21*), where the rate-limiting step is product release (*22*, *23*). At rate-limiting concentrations of ATP, the 120° rotational steps occur in 80° and 40° substeps (*14*, *24*) that result in two different dwells. The duration of the dwell prior to the 80° substep is inversely proportional to the substrate concentration, indicating that further rotation requires ATP binding. This dwell occurs at the 0° position and is often referred to as the ATP-waiting dwell. The dwell prior to the 40° rotational step does not change with ATP concentration and is likely the same dwell observed at saturating ATP. However, for the mutant βD190E where the rate-limiting step is hydrolysis (*25*), the enzyme follows an alternative reaction pathway. In this pathway a 120° power stroke occurs after a dwell at the 0° position without stopping at the 80° position (*26*). A dwell at the 0° position also results from an application of external load to the motor that has been shown to alter the rate constant of ATP binding (*9*).

We now present measurements of the power stroke and dwell duration of single molecules of *E. coli* F_1-ATPase in

---

[†] This project was supported by Award R01GM50202 to W.D.F. from NIGMS. The content is solely the responsibility of the authors and does not necessarily represent the official views of the National Institute of General Medical Sciences or the National Institutes of Health.

*Corresponding author. Tel: 480-965-8663. Fax: 480-965-6899. E-mail: Frasch@asu.edu.

response to viscous loads applied to the motor. We show that an increase in the duration of the power stroke is correlated with a 20-fold increase in the length of the dwell. The results presented here show that the dwell duration is extended by application of an external load on the motor and/or by inhibition of ATP hydrolysis. These results suggest that the order of hydrolysis, product release, and substrate binding may change as the result of external load on the motor and inhibition of hydrolysis.

EXPERIMENTAL PROCEDURES

The F_1-ATPase was purified from *E. coli* XL-10 strain. F_1 contains a His_6 tag on the N-terminus of the α subunit and γS193C for biotinylation as described previously (*27*, *28*). Membranes were resuspended in buffer A containing 5.0 mM TES, pH 7, 40 mM ε-aminocaproic acid, 1 mM EDTA, 1 mM DTT, and 5.0% (v/v) glycerol, and the mixture was centrifuged at 180000*g* for 1 h at 4 °C. The supernatant was mixed with buffer B (0.5 M Tris, pH 8.0, 1 M KCl, 300 mM imidazole, 50 mM $MgCl_2$) at a 10:1 (v/v) ratio. Glycerol was added to 15% (v/v), and this mixture was loaded on a Ni-NTA column (0.8 cm in diameter, 1.5 cm^3 of resin) washed initially with water and equilibrated with buffer C (50 mM Tris, pH 8.0, 100 mM KCl, 30 mM imidazole, 5 mM $MgCl_2$, 15% glycerol) to bind the F_1-ATPase to the column, and the column was washed with 20 mL of buffer C. To elute F_1-ATPase, the column was then flushed with 3 mL of buffer C containing 180 mM imidazole instead of 30 mM. To biotinylate the enzyme, 200 μL of F_1 solution was mixed with an equimolar amount of biotin-maleimide (Pierce) and passed through a desalting column (Pierce) equilibrated with buffer C. Biotinylated F_1 was stored at 0.1 mg/mL at −80 °C prior to use.

Where PEG-400 was present, the desired volume of PEG-400 was mixed with buffer D (50 mM Tris-HCl, pH 8.0, 10 mM KCl), 60 μM phenol red pH indicator, and the desired amount of $MgCl_2$ and ATP. A 1:2 mol ratio of Mg^{2+}-ATP was maintained to minimize the presence of free Mg^{2+}. Since high concentrations of PEG-400 interfere with the accuracy of measurements by a pH meter, the pH was adjusted by comparing absorbance of the phenol red at 557 nm in the presence and absence of PEG-400. The viscosity of the solutions was measured with a Brookfield LVDV viscometer with UL adaptor at 28 °C and varied between 1 and 20 cP (*16*). The F_1-ATPase activity was measured as described (*29*) in 5 mM Tris, pH 8, and 55 mM KCl with the indicated amount of Mg^{2+}-ATP in a Cary 100 spectrophotometer at 28 °C.

The power stroke of the enzyme was characterized by measuring the transition time, defined as the time required for the γ subunit to travel any 90° of the 120°. Single molecule rotation assays were performed as described by Spetzler et al. (*15*) with the following modifications. The F_1-ATPase was bound to the surface of nonfunctionalized glass coverslips since there was no measurable difference in dwell or transition times from enzyme bound to Ni-NTA coated coverslips. On average 25% were observed to rotate (*27*). Gold nanorods were made as previously described (*15*) except for the 91 × 45 nm rods, which were purchased from Nanopartz Inc. Single gold nanorods were initially identified to undergo F_1-ATPase-dependent rotation by observing oscillations in light intensity through a polarizing filter via a Zeiss HSC color CCD camera at 55 fps. Each molecule was aligned confocal to a Perkin-Elmer SPCM-AQR-15 single photon detector to quantitate changes in scattered light intensity from the nanorods as a function of time. A total of 100 s of data was collected in successive 5 s data sets at each acquisition speed from 10 to 200 kHz in 10 kHz increments for each molecule. Temperatures of the slide on the microscope while making the measurements were observed to vary between 27 and 29 °C. The viscosity of the buffer used in these single molecule measurements was varied by increasing the concentration of poly(ethylene glycol) 400 (PEG-400) in the rotation assay buffer (*16*).

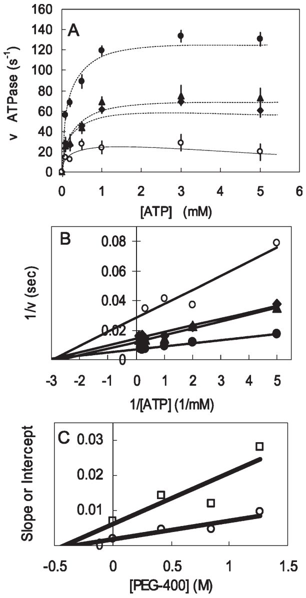

FIGURE 1: Noncompetitive inhibition of F_1-ATPase activity by PEG-400. (A) Effect of PEG-400 on the bulk ATPase activity of F_1 without nanorods. The linear initial rate of F_1-ATPase activity was determined in triplicate with phenol red as indicated in Experimental Procedures using 10 μg of F_1 in the presence of (●) 0% PEG-400, (▲) 15% PEG-400, (◆) 30% PEG-400, and (○) 45% PEG-400 (v/v). (B) Double reciprocal plot of the data from (A). (C) Plot of the slopes (□) and *y*-intercepts (○) of each trend line from (B) versus PEG-400 concentration. The absolute values of the *x*-intercepts determined by linear regression are defined as the inhibition constants K_{is} (slopes) and K_{ii} (intercepts).

The average dwell time was calculated by determining the number of hydrolysis events that occurred in a given time frame. This was measured by counting the number of times that the scattered light intensity spanned the 5th and 95th percentile of the dynamic range of the intensity of that data set. The average dwell time was calculated by dividing the total time by the number of 5th−95th percentile events.

The direction of rotation was determined by splitting the signal from a single gold nanorod and passing it through two polarizing filters that were offset from one another. The signals follow the relations $I_1 = A\cos(Bx_1 + C)$ and $I_2 = A\cos(Bx_2)$. This provides enough information to determine the direction that the gold nanorod has traveled between consecutive data points. The direction and magnitude of the movement were used to generate Figure 1A,B.

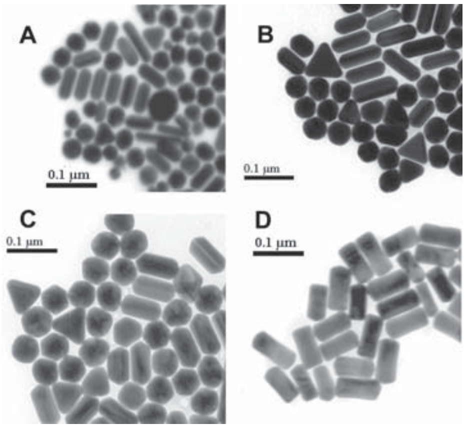

FIGURE 2: Electron micrographs of gold nanorod preparations used as probes to measure rotation. Triangles and spheres that appear in the preparations do not scatter both red and green light and are therefore excluded from rotation measurements. The average size of nanorods in each preparation was (A) 75 × 35 nm, (B) 87 × 36 nm, (C) 90 × 46 nm, and (D) 91 × 45 nm.

RESULTS

In an effort to understand the effects of viscous load on the enzyme, the velocity of the 120° power stroke was measured as a function of load. The load was varied by changing the size of the nanorod attached to the γ subunit and the viscosity of the medium. Increasing concentrations of poly(ethylene glycol) 400 (PEG-400) were used to vary the viscosity. This fluid is Newtonian and increases the viscosity to 20 cP at 60% (v/v) (*16*). Since crystal structures of F_1 do not differ significantly when derived from crystals grown in PEG (*30*), this reagent is unlikely to alter tertiary structure of the enzyme significantly. However, as shown in Figure 1, PEG-400 was observed to inhibit F_1-ATPase activity in bulk measurements. The lines of the double reciprocal plot converge on the *x*-axis (Figure 1B), indicating that PEG-400 inhibition causes equivalent changes in k_{cat} and $k_{\mathrm{cat}}/K_{\mathrm{M}}$, characteristic of pure noncompetitive inhibition. Figure 1C shows a plot of the slopes and *y*-intercepts from each trend line from Figure 1B versus PEG-400 concentration. The *x*-intercepts determined from linear regression show that the inhibition constants K_{is} (slopes) and K_{ii} (intercepts) are equivalent, indicating that PEG-400 is a pure noncompetitive inhibitor. Thus, the PEG-400-dependent decreases in ATPase activity are not due to a decrease in the rate of either substrate binding or product release and must therefore be due to the influence of PEG-400 on the rate of ATP hydrolysis.

Since PEG-400 inhibits F_1-ATPase activity, the load on the enzyme was varied in a manner independent of PEG-400 concentration. This was accomplished by using gold nanorods of 75 × 35, 87 × 36, 90 × 46, and 91 × 45 nm sizes (Figure 2). It is noteworthy that the 91 × 45 nm nanorods had a rectangular profile compared to the 90 × 46 nm nanorods that had rounded ends, and thus while these two preps had similar size, their respective shapes were substantially different.

Rotation was observed as a change in the intensity of red light scattered from the nanorod (*15*), where the scattered light intensity is maximal and minimal when the long axis is parallel and perpendicular to the plane of polarization, respectively (*31*). Consequently, the intensity of light scattered from a nanorod changes in a sinusoidal manner as a function of the rotary position of the gold nanorod (*15*). To determine if the changes in scattered light intensity were the result of F_1-driven unidirectional rotation, the light scattered from a single nanorod was split into two parts, each of which was directed through a separate polarizer to a photon counter. The difference in the planes of polarization caused a constant phase shift in the maxima between the photon counters that defines the direction of rotation (*32*).

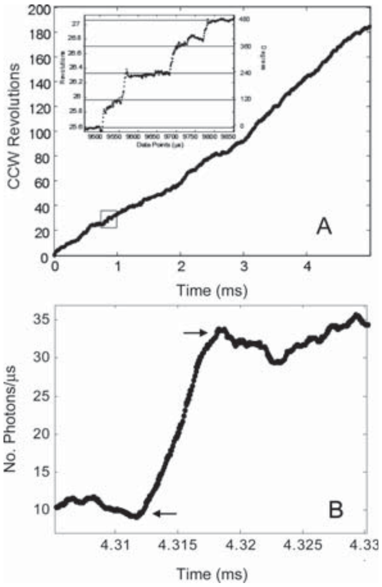

FIGURE 3: Single molecule rotation profile. (A) Time course of rotational position of a single F_1 molecule determined from the offset between two polarizers with data acquired at 10 kHz. All single molecule measurements were performed with 1 mM $MgCl_2$ and 2 mM ATP. (Inset) Detail of the rotational stepping of the boxed region. Horizontal lines show the 120° dwell positions. (B) Individual power stroke collected at 100 kHz using 91 × 45 nm nanorods in the presence of 0% PEG-400. Arrows indicate the beginning and end of the transition used to determine the rate of the power stroke.

The rotational position of a single gold nanorod attached to F_1 in the presence of saturating ATP is shown in Figure 3A. Under these conditions, the F_1-ATPase was observed to rotate almost exclusively counterclockwise in 120° steps (Figure 3A inset). Since this assay allows rotation data to be acquired for relatively long periods of time, it was possible to observe that the CCW rotation catalyzed by the enzyme was sustained. Figure 3B shows a typical individual power stroke in the absence of PEG-400. The intensity of scattered light follows a sinusoidal pattern in response to rotation of the nanorod. Thus, the greatest sensitivity with which to quantitate the power stroke velocity occurs during that 90° of rotation in which the intensity changes between minimum and maximum values. Consequently, velocities were calculated based on the time required for the nanorod to travel 90° that we designate as the transition time.

The transition times of several thousand power strokes were measured and averaged for each F_1-ATPase molecule for each

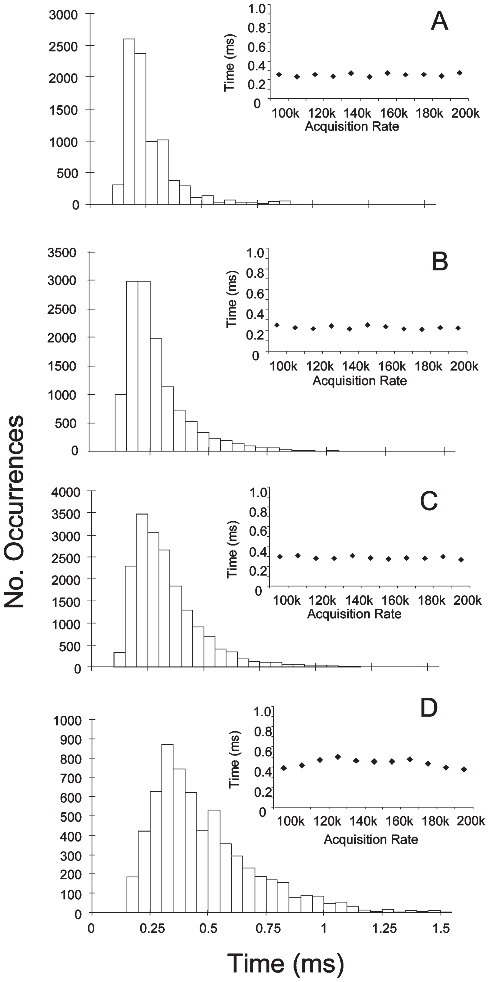

FIGURE 4: Distributions of transition times from single molecules collected at 1 mM $MgCl_2$ and 2 mM ATP at 100 kHz using (A) 75 × 35 nm, (B) 87 × 36 nm, (C) 90 × 46 nm, and (D) 91 × 45 nm nanorods. (Insets) The average time of each distribution for each nanorod preparation, respectively, as a function of data acquisition rate.

size of nanorod (Figure 4). A data set to characterize a single condition was considered complete when it contained at least 20000 power strokes from at least 15 different molecules. The rate of data acquisition was varied to ensure that the transition times measured were independent of the method used to collect data. Measurements of the transition times for single F_1 molecules were acquired at rates ranging from 100 to 200 kHz in increments of 10 kHz. The average transition time from each acquisition rate did not change significantly (Figure 4 insets). Thus, the average of the distributions formed from measurements at all acquisition rates was used to describe the transition times for any given molecule.

The mean power stroke duration for each nanorod size as a function of PEG-400 concentration is shown in Figure 5A.

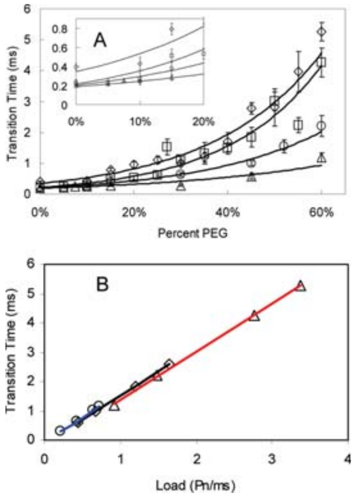

FIGURE 5: Transition times as a function of PEG-400 concentration and nanorod size at 1 mM $MgCl_2$ and 2 mM ATP. (A) Average transition times as a function of PEG-400 concentration measured using 75 × 35 nm (Δ), 87 × 36 nm (○), 90 × 46 nm (□), and 91 × 45 nm (◇) nanorods. (Inset) Expansion of data between 0% and 20% PEG-400 shows that the transition times for the three smallest nanorods converge to a single value of ~250 μs. (B) Transition times plotted as a function of increasing nanorod size at fixed PEG-400 concentrations. Lines are the linear best fit for 30% (blue), 45% (black), and 60% (red) PEG-400.

The duration of the transition for the three smallest nanorods converged to ~250 μs at low viscosities (Figure 5A inset), indicating that the velocity of the power stroke was limited by intrinsic properties of the enzyme. The transition times of the 91 × 45 nm nanorods never reached ~250 μs, indicating that the power stroke velocity was always limited by the viscous load on the motor. The difference in performance between these nanorods and the 90 × 46 nm nanorods is likely due to the fact that the ends of the former nanorods are more rounded (Figure 2). This difference in shape results in a difference in a significantly larger drag for the 91 × 45 nm nanorods (*33*).

The transition time for each nanorod size at various fixed PEG-400 concentrations was plotted as a function of the load (Figure 5B). Load was estimated using the relation $\Gamma = T/\omega$, where T is the torque, 61 pN nm (*16*), and ω is the velocity determined from the transition time (the measured transition time, t, is reciprocal to ω, and hence t is proportional to Γ/T). Linear best fit trend lines ($r^2 > 0.999$) for the transition times at 30%, 45%, and 60% PEG-400 showed no significant differences in the slopes or intercepts. This indicates that increases in transition time resulted solely from an increase in the viscous load and not from decreases in ATPase activity resulting from PEG-400 inhibition. The transition times for 0%, 5%, and 15% PEG-400 were not included since they were limited by intrinsic properties of the enzyme and thus did not change. The linear plot in Figure 5B implies that the torque produced during the power strokes is independent of the addition of PEG-400 and of using nanorods of different sizes and is consistent with previous results that show the torque is constant at different PEG-400 concentrations (*16*).

Figure 6A,C shows representative dwells at each PEG-400 concentration examined where the duration of each dwell is

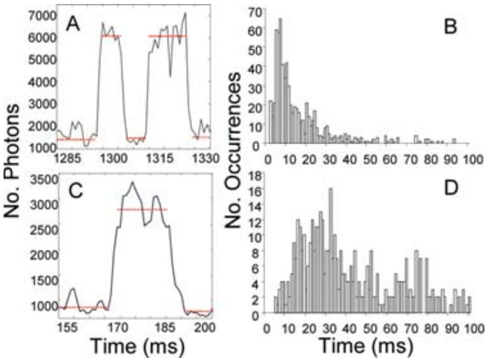

FIGURE 6: Dwell times in the absence (A, B) and presence (C, D) of 60% PEG-400 at 1 mM $MgCl_2$ and 2 mM ATP. (A, C) Changes in the intensity of scattered light from a single 75 × 35 nm nanorod attached to an F_1-ATPase molecule during rotation for 45 ms acquired at 100 kHz for 0% and 60% PEG-400, respectively. Each data point is 10 μs, and dwells are indicated by dotted lines. (B, D) Histograms of average F_1 dwell times acquired at 100−200 kHz using the same nanorods and PEG-400 concentrations as in (A) and (C), respectively.

indicated by a red dotted line. Histograms of the average dwell time for each molecule for the 75 × 35 nm nanorods (Figure 6B, D) showed an increase in the duration of the dwell with increasing PEG-400 concentration. The median of the dwell time population was used to compare dwell times between different conditions to avoid the error in the mean caused by long dwells that resulted from entrapped Mg^{2+}-ADP. The results in the absence of PEG-400 are consistent with previous studies where the dwell time from single molecule experiments was compared to the inverse of k_{cat} for the ATP hydrolysis rate measured in bulk solution (*14*, *15*, *34*).

The dwell duration as a function of PEG-400 concentration for all sizes of nanorods is shown in Figure 7A. The solid circles show the inverse of the k_{cat} from bulk ATPase experiments in the absence of nanorods and are comparable to the dwell times observed with the smallest nanorods; i.e., the decrease in activity observed in the bulk experiments is equivalent to the decrease observed in the dwell time. Thus the inhibition of ATPase activity by PEG-400 dominates any contribution to the dwell duration from the load of the smallest nanorods. The three largest nanorods have dwell times that are significantly longer than the inverse of the k_{cat} of the ATP hydrolysis rate. This indicates that the load significantly contributes to the dwell duration under these conditions. The heterogeneity of the nanorods was significantly smaller than the stochastic variation in the transition and dwell times and thus did not significantly contribute to deviations in the measurements, as can be seen by the comparison of the bulk ATPase rates and the dwell times with the smallest rods (Figure 7A). A linear trend was observed between transition time and the dwell over the large range of viscous loads examined. A scatter plot of the dwell times versus the transition times revealed a strong linear correlation (correlation coefficient = 0.935) between these two variables (Figure 7B) with about a 20-fold increase in the dwell time in response to increases in the transition time.

DISCUSSION

At saturating ATP concentrations in the absence of PEG-400, rotation occurred in CCW 120° steps (Figure 3) as has been observed elsewhere (*15*, *17*, *23*). Under these conditions, the enzyme follows the conventional reaction pathway that involves a catalytic dwell at the −40° (equivalent to 80°) position followed by a 120° power stroke initiated by product release (Figure 8A) (*13*, *15*, *21*). In this three-site model (*35*), ATP hydrolysis and ATP binding occur prior to product release, which may be ADP (*22*, *23*) or P_i (*36*), though only ADP is shown for simplicity in Figure 8. Thus the presence of product at site 2 is thought to prohibit rotation past the 80° position. At limiting ATP concentrations (Figure 8B), ATP binding occurs after product release, resulting in a second dwell at the 0° position (ATP-waiting dwell) (*14*, *24*). This dwell can also be induced by the application of an external load sufficient to slow the power stroke that in turn reduces the rate constant of ATP binding (*9*). Based on these observations, substrate binding at site 3 is thought to be required to initiate rotation past the 0° position (*14*).

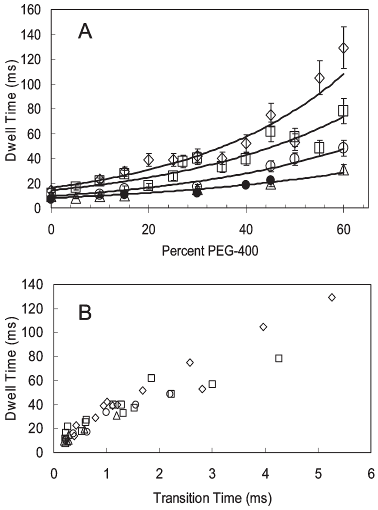

FIGURE 7: (A) Average dwell times of F_1 as a function of percent PEG-400 using 75 × 35 nm (Δ), 87 × 36 nm (○), 90 × 46 nm (□), and 91 × 45 nm (◇) nanorods at 1 mM $MgCl_2$ and 2 mM ATP. The inverse of the k_{cat} from bulk ATPase measurements (●) from Figure 1. (B) Linear correlation between the transition time and dwell time (correlation coefficient = 0.935) for 75 × 35 nm (Δ), 87 × 36 nm (○), 90 × 46 nm (□), and 91 × 45 nm (◇) nanorods.

The results presented here show that application of an external load on the motor causes the dwell to lengthen (Figure 7A), consistent with a decrease in the rate constant of ATP binding as is observed in *PS3*-F_1 (*9*). The dwell duration also increases as a result of inhibition of ATP hydrolysis by PEG-400 (Figure 7A, solid dots). Similar increases in dwell duration have been observed with the βD190E mutant of the catalytic base in the thermophilic bacterium *PS3* enzyme that slow the rate of hydrolysis (*25*, *26*). The βD190E mutant follows an alternate reaction pathway where product release occurs before substrate binding that causes the γ subunit to dwell in the 0° position after which it rotates by 120°, skipping the dwell at the 80° position (Figure 8C) (*28*). In this proposed alternate reaction pathway the order of events is hydrolysis at site 1, followed by product release at site 2, and then substrate binding at site 3. This leads to a nucleotide occupancy state where two ADP are bound at one

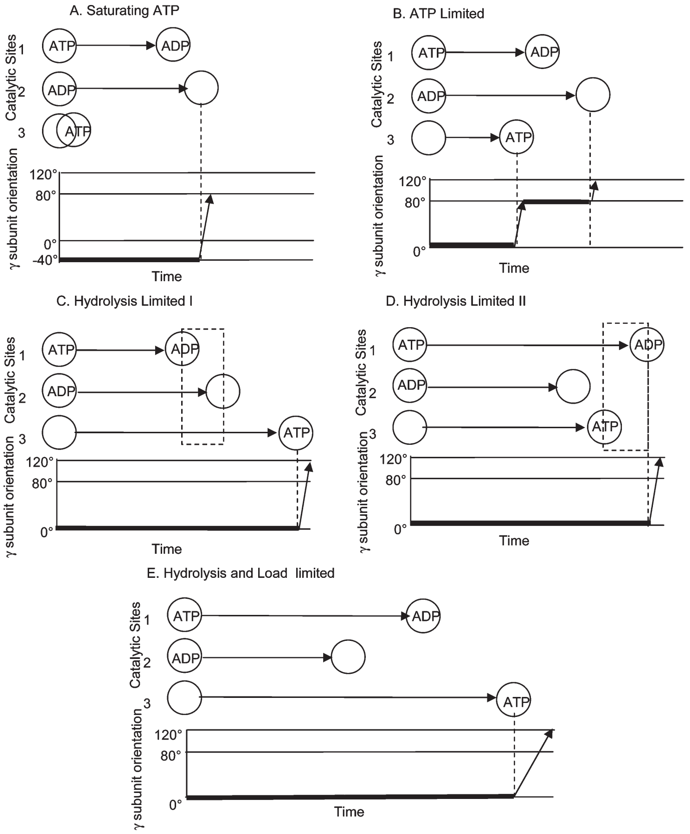

FIGURE 8: (A) The conventional reaction pathway at saturating ATP concentrations. (B) The conventional reaction pathway at limiting ATP concentrations. (C) The alternate reaction pathway from Shimabukuro et al. (*26*). The dotted box shows when the enzyme has two ADP bound. (D) Modifications to the alternate reaction pathway compatible with the data presented here when only hydrolysis is limiting. The dotted box shows when the enzyme has two ATP bound. (E) Additional modifications to the alternate reaction pathway when both hydrolysis and ATP binding are limited, compatible with the data presented here.

time (dotted box, Figure 8C), similar to that observed in three F_1 crystal structures (*30*, *37*, *38*).

We propose two additional reaction pathways that could occur when the rate of hydrolysis has been decreased and/or the load on the γ subunit decreases the rate constant for ATP binding. The first occurs when ATP binds to site 3 prior to hydrolysis in site 1 but after product release in site 2 (Figure 8D). Under these conditions, the dwell duration is determined by the rate of hydrolysis at site 2 and is not additionally extended by increases in the time required to bind ATP to site 3 (Figure 7, solid dots and open triangles) caused by external load on the motor that slows the power stroke (Figure 5, open triangles). This model requires that rotation be inhibited when two ATP are bound and that hydrolysis at site 1 initiates the power stroke at the 0° position. This leads to a nucleotide occupancy state where two ATP are bound at one time while the third site is empty (dotted box, Figure 8D). It is noteworthy that two ATP or ATP analogues are bound to the enzyme simultaneously in six F_1 crystal structures with one site empty (*11*, *39*, *40*).

In the second possible reaction pathway, ATP hydrolysis in site 1 occurs before ATP binding in site 3 but after product release in site 2 (Figure 8E). Under these conditions, the external load on the motor increases the time required for ATP to bind (*9*) to a greater extent than the time required for hydrolysis to occur when inhibited by PEG-400. This is consistent with the results presented here, where the three largest sizes of nanorods significantly increase the duration of the power stroke (Figure 5, open circles, squares, and diamonds) and have longer dwell durations than when the enzyme is limited by hydrolysis (Figure 7, solid circles, open circles, squares, and diamonds).

The reaction pathways of Figure 8C−E differ from the conventional pathway (Figure 8A,B) with regard to the order of hydrolysis, product release, and substrate binding events. This change in order may account for the absence of the dwell at the 80° position in the alternate reaction pathways. The presence of product at site 2 prohibits rotation past the 80° dwell position (*24*, *25*). Thus, when product has been released from site 2 before rotation has been triggered by either substrate binding at site 3 (Figure 8C,E) or hydrolysis at site 1 (Figure 8D), the 80° dwell position does not occur. Instead, rotation continues past this point and ends after 120°. Consequently, when rotation is triggered at the 0° position and there is no product in site 2, rotation occurs in a single 120° event. The results presented here suggest two new forms of the alternate reaction pathway (Figure 8D,E) but do not eliminate the reaction pathway of Figure 8C. Since crystal structures provide evidence that both situations occur, it appears that hydrolysis, product release, and substrate binding may occur in different orders, depending upon the conditions.

ACKNOWLEDGMENT

We thank Dr. Michael Berg for insightful discussions and editorial review.

REFERENCES

1. Spudich, J. A. (2006) Molecular motors take tension in stride. *Cell 126*, 242–244.
2. Veigel, C., Schmitz, S., Wang, F., and Sellers, J. R. (2005) Load-dependent kinetics of myosin-V can explain its high processivity. *Nat. Cell Biol. 7*, 861–869.
3. Toba, S., Watanabe, T. M., Yamaguchi-Okimoto, L., Toyoshima, Y. Y., and Higuchi, H. (2006) Overlapping hand-over-hand mechanism of single molecular motility of cytoplasmic dynein. *Proc. Natl. Acad. Sci. U.S.A. 103*, 5741–5745.
4. Reck-Peterson, S. L., Yildiz, A., Carter, A. P., Gennerich, A., Zhang, N., and Vale, R. D. (2006) Single-molecule analysis of dynein processivity and stepping behavior. *Cell 126*, 335–348.
5. Purcell, T. J., Sweeney, H. L., and Spudich, J. A. (2005) A force-dependent state controls the coordination of processive myosin V. *Proc. Natl. Acad. Sci. U.S.A. 102*, 13873–13878.
6. Mallik, R., Carter, B. C., Lex, S. A., King, S. J., and Gross, S. P. (2004) Cytoplasmic dynein functions as a gear in response to load. *Nature 427*, 649–652.
7. Altman, D., Sweeney, H. L., and Spudich, J. A. (2004) The mechanism of myosin VI translocation and its load-induced anchoring. *Cell 116*, 737–749.
8. Baker, J. E., Krementsova, E. B., Kennedy, G. G., Armstrong, A., Trybus, K. M., and Warshaw, D. M. (2004) Myosin V processivity: multiple kinetic pathways for head-to-head coordination. *Proc. Natl. Acad. Sci. U.S.A. 101*, 5542–5546.
9. Watanabe-Nakayama, T., Toyabe, S., Kudo, S., Sugiyama, S., Yoshida, M., and Muneyuki, E. (2008) Effect of external torque on the ATP-driven rotation of F1-ATPase. *Biochem. Biophys. Res. Commun. 366*, 951–957.
10. Guydosh, N. R., and Block, S. M. (2006) Backsteps induced by nucleotide analogs suggest the front head of kinesin is gated by strain. *Proc. Natl. Acad. Sci. U.S.A. 103*, 8054–8059.
11. Bowler, W., Montgomery, M., Leslie, A., and Walker, J. E. (2007) Ground State Structure of F_1-ATPase from Bovine Heart Mitochondria at 1.9 Å Resolution. *J. Biol. Chem. 282*, 14238–14242.
12. Borsch, M., Turina, P., Eggeling, C., Fries, J. R., Seidel, C. A., Labahn, A., and Graber, P. (1998) Conformational changes of the H^+-ATPase from *Escherichia coli* upon nucleotide binding detected by single molecule fluorescence. *FEBS Lett. 437*, 251–254.
13. Noji, H., Yasuda, R., Yoshida, M., and Kinosita, K. Jr. (1997) Direct observation of the rotation of F1-ATPase. *Nature 386*, 299–302.
14. Yasuda, R., Noji, H., Yoshida, M., Kinosita, K., and Itoh, H. (2001) Resolution of distinct rotational substeps by submillisecond kinetic analysis of F-1-ATPase. *Nature 410*, 898–904.
15. Spetzler, D., York, J., Daniel, D., Fromme, R., Lowry, D., and Frasch, W. (2006) Microsecond time scale rotation measurements of single F(1)-ATPase molecules. *Biochemistry 45*, 3117–3124.
16. Hornung, T., Ishmukhametov, R., Spetzler, D., Martin, J., and Frasch, W. D. (2008) Determination of torque generation from the power stroke of *Escherichia coli* F_1-ATPase. *Biochim. Biophys. Acta 1777*, 579–582.
17. Pilizota, T., Bilyard, T., Bai, F., Futai, M., Hosokawa, H., and Berry, R. M. (2007) A programmable optical angle clamp for rotary molecular motors. *Biophys. J. 93*, 264–275.
18. Cherepanov, D. A., and Junge, W. (2001) Viscoelastic dynamics of actin filaments coupled to rotary F-ATPase: curvature as an indicator of the torque. *Biophys. J. 81*, 1234–1244.
19. Panke, O., Cherepanov, D. A., Gumbiowski, K., Engelbrecht, S., and Junge, W. (2001) Viscoelastic dynamics of actin filaments coupled to rotary F-ATPase: angular torque profile of the enzyme. *Biophys. J. 81*, 1220–1233.
20. Panke, O., Cherepanov, D. A., Gumbiowski, K., Engelbrecht, S., and Junge, W. (2002) Viscoelastic dynamics of actin filaments coupled to rotary F-ATPase: Angular torque profile of the enzyme. *Biophys. J. 83*, 582–582.
21. Yasuda, R., Noji, H., Kinosita, K. Jr., and Yoshida, M. (1998) F1-ATPase is a highly efficient molecular motor that rotates with discrete 120 degree steps. *Cell 93*, 1117–1124.
22. Sielaff, H., Rennekamp, H., Engelbrecht, S., and Junge, W. (2008) Functional halt positions of rotary F_oF_1-ATPase correlated with crystal structures. *Biophys. J. 95*, 4979–4987.
23. Adachi, K., Oiwa, K., Nichizaka, T., Furuike, S., Noji, H., Itoh, H., Yoshida, M., and Kinosita, K. Jr. (2007) Coupling of rotation and catalysis in F_1-ATPase revealed by single-molecule imaging and manipulation. *Cell 130*, 309–321.
24. Sakaki, N., Shimo-Kon, R., Adachi, K., Itoh, H., Furuike, S., Muneyuki, E., Yoshida, M., and Kinosita, K. (2005) One rotary mechanism for F1-ATPase over ATP concentrations from millimolar down to nanomolar. *Biophys. J. 88*, 2047–2056.
25. Shimabukuro, K., Yasuda, R., Muneyuki, E., Hara, K. Y., Kinosita, K. Jr., and Yoshida, M. (2003) Catalysis and rotation of F1 motor: cleavage of ATP at the catalytic site occurs in 1 ms before 40 degree substep rotation. *Proc. Natl. Acad. Sci. U.S.A. 100*, 14731–14736.
26. Shimabukuro, K., Muneyuki, E., and Yoshida, M. (2006) An alternative reaction pathway of F1-ATPase suggested by rotation without 80 degrees/40 degrees substeps of a sluggish mutant at low ATP. *Biophys. J. 90*, 1028–1032.
27. York, J., Spetzler, D., Hornung, T., Ishmukhametov, R., Martin, J., and Frasch, W. D. (2007) Abundance of *Escherichia coli* F_1-ATPase molecules observed to rotate via single-molecule microscopy with gold nanorod probes. *J. Bioenerg. Biomembr. 39*, 435–439.
28. Greene, M. D., and Frasch, W. D. (2003) Interactions among gamma R268, gamma Q269, and the beta subunit catch loop of *Escherichia coli* F_1-ATPase are important for catalytic activity. *J. Biol. Chem. 278*, 51594–51598.
29. Ishmukhametov, R. R., Galkin, M. A., and Vik, S. B. (2005) Ultrafast purification and reconstitution of His-tagged cysteine-less *Escherichia coli* F_1F_o ATP synthase. *Biochim. Biophys. Acta 1706*, 110–116.
30. Gibbons, C., Montgomery, M. G., Leslie, A. G., and Walker, J. E. (2000) The structure of the central stalk in bovine F(1)-ATPase at 2.4 Å resolution. *Nat. Struct. Biol. 7*, 1055–1061.
31. Sonnichsen, C., and Alivisatos, A. P. (2005) Gold nanorods as novel nonbleaching plasmon-based orientation sensors for polarized single-particle microscopy. *Nano Lett. 5*, 301–304.
32. Spetzler, D., York, J., Martin, J., Ishmukhametov, R., Frasch, W. D. (2008) Microsecond resolution of enzymatic conformational changes using dark-field microscopy. Methods, in press, doi:10.1016/j.ymeth.2008.05.004.
33. Rudyak, V. Y., Belkin, A. A., and Tomilina, E. A. (2008) Force acting on a nanoparticle in a fluid. *Tech. Phys. Lett. 34*, 76–78.
34. Nakanishi-Matsui, M., Kashiwagi, S., Hosokawa, H., Cipriano, D. J., Dunn, S. D., Wada, Y., and Futai, M. (2006) Stochastic high-speed rotation of *Escherichia coli* ATP synthase F_1 sector: the epsilon subunit-sensitive rotation. *J. Biol. Chem. 281*, 4126–4131.
35. Ariga, T., Muneyuki, E., and Yoshida, M. (2007) F_1-ATPase rotates by an asymmetric, sequential mechanism using all three catalytic subunits. *Nat. Struct. Mol. Biol. 14*, 841–846.
36. Hirono-Hara, Y., Noji, H., Nishiura, M., Muniyuki, E., Hara, K., Yosuda, R., Kinosita, K., and Yoshida, M. (2001) Pause and rotation of F_1-ATPase during catalysis. *Proc. Natl. Acad. Sci USA 98*, 13649–13654.
37. Kagawa, R., Montgomery, M. G., Braig, K., Leslie, A. G., and Walker, J. E. (2004) The structure of bovine F_1-ATPase inhibited by ADP and beryllium fluoride. *EMBO J. 23*, 2734–2744.
38. Gledhill, J. R., Montgomery, M. G., Leslie, A. G., and Walker, J. E. (2007) How the regulatory protein, IF(1), inhibits F(1)-ATPase from bovine mitochondria. *Proc. Natl. Acad. Sci. U.S.A. 104*, 15671–15676.
39. Cabezon, E., Montgomery, M., Leslie, A., and Walker, J. E. (2003) The Structure of Bovine F_1-ATPase in Complex with its Regulatory Protein IF1. *Nat. Struct. Mol. Biol. 10*, 744–750.
40. Kabaleeswaran, V., Puri, N., Walker, J., Leslie, A., and Mueller, D. (2006) Novel Features of the rotary catalytic mechanism revealed in the structure of yeast F_1 ATPase. *EMBO J. 25*, 5433–5442.

APPENDIX C

PERMISSION TO PUBLISH

I, James L Martin, have communicated with and have received permission to include the published works contained herein from those individuals that are co-authors with me.